Cape Peninsula
University of Technology

EVALUATION AND CHARACTERISATION OF AN ULTRASOUND BASED IN-LINE RHEOMETRIC SYSTEM FOR INDUSTRIAL FLUIDS

By

TAFADZWA JOHN SHAMU
(210227702)

Thesis submitted in fulfilment of the requirements for the degree

Master of Technology: Electrical Engineering

in the Faculty of Engineering

at the

CAPE PENINSULA UNIVESITY OF TECHNOLOGY

Supervisors:
Dr Reinhardt Kotzé &
Prof Rainer Haldenwang

External supervisor:
Dr Johan Wiklund: SP - Technical Research Institute of Sweden

Cape Town
October 2015

DECLARATION

I, Tafadzwa John Shamu, declare that the contents of this dissertation/thesis represent my own unaided work, and that the dissertation/thesis has not previously been submitted for academic examination towards any qualification. Furthermore, it represents my own opinions and not necessarily those of the Cape Peninsula University of Technology.

Some of the very detailed specifications of the Flow-Viz^{TM} system have been omitted due to patent confidentiality.

25 November 2015

Signed **Date**

EVALUATION AND CHARACTERISATION OF AN ULTRASOUND BASED IN-LINE RHEOMETRIC SYSTEM FOR INDUSTRIAL FLUIDS

Tafadzwa John Shamu

ABSTRACT

Pulsed Ultrasound Velocimetry combined with Pressure Difference (PUV+PD) measurement is a non-invasive in-line rheometric technique which is used to analyse the complex flow properties of industrial fluids for quality control purposes. Cape Peninsula University of Technology (CPUT) and Technical Research Institute of Sweden (SP) have developed and patented a new PUV+PD based system, called Flow-Viz™. Despite this advancement, the system and ultrasound sensor technology have not been fully tested and evaluated in a wide range of industrial fluids. Acoustic characterisation tests were carried out at SP, with the aim of understanding the ultrasound beam properties after propagating through industrial stainless steel (316L) pipe walls. For these tests, a high-precision robotic XYZ-scanner and needle hydrophone setup were used. Different ultrasound sensor configurations were mounted to a stainless steel pipe while using different coupling media between the transducer-to-wedge and sensor wedge-to-pipe boundaries. The ultrasound beam propagation after the wall interface was measured by navigating the needle hydrophone within a predefined 2-dimensional spatial grid. The most suitable coupling material was determined from the acoustic characterisation, and then used in the in-line rheological characterisation tests to evaluate the performance of the Flow-Viz™ rheometric unit against conventional tube viscometry. The in-line rheological tests were conducted with bentonite, kaolin and Carboxymethyl cellulose (CMC) model fluids. The flow loop used consisted of three different pipe test sections; and two concentrations of each fluid were tested in order to ascertain the consistency of the measurements. The in-line rheological tests showed good agreement (±15%) between the two techniques and Flow-Viz™ was able to provide important data at very low shear rates. Acoustic characterisation indicated that variations in the beam properties were highly dependent on the acoustic couplants used to mount the sensors to the stainless steel pipes. Furthermore, the in-line results showed the effectiveness of Flow-Viz™ as an industrial rheometer. The non-invasive ultrasound sensor technology, was for the first time acoustically characterised through stainless steel. This information will now be used to further optimise the unique technology for advanced industrial applications, e.g. oil drilling fields, complex cement grout and food processing applications.

ACKNOWLEDGEMENTS

I wish to thank:

- God almighty for providing me with the strength and capacity to see this work come to completion.
- Cape Peninsula University of Technology (CPUT) and Technical Research Institute of Sweden (SP), for providing the platform, funding and necessary facilities needed to conduct this research work.
- My supervisor Dr. Reinhardt Kotzé for his support and knowledge throughout the course of the experimental and writing phases of the project.
- My external supervisor Dr. Johan Wiklund from SP Sweden for his invaluable knowledge and support which he gave during my stay in Sweden.
- Prof Haldenwang my co-supervisor from the Flow Process and Rheology Centre (FPRC) for his support, guidance and especially with the analysis of conventional tube viscometry data.
- Mr. Andrew Sutherland for his assistance with error and tube viscometry data analysis.
- Mr. Richard Du Toit and Mr. Naziem George for their support at the FPRC laboratories.
- All my colleagues at the FPRC for their support throughout the research period, especially Willy Mbasha who assisted with rheological analysis of data.
- All those who contributed to the completion of this research project.

DEDICATION

Dedicated to my loving mother Shingirai Beatrice Shamu who has been a pillar of support in life and throughout the course of my research work.

NOMENCLATURE

Symbol	Description	Unit
A	cross sectional area	m^2
A_{max}	wave amplitude	mm
c	sound velocity	ms^{-1}
Δd	measurement distance along US beam or measuring line	mm
F	Fourier transform	-
F^{-1}	inverse Fourier transform	-
f	Fanning friction factor	-
f_d	Doppler shift frequency	Hz
f_e, f_0	frequency of emitted ultrasound wave	Hz
f_r	Frequency of reflected ultrasound wave	Hz
f_{res}	resonant frequency	Hz
g	gravitational acceleration	ms^{-2}
H	flow depth / distance between two transducers	m
h_f	frictional head	m
I	US intensity	Wcm^{-2}
ID	Pipe inner diameter	m
IQ	in-phase, quadrature echo data	-
K	fluid consistency index	$Pa.s^n$
L	pipe length, characteristic length	m
L_c	thickness of piezoelectric crystal	m
N_{rep}	number of pulse repetitions	-
N_f	near-field distance of US transducer	m
n	flow behaviour index	-
P, p	pressure, acoustic pressure	Pa
PRF	Pulse repetition frequency	Hz

Q	volumetric flow rate	m^3s^{-1}
R	pipe radius (inner)	m
R_{plug}	plug radius	m
Re, Re_2	Reynolds number, non-Newtonian Reynolds number *(Slatter)*	-
r	radial position	m
S	power spectrum	-
Δs	moving distance along main stream direction	mm
T	Temperature	^oC
t	Time	s
T_{prf}	periodic interval between two ultrasound pulse emissions	s
t_d	time delay	s
u, v	point velocity	ms^{-1}
V^+	Non-dimensionalised velocity	-
V	average velocity	ms^{-1}
V_n	velocity across area segment	ms^{-1}
V_{pk-pk}	Peak to peak voltage	V
V_{tr}	target velocity	mms^{-1}
V_t	velocity in direction of US beam or measuring line	mms^{-1}
V_m	measured velocity profile as function of k	-
V_z	velocity distribution across flume flow depth	ms^{-1}
XYZ	3 dimensional coordinate system	mm
y^+	Non-dimensionalised wall units	-
Z	specific acoustic impedance	$grcm^{-2}s^{-1}$

GREEK SYMBOLS

α_0	spatial attenuation coefficient	dB/cm
$\dot{\gamma}$	Pseudo shear rate	s^{-1}
p_0	reference acoustic pressure of ultrasound sensor	Pa
$\dot{\gamma}_w$	Wall pseudo shear rate	s^{-1}
ρ	density of fluid or material	kgm^{-3}
θ	Doppler angle	degrees
κ	adiabatic compressibility	-
λ , λ_0	wavelength	m
τ_w	Wall shear stress	Pa
τ_y	Yield stress	Pa

ABBREVIATIONS AND ACRONYMS

AToM	Acoustic Time of Flight Measurement
CMC	Carboxymethyl cellulose
CPUT	Cape Peninsula University of Technology, Cape Town
ERT	Electrical resistance tomography
FPRC	Flow Process and Rheology Centre
LDA	Laser Doppler Anemometry
MRI	Magnetic resonance imaging
PRF	Pulse Repetition Frequency
PUV	Pulsed Ultrasound (Doppler) Velocimetry
PUV+PD	Pulsed Ultrasound (Doppler) Velocimetry combined with Pressure Difference measurement
SP	Technical Research Institute of Sweden, Sweden
SNR	Signal-to-Noise Ratio
TDX	Ultrasound transducer
US	Ultrasound

TERMS AND CONCEPTS CITED

Aliasing:	Measurement artefact that occurs when the Doppler frequency shift exceeds one half of the pulser repetition frequency (PRF).
Acoustic map	A two dimensional grid showing the acoustic intensity distribution of an ultrasound beam measured within a predefined two-dimensional scanning area.
Gate Distance:	The distance between two measuring volumes.
Gate width:	The length of the measuring volume, also called sample volume or ultrasonic burst. It influences directly the special resolution of Doppler shift frequency determination.
Gates:	A gate (channel) within a Doppler ultrasound system is described as an ultrasound burst which gives the measuring sample or measuring volume at a particular measuring depth.
Couplant	Impedance matching material used to facilitate ultrasound beam transmission from outer pipe wall into fluid medium.
Doppler effect:	The apparent change in frequency and wavelength of a wave that is perceived by an observer moving relative to the source of the waves.
Far-field:	The region where the pressure field variation of the ultrasonic beam is linear.
In-line	Measurement is performed directly in the process line
Laminar flow:	Streamline flow in parallel layers.
Maximum Depth:	Maximum measurable depth of the ultrasonic beam.
Measurement Window:	Distance between the first measuring gate and the last one throughout the measuring depth.
Near-field:	The region where the pressure field variation of the ultrasonic beam is non-linear.
Newtonian fluid:	Any fluid which exhibits a linear relationship between the applied shear stress and the resultant shear rate, at a specific temperature. Water is an example of a Newtonian fluid.
Non-Newtonian fluid:	A fluid with a viscosity value which is dependent on the shear rate at a specified temperature. The shear rate history also influences the measured viscosity.
Off-line	Measurement performed on sample taken from process line

Reynolds number:	A dimensionless quantity which describes the flow regime of a fluid. It can be expressed as a ratio of the fluid's viscous and inertial forces.
Reynolds number (Non-Newtonian)	The non-Newtonian Reynolds number describes the flow regime for non-Newtonian fluids, different definitions of this number exist and it is dependent on the rheological properties of the fluid such as the flow-behaviour index, *n*, flow consistency coefficient, *K* and τ_y the yield stress.
Spatial Resolution:	Pointwise distance between the centre of two adjacent gates or channels within a measurement window (depth)..
Time Resolution:	Sampling time of one velocity profile measurement. Directly influenced by the number of ultrasonic repetitions per profile.
Transducer:	A measurement device that converts energy from one form to another. A transducer is usually integrated as the primary detection element within a sensor unit.
Transition:	The region where laminar flow streamlines in a fluid approach full turbulence.
Turbulent flow:	Flow regime which is characterised by non-uniform streamlines and flow is erratic.
Ultrasound Sensor unit	Ultrasound transducer on a mounting wedge or integrated in a case.
Viscosity:	A measure of the resistance to flow of a fluid under an applied force.

TABLE OF CONTENTS

LIST OF FIGURES

LIST OF TABLES

CHAPTER ONE: INTRODUCTION

1.1 BACKGROUND

In most industrial setups, rheological characterisation of complex industrial suspensions is carried out off-line, which is time consuming. The off-line tests are also subject to several inaccuracies since the test sample might differ considerably from the actual fluid under process conditions. In-line techniques for flow visualisation and rheometry have been developed with the most prominent being Pulsed Doppler Ultrasound Velocimetry (PUV).

Before discussing the PUV method in detail, a brief overview of the different techniques used for flow visualisation and fluid characterisation is given. Off-line techniques are extensively used to rheologically characterise fluids, however, a number of inadequacies associated with these techniques have been reported in literature (Chhabra & Richardson, 1999). These inadequacies are mostly related to rheological properties such as time dependence and shear history of the test fluid. For instance, a test sample whose structure is dominantly time dependant might not be characterised accurately if the off-line test is delayed even by a few minutes. In the past two decades, technological advancements have resulted in the use of flow visualisation methods such as: Laser Doppler Anemometry (LDA), Magnetic Resonance Imaging (MRI), Electrical Resistance Tomography (ERT) and PUV techniques. LDA and MRI are well established techniques however, the former is dependent on the detection of visible light and therefore cannot be used in opaque complex suspensions, whereas MRI is very costly and complex, requiring highly skilled personnel to operate the equipment (Powell, 2008). ERT has not yet been fully developed for industrial use and data analysis of measured results is also very technical and complex. From the previously discussed flow visualisation techniques PUV and LDA are more suited for in-line rheometry although LDA cannot be used for opaque industrial suspensions. With this in mind, the PUV technique stands out as the most suitable method for in-line rheometry.

The PUV technique has been studied and developed by a number of research groups as the main tool for determining the rheometric parameters of complex industrial suspensions in line (Windhab and Ouriev, 2002; Birkhofer et al., 2004; Wiklund and Stading, 2008; Kotzé et al., 2012). For the past decade, PUV combined with pressure difference measurement (PUV+PD) methodology has been continually optimised and evaluated for a wide range of complex industrial suspensions, however, no commercial in-line rheometric system was developed for industrial implementation. Recently, Flow-Viz™ a novel, non-invasive rheometric system based on the PUV+PD methodology was developed under collaborative research between SP – Technical Research Institute of Sweden (SP), Gothenburg, Sweden and Flow Process and

Rheology Centre (FPRC) at Cape Peninsula University of Technology (CPUT). The Flow-Viz™ system offers a number of advantages which include its ability to characterise opaque, non-Newtonian industrial fluids and suspensions. Rheometric measurements using the system are carried out non-invasively through process pipes including high grade stainless steel pipes. The system also delivers real-time data such as instantaneous velocity profiles and rheological parameters (yield-stress, apparent viscosity) of complex industrial fluids. These measurements can then be used to enhance process monitoring and quality control.

1.2 CURRENT STATUS

In spite of this development, optimisation of the Flow-Viz™ system for industrial use is still required due to a number of persistent technical issues (Kotze et al., 2015b). These issues are related to, and include the following: inaccurate pipe wall estimation during measurement, the need for specialised ultrasonic transducers (characterised and evaluated specifically for the application) and optimised signal processing algorithms to accurately estimate the velocity gradient close to the wall interfaces. The main problem which still persists, and requires more attention is related to the development of more advanced non-invasive ultrasound sensor technology (Kotze et al., 2015b). This difficulty can be dealt with by studying the acoustic sensor beam properties. The ideal ultrasound beam required for accurate measurements should be as narrow as possible throughout the measurement depth (Kotzé et al., 2013). The geometry of the acoustic field is determined by the diameter of the emitter and the wavelength of the ultrasonic waves. Characterising beams from existing sensors will facilitate the development of advanced ultrasonic sensor technology, with narrower beams thus focusing all the acoustic energy throughout the measurement depth for improved results. With characterised and improved sensor technology, in-line PUV+PD measurements will greatly be improved and hence fluid characterisation based on the method will be more reliable. This will also allow testing in industrial applications with larger pipe diameters, for example in mining or oil drilling applications.

1.3 STATEMENT OF THE PROBLEM

The newly developed, non-invasive rheometric Flow-Viz™ system has not yet been fully tested and evaluated in a wide range of industrial fluids and applications. The new ultrasonic sensor technology used within the system still needs to be fully acoustically characterised in order to optimise measurements for more accurate results. Detailed information about the beam's focal zone shape is important. Non-invasive ultrasound sensors for pulsed ultrasound velocimetry should have a focal zone which starts at the pipe wall and is narrow throughout the measurement depth. By having the focal zone within the measuring section, the near field is

eliminated and the overall accuracy of the velocity profiles is greatly improved (Kotzé, et al., 2014).

Different industrial fluids vary in terms of their particle structures and compositions which tends to present different problems for the PUV measuring technique. Attenuation of the ultrasound beam inhibits the proper measurement of accurate velocity profiles. These factors need to be studied carefully in order to clearly understand the limitations of the Flow-Viz™ system. Therefore the technology's limitations and capabilities need to be tested and evaluated in a wide range of complex industrial fluids. In addition, the experimental tests will also illuminate the major factors which need to be taken into consideration in the application of the newly developed Flow-Viz™ system. Factors to consider during in-line tests include automatic wall detection for different fluid applications, accurate velocity of sound and optimum ultrasound parameter settings which are specific to a fluid e.g. emission voltage, voltage gain settings and also on board FFT processing (handling of higher amounts of data to combat effects of attenuation). Critical parameters which need more attention during optimisation procedures, include the velocity of sound and the Doppler angle. If these parameters are not determined correctly prior to measurement, all the experimental data is rendered inaccurate.

1.4 RESEARCH OBJECTIVES

The main objective of this research was to investigate the capabilities and limitations of the PUV+PD rheometric technique, using the Flow-Viz™ system as an in-line rheometer for measuring the rheological parameters of different industrial fluids. These objectives are outlined as follows:

- Acoustically characterise and evaluate ultrasound sensor technology for non-invasive flow profile measurements through stainless steel pipes (nominal inner diameters of 22.4 mm and 47.8 mm). The purpose of these tests was to investigate the propagation of the pulsed ultrasound beam using different coupling, wedge and transducer technologies.
- Evaluate the capabilities and limitations of the Flow-Viz™ system in the rheological characterisation of different concentrations of fluids against conventional tube viscometry. The complex suspensions that were tested include mineral suspensions of bentonite and kaolin clay as well as Carboxymethyl Cellulose (CMC) solutions.

1.5 DELINIATION

In relation to the objectives, the following delineations were set as guidelines for this research project:

- The scope of this research was limited to evaluating and optimising the PUV+PD in-line rheometric method.
- Although rotary rheometry is a widely accepted technique, it was not used for validation purposes since the shearing geometry provided by rotary rheometers does not truly represent pipe-flow dynamics accurately as compared to an in-line technique such as tube viscometry. Furthermore, the fluid sample used in an off-line test might differ considerably from that which was in the pipe, owing to some time-dependency characteristic of the test fluid (Roberts, 2001). Therefore, only tube viscometry was used for comparison and validation purposes. Like PUV+PD, tube viscometry determines the rheological parameters of a fluid in-line by measuring the pressure difference across a test pipe section at different flow-rates.
- Other methods such as MRI and LDA where not used for validation since they were not readily available and are technically complex. Furthermore a technique such as LDA cannot be used with opaque fluids.
- Only ultrasonic sensor technology from Flow-Viz™ was characterised and tested. No other commercial transducers were used.

1.6 METHODOLOGY AND THESIS OUTLINE

The experimental work consisted of two major components which were, acoustic characterisation of the non-invasive sensor technology and in-line rheological characterisation with two techniques i.e. PUV+PD compared with tube viscometry. The acoustic characterisation tests were carried out at SP, Gothenburg, whereas the in-line rheological characterisation tests were conducted at the Flow process and Rheology Centre (FPRC) within the Cape Peninsula University of Technology.

Figure 1.1 shows a flow chart with the adopted research methodology. The flow chart was used as a guideline in conducting the research work.

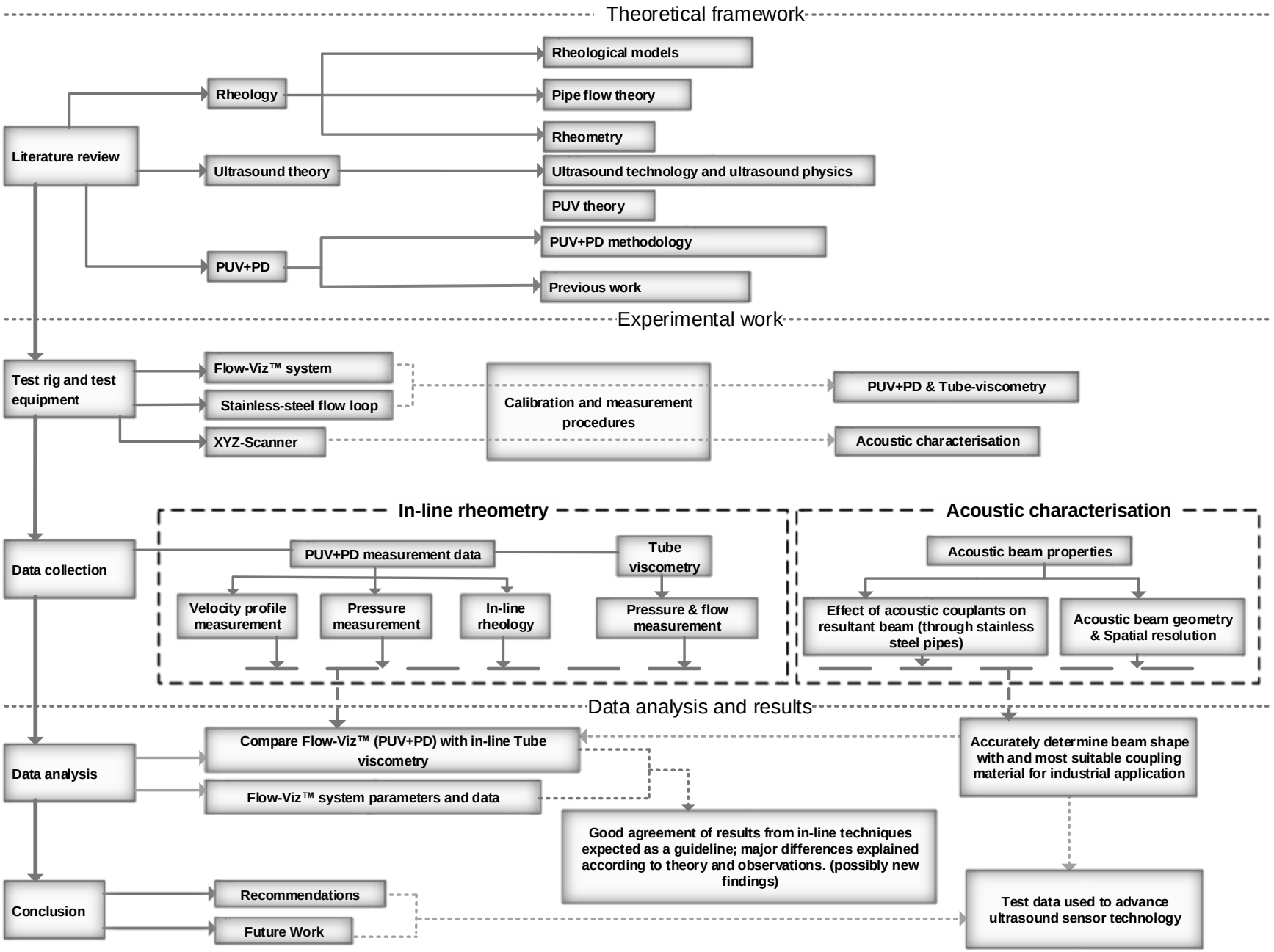

Figure 1.1: Flow diagram of overall research methodology

1.6.1 Literature review and fundamental theory (Chapter 2)

The literature review is divided into three major sections which are rheology, ultrasonics and PUV+PD. The rheology section will describe principles of Newtonian and non-Newtonian fluids and the common constitutive models which are used to characterise different fluids encountered within the processing industries including the ones used for the purpose of this research. The ultrasonics section gives a brief background on ultrasound physics and then narrows down to how the basic properties of ultrasound are used in PUV. Lastly, the PUV+PD technique is then discussed. The technique is the basis upon which the Flow-Viz™ system operates in order to deliver real-time, in-line rheometric data about the fluid under observation. Previous literature on the PUV+PD technique is also discussed to give a detailed overview of the subject matter and to show the gap which this research work fills. General industrial applications which could benefit from the use of Flow-Viz™ as a tool for in-line rheometry are briefly discussed.

1.6.2 Methodology and apparatus (Chapter 3)

The methodology followed to carry out the experimental aspect of this research work is presented in Chapter 3. Ultrasound sensor acoustic characterisation was carried out at SP, which provided the necessary equipment required for this research component. SP has a high precision needle hydrophone and XYZ-scanner setup, which were used for the tests. Stainless steel pipes cut in half had sensors mounted onto them in order to measure the ultrasound beam after the wall interface, that is from the inside of the pipe. Several acoustic couplants were utilised to determine the most suitable mounting setup for industrial applications. Important information obtained from the acoustic characterisation such as the beam properties e.g. Doppler angle, was then used as parameters for the in-line PUV+PD tests.

The Flow-Viz™ system was the main tool used for the in-line rheometric tests. The Flow-Viz™ system was integrated as part of a portable stainless steel flow loop at the FPRC. This flow loop consisted of a rotary-lob pump *(SPX Process Equipment, Sweden)* suitable for conveniently pumping highly viscous fluids, as it facilitates fluid movement without altering the rheology (non-shearing action). The flow loop was fitted with instrumentation (magnetic flow meters, thermocouples and differential pressures sensors) for in-line viscometric measurements. The instrumentation also served to verify and validate results obtained using the Flow-Viz™ system. Since the core of this research work was to perform an evaluation of the Flow-Viz™ and how well it rheologically characterises complex industrial fluids, several fluids of varying concentrations were used. The fluids included dilute bentonite, kaolin and

CMC (Carboxymethyl cellulose). These model fluids were selected as they exhibit a wide range of rheological characteristics which are common to most fluids found in industry, e.g. bentonite a typical drilling mud, which exhibits a characteristic yield-stress component. Two concentrations (high and low) of each model fluid were tested in order to assess the sensitivity of the measurement technique at different viscosities of the same fluid. Results obtained using the in-line Flow-Viz™ system were compared against results obtained using conventional tube viscometry.

1.6.3 Analysis of experimental results (Chapter 4)

The analysis for the different sections of this work was combined into one chapter. The first part included the acoustic characterisation of different sensor technologies which were characterised, with more emphasis on the important velocimetry parameter (Doppler angle) and the length of the beam focal zone. The second part utilised the acoustic characterisation data in in-line rheological characterisation tests, to evaluate the new Flow-Viz™ non-invasive rheometric system against conventional tube viscometry over the same shear rate ranges.

- **Acoustic characterisation of non-invasive sensor technology**

Chapter 4 describes the test data (acoustic maps) which were obtained from the acoustic characterisation tests. The purpose of the acoustic characterisation was to determine important parameters such as the Doppler angle and the start distance of the focal zone from the transducer front or inner pipe wall. The shape and location of the focal zone was also noted for different transducers and how it was affected by different acoustic couplants. With information about the distribution of the beam shape after the pipe wall, important conclusions can are made towards the configuration and sensor mountings for more enhanced measurements.

- **Evaluation of Flow-Viz™ against conventional tube viscometry**

The second part of Chapter 4 describes the results obtained from evaluating the Flow-Viz™ system for in-line rheometry. The measured profiles and the rheological data obtained from the tests of each fluid are discussed in detail. Percentage deviation curves on rheological data were also included to graphically illustrate the differences in the measurement values from the different techniques, hence making the experimental differences more understandable and reliable. Power spectrum images were also presented and analysed in relation to the attenuating effects of the fluids on the velocity profile. Differences between the two in-line methods are highlighted and discussed.

1.6.4 Research summary, contributions, recommendations, future work and conclusions (Chapter 5)

This section brings together the main points highlighted and described within the context of each chapter and the research work as a whole. This chapter also outlines the key technical areas which still need to be addressed and improved in the existing Flow-Viz™ system and the PUV+PD technique as a whole. Recommendations are outlined for further research and advancement of the PUV+PD rheometric technique.

CHAPTER TWO: THEORY AND LITERATURE REVIEW

2.1. INTRODUCTION

The main aim of this chapter is to provide a brief and concise theoretical foundation on rheology, ultrasound principles and PUV+PD. The first section discusses some rheology basics. The scope is limited to the description of rheology within the context of in-line rheometry using the PUV+PD principle. Following the rheology section, ultrasound principles are discussed in detail to elaborate on the working principle of PUV. The rheology section on fluid pipe flow is first presented before ultrasound theory, in this way, there is more clarity as to how pulsed-ultrasound properties are manipulated to obtain the rheological properties of the fluid medium. The fundamentals of PUV are discussed in conjunction with the currently used PUV+PD in-line rheometric method. Previous and current works done on the PUV+PD technique are presented, narrowing down the discussion to the most recent development in in-line rheometry: that is, the Flow-Viz™ in-line rheometric system.

2.2. RHEOLOGY

The rheology section is presented in a sequential manner and targeted at describing fundamental principles of the subject matter for fluids in laminar pipe flow. Using this approach, the description of a particular fluid model is carried out using a mathematical relationships which describes its flow in a pipe. During the discussion of fluid flow in pipes, velocity profiles will be of particular interest since velocity profile measurements are required for the PUV+PD methodology.

2.2.1. Introduction to rheology

From most scholarly articles which deal with rheology, the term *rheology* is defined as the study of deformation and flow of matter (Barnes, 2000). The term is derived from the Greek word "*rheos*" which when literally translated means flow science (Metzger, 2002). In the context of this thesis and research work, *rheology* was used to describe the flow behaviour of a fluid by its rheological or flow parameters. Several parameters can be used to classify the flow behaviour of a particular fluid depending on the mathematical model used to describe its behaviour. The most important parameter is the viscosity of a fluid which is simply a measure of how the fluid resists gradual deformation due to the action of shear stress or tensile stress. To facilitate fluid characterisation, several constitutive models have been presented in literature, for example the Power-law and Herschel-Bulkley models. These models give rise to the use of rheological parameters such as the yield stress τ_y, flow behaviour index *n* and fluid

consistency coefficient *K*. More details on the different fluid models and rheological parameters are given in Section 2.2.4.1.

2.2.2. Flow Regimes

Before examining fluid rheological behaviour in depth, it is necessary to address the different flow regimes which are observed whilst the fluid is in motion. In simple terms, a flow regime is the geometric distributions or flow patterns observed as the fluid flows. When a fluid flows, it forms a certain pattern depending on its velocity, the conduit through which it flows and the properties of the fluid itself. These patterns can be orderly or random in terms of the packing order of the fluid's particles flowing at different depths. When the flow is headed in one direction and the fluid is uniformly stacked in layers of different flow velocities, the flow is termed to be *laminar*. The extreme opposite of laminar flow is *turbulence*, which is characterised by the absence of orderly arrangement and lack of uniformity in the flow direction. The unstable region between laminar and turbulence is called the *transition* zone. The Reynolds number *Re*, is a dimensionless quantity that is used to give an indication whether a fluid is in laminar or turbulent flow and was named after Osborne Reynolds (1842–1912). It is a ratio of the inertial and viscous forces and is defined by the relationship:

$$Re = \frac{\rho V D}{\mu} \tag{2.1}$$

2.2.2.1. Description of flow regimes in terms of Reynolds Number

The three flow regimes mentioned above (Section 2.2.2) simply describe the pattern of the fluid flow at a particular velocity.

The laminar flow regime is characterised by smooth streamlines and highly ordered motion, and turbulence is the case characterised by velocity fluctuations and highly disordered motion (Cengel, 2010). Laminar flow is encountered when highly viscous fluids such as oils flow in small pipes or narrow passages. The laminar region is of particular interest because it is within this flow regime that rheological characterisation using tube viscometry and related methods is carried out. When the laminar flow regime becomes unstable, the flow regime shifts to turbulence. The transition zone is realised when the laminar flow regime changes to turbulent flow. Fully turbulent flow is then realised at higher flow rates than those which are noted in transitional flow. As presented by Cengel (2010) the flow regimes can be grouped in terms of *Re* as follows:

- *laminar* when *Re < 2300*
- *transition* when *2300 < Re < 4000*
- *turbulent* when *4000 < Re*

An illustration of the flow patterns formed within the laminar, transition and turbulent regions is shown in Figure 2.1.

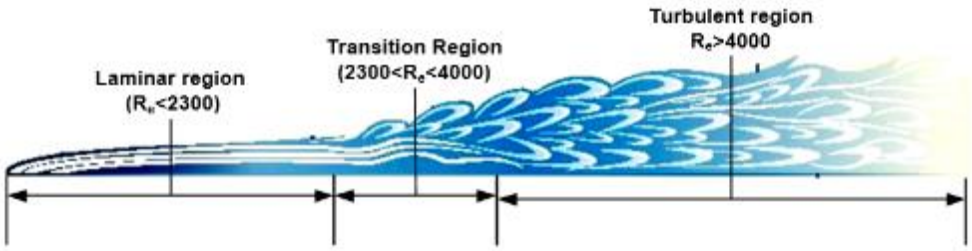

Figure 2.1: Illustration of laminar and turbulent flow patterns (Federal Aviation Administration, 2008)

The above Reynolds number is merely descriptive of Newtonian fluids. A number of different Reynolds numbers have been presented in literature to describe flow conditions of non-Newtonian fluids. An example is that described by Slatter (1993), which takes the form of:

$$Re_2 = \frac{8\rho V^2}{\tau_y + K\left(\frac{8V}{D}\right)^n} \tag{2.2}$$

In Equation (2.2), *n* is the Power-law flow behaviour index and *K* is the fluid consistency coefficient. The consistency coefficient *K* has the units Pa.s^n and the exponent *n*, the flow behavior index, is dimensionless and reflects the closeness to Newtonian flow. The yield-stress of the fluid is described by τ_y. The use of these parameters is described under Section (2.2.4). The non-Newtonian Reynolds number, Re_2 used for this research work.

2.2.3. Fluid behaviour

According to (Chhabra & Richardson, 1999), one can classify fluids in two different ways; either based on their response to externally applied pressure or according to the effects produced under the action of shear stress. Assuming incompressibility for most of the fluids which are encountered in practice, the main focus is drawn to fluid behaviour based on the action of shear stress. This narrows down the discussion to fluid behaviour of Newtonian and non-Newtonian fluids which will be discussed in detail in Sections 2.2.4 and 2.2.5. The discussion on fluid behaviour starts off by describing Newtonian fluids since the mathematical relationships and models describing their flow-curves are less involved. The flow properties

discussed will be restricted to treat the laminar flow regime within circular pipes. After the discussion of Newtonian fluids, complex non-Newtonian pipe flow will be discussed with relevant rheological models. These basic principles which address fluid flow behaviour in circular pipes are paramount to the optimal design of flow networks. Furthermore knowledge of these factors facilitates more controlled flow of complex fluids within process pipes, since the flow properties are known in advance (Metzner & Reed, 1963).

2.2.3.1. Newtonian fluid behaviour and pipe flow

The concept of a Newtonian fluid is explained by Figure 2.2 which illustrates a thin film of fluid contained between two parallel plates. If a shearing force is applied on the top layer (plane) of the fluid element, an equal and opposite reaction will result due to the fluid's internal frictional forces. The magnitude of the shearing force decreases linearly from the top plane to the bottom plane.

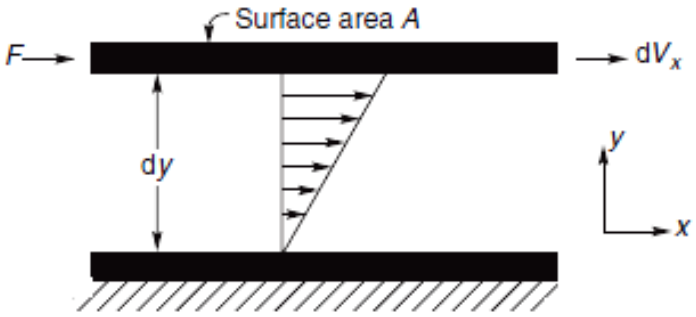

Figure 2.2: Unidirectional shearing flow (Chhabra & Richardson, 2008)

Equation 2.3 shows the linear relationship between the applied shear stress and the resultant shear rate for Newtonian fluids. The shear rate $\dot{\gamma}_{yx}$ is then expressed as the velocity gradient, in a direction perpendicular to the shear force:

$$\frac{F}{A} = \tau_{yx} = \mu\left(-\frac{dV_x}{dy}\right) = \mu\dot{\gamma}_{yx} \tag{2.3}$$

The direction coordinates i.e. subscripts *(x, y)*, show the direction parallel to the flow *(x)* and that which is perpendicular to the bulk flow *(y)* (Chhabra & Richardson, 1999). By plotting values of shear stress (τ_{yx}) against the corresponding shear rate ($\dot{\gamma}_{yx}$) a graphical representation of the fluids flow properties known as a rheogram is obtained. For a Newtonian fluid, the rheogram is therefore a straight line of slope, μ, which passes through the origin. The slope of the rheogram is the viscosity of the fluid and it characterises the flow behaviour of a Newtonian fluid at a fixed temperature and pressure.

- Newtonian pipe flow

Figure 2.3 illustrates the force balance which can be observed in laminar Newtonian pipe-flow, and the Equation (2.4) shows the relationship of the pressures acting on the fluid element.

$$p\left(\pi r^2\right)-\left(p+\Delta p\right)\pi r^2=\tau_{rz}2\pi rL \tag{2.4}$$

$$\tau_{rz}=\frac{r}{2}\left(\frac{-\Delta P}{L}\right) \tag{2.5}$$

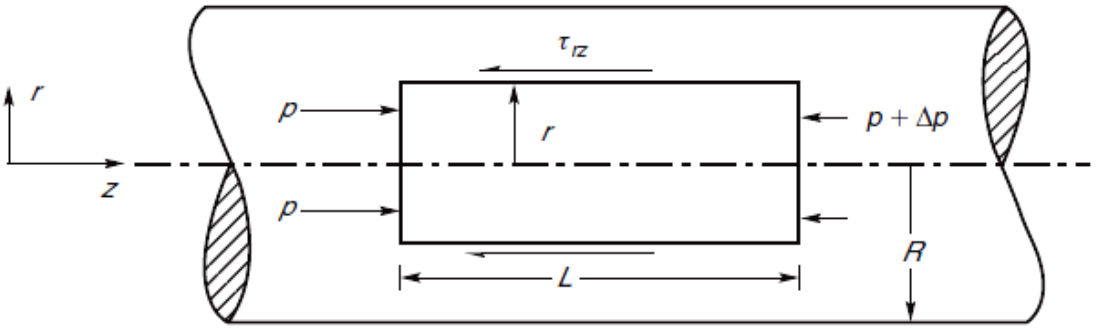

Figure 2.3: Flow through a horizontal pipe (Chhabra & Richardson, 1999)

Figure 2.3 and Equation 2.4 are applicable to laminar and turbulent flow of any fluid since it is based on a simple force balance and no assumption has been made so far concerning the type of flow or fluid behaviour. Figure 2.4 below shows the shear stress and velocity distribution across the pipe wall. As the shear stress decreases towards the centre of the pipe, the radial velocity conversely increases to a maximum.

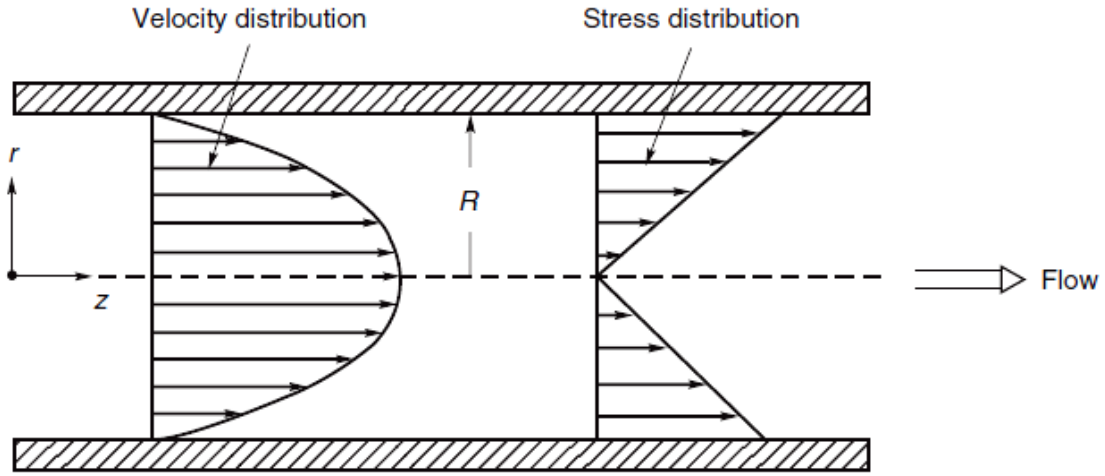

Figure 2.4: Shear stress and velocity distribution across pipe diameter (Chhabra & Richardson, 1999)

The Hagen–Poiseuille equation, which applies to fully developed laminar Newtonian flow is described in Equation (2.6) in terms of *V*, the mean velocity.

$$V = \frac{R^2}{8\mu}\left(\frac{-\Delta P}{L}\right) \tag{2.6}$$

2.2.4. Non-Newtonian fluid behaviour and pipe flow

A non-Newtonian fluid is one whose shear stress against shear rate plot is non-linear or has a yield stress component which is seen as an intercept on the shear stress axis of the rheogram. Non-Newtonian fluids cannot be completely characterised by a single value of the viscosity since they exhibit a complex flow behaviour. The relationship between the shear stress and the shear rate of these fluids is dependent on a number of factors which include: flow conditions such as the shear rate, flow geometry and the kinematic history of the fluid itself (Chhabra & Richardson, 1999). This complex behaviour of non-Newtonian fluids makes it evident that special care needs to be taken when determining their rheology. Typical flow curves of the different types of time-independent flow behaviour are displayed in Figure 2.5.

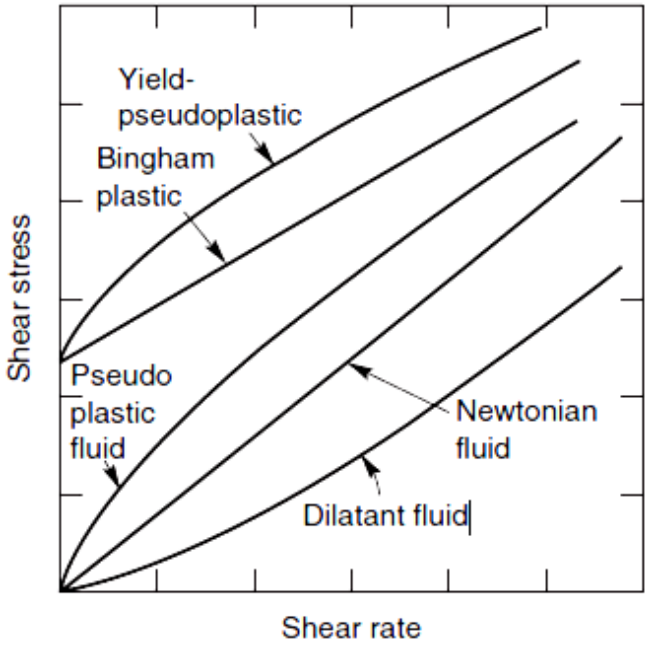

Figure 2.5: Flow curves for non-Newtonian and Newtonian fluids (Chhabra & Richardson, 1999)

Both non-Newtonian and Newtonian fluids can be better understood by the different models which mathematically describe their behaviour. Several models have been presented in literature to rheologically classify fluid behaviour. Only the common models used for practical applications and especially for the purpose of this work were discussed within this thesis. Figure 2.6 is a generalised chart which gives an overview of these models as described in

Chhabra & Richardson (2008). Within the chart mathematical models which describe the rheological models are also highlighted.

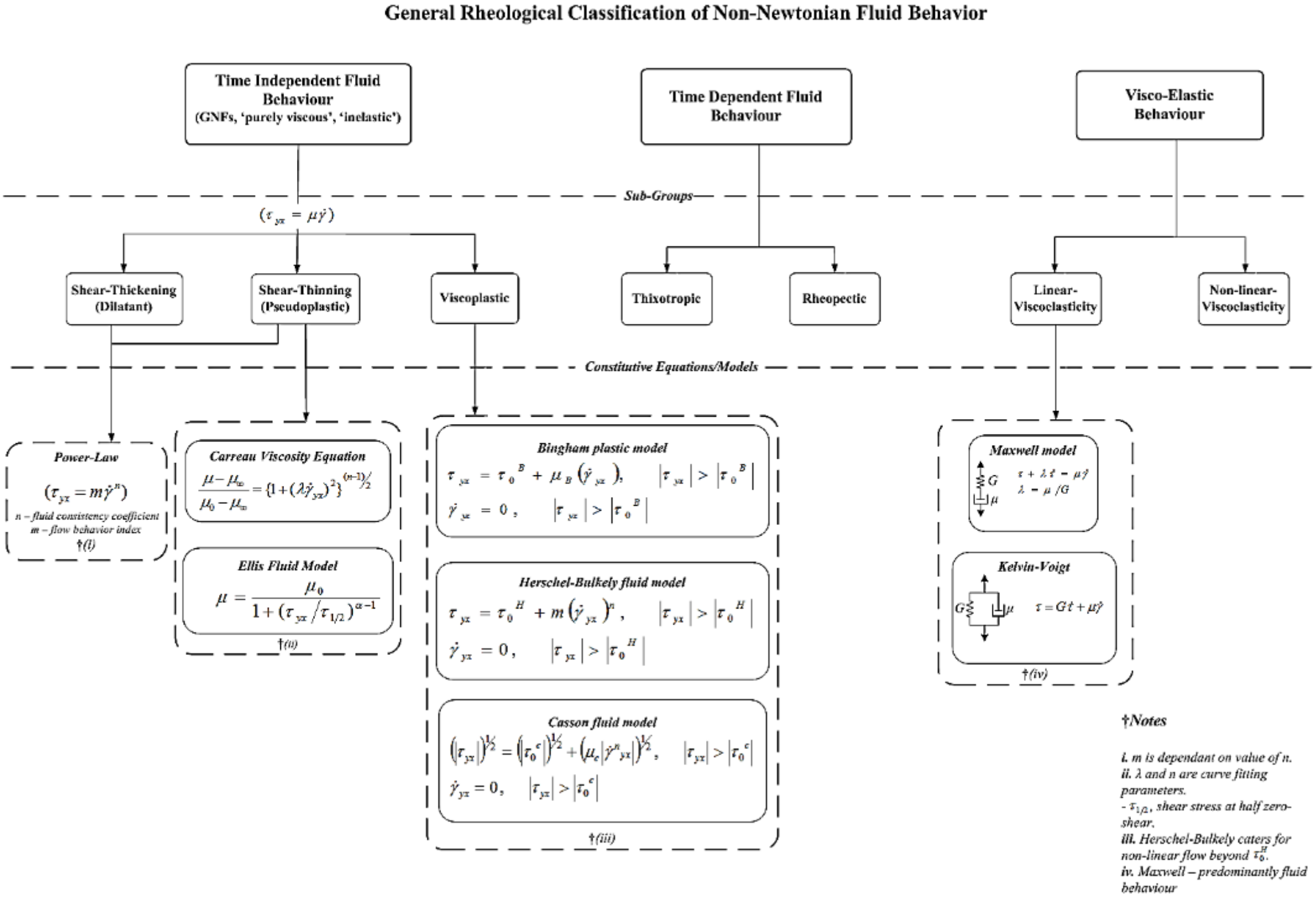

Figure 2.6: General rheological characterisation of Non-Newtonian fluid behaviour based on (Chhabra & Richardson, 1999)

Non-Newtonian fluids display complex behaviour during the flow process. Generalised models to describe flow in circular tubes of these models are available. These models depend on the velocity and shear rate distribution across the pipe radius. Mathematical models of this nature facilitate the design process for the realisation of more accurate pipeline designs. For example the velocity distribution, that is the flow profile of a fluid, can be considered as a valuable predictor of fluid properties at that point in time and hence the pumping power required. Thus it is important to discuss non-Newtonian rheological models such as the Power-law, Herschel-Bulkley and Bingham plastic models within this section.

2.2.4.1. Pseudoplastic or Power-law fluid model

The shear-thinning fluids are the most common type of time-independent fluid encountered within the environment and in industry. Shear thinning fluids exhibit a decrease of viscosity with shear rate. The mathematical model used to describe the pseudoplastic fluids is the Power-law model and it is given as:

$$\tau = K\left(\dot{\gamma}\right)^{n} \tag{2.7}$$

where *K* is the flow consistency coefficient and *n* is flow behaviour index. Using Equation 2.3 the value of the viscosity can be written as:

$$\mu = K\left(\dot{\gamma}\right)^{n-1} \tag{2.8}$$

Different values of the flow behaviour index, *n* characterise the flow using the Power-law model for three cases. With a value of ($n < 1$), shear-thinning behaviour is modelled, whereas ($n = 1$) is Newtonian and ($n > 1$) describes shear-thickening behaviour.

Figure 2.7 illustrates the variation in the shape of the velocity profile with a change in the value of the flow behaviour index, *n*.

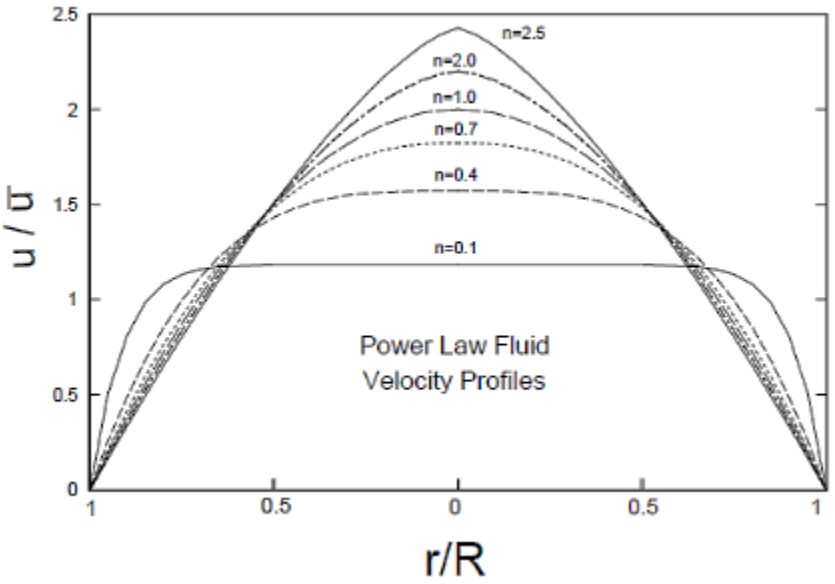

Figure 2.7: Typical velocity profiles of Power-law fluids in laminar flow, with changing flow behaviour index (Steffe, 1996)

2.2.4.2. Bingham plastic model

Some fluids have a greater resistance to flow when subjected to an external force. A threshold force needs to be exceeded before the fluid can flow. This type of fluid behaviour is characterised by the existence of a yield stress, τ_y which needs to be exceeded before the fluid flows. After the yield stress has been exceeded different fluids behave differently. Some fluids are characterised by a non-linear flow curve after the yield-stress point whilst others are described by a linear or Newtonian curve after this point (Barnes, 2000). The Bingham plastic model mathematically describes the latter behaviour, which is linear after the yield point. The mathematical equation governing the Bingham plastic behaviour is given by:

$$\begin{aligned} \tau_{yx} &= \tau_{y_B} + \mu_B\left(\dot{\gamma}_{yx}\right), \quad \left|\tau_{yx}\right| > \left|\tau_{yB}\right| \\ \dot{\gamma}_{yx} &= 0, \quad \left|\tau_{yx}\right| < \left|\tau_{yB}\right| \end{aligned} \tag{2.9}$$

In this case the consistency coefficient *K* is equal to μ_B, the Bingham viscosity.

2.2.4.3. Yield-pseudoplastic or Herschel-Bulkley model

Like the Bingham-plastic model, the Herschel-Bulkley describes fluids with an apparent yield stress which must be exceeded first before deformation occurs and fluid flow is initiated. The only difference is that this model incorporates the Power-law model as given by Equation 2.7 so that it describes Power-law (non-linear) flow behaviour after the yield stress value.

$$\begin{aligned} \tau_{yx} &= \tau_{yH} + K\left(\dot{\gamma}_{yx}\right)^n, \qquad \left|\tau_{yx}\right| > \left|\tau_{yH}\right| \\ \dot{\gamma}_{yx} &= 0, \qquad \left|\tau_{yx}\right| < \left|\tau_{yH}\right| \end{aligned} \tag{2.10}$$

Again, as demonstrated in Section 2.2.4.1 the value of the flow behaviour index *n* can be varied to describe Newtonian, shear-thinning or shear-thickening behaviour after the yield-stress point of Herschel-Bulkley fluids. The velocity profile relationship for these fluids in terms of rheological parameters *n*, and *K* is described under Appendix B.1.

2.2.5. Methods for fluid characterisation and rheometry

Rheological characterisation is the process of closely predicting a fluids behaviour based on some measured fluid properties like the fluid's viscosity and then categorising it under a certain class of fluids (for example Bingham plastic, Herschel-Bulkley fluid etc. as discussed under Section 2.2.4). Thus, viscometry is used for fluid characterisation and it is described as the science of the measurement of viscosity (Barnes, 2000). Viscometry establishes the relationship between shear-stress and shear-rate and also other important rheological parameters of a fluid. Viscometry tests for non-Newtonian fluids may become complex and inaccurate due to the time-dependency characteristic of these fluids. Correctly determining the rheological parameters is important as these parameters give an insight to how the fluid will behave when sheared at a certain rate and under particular conditions. Several techniques for viscometry have been tried and tested over the years. Some of these techniques include conventional rotational and tube viscometry. Tube viscometry is presented in this section since it is the most common in-line method and was used for validation purposes in this research work. Rotary rheometry which is an off-line technique is also presented. To conclude the discussion on fluid characterisation, more advanced in-line rheometric techniques such as PUV+PD and current trends in on-line/in-line process viscometry are discussed in brief.

2.2.5.1. Rotational rheometry

Generally the principle of operation of most rheometric equipment is that of applying either a force *F* or a velocity *V* at a surface in contact with a contained test liquid. The response of this liquid to either the velocity or the force is measured at that surface or at some other nearby surface which is also in contact with the liquid. Therefore in simple terms, rheometers rely on:

- converting the applied force *F* to a shear stress τ, and
- converting the velocity *V* to a shear rate $\dot{\gamma}$

There are two main types of rotational rheometers, namely: the controlled shear rate instruments (also known as controlled rate devices) and controlled stress instruments. Both types are usually supplied with the same range of measuring geometries, principally the concentric cylinder, cone and-plate and parallel-plate systems (Chhabra & Richardson, 1999). Many types of viscometers rely on rotational motion to achieve a simple shearing flow. Figure 2.8 illustrates these types of rotational viscometers. The working principle is based on measuring the minimum amount of torque required to continuously shear the fluid under test at a particular constant rate.

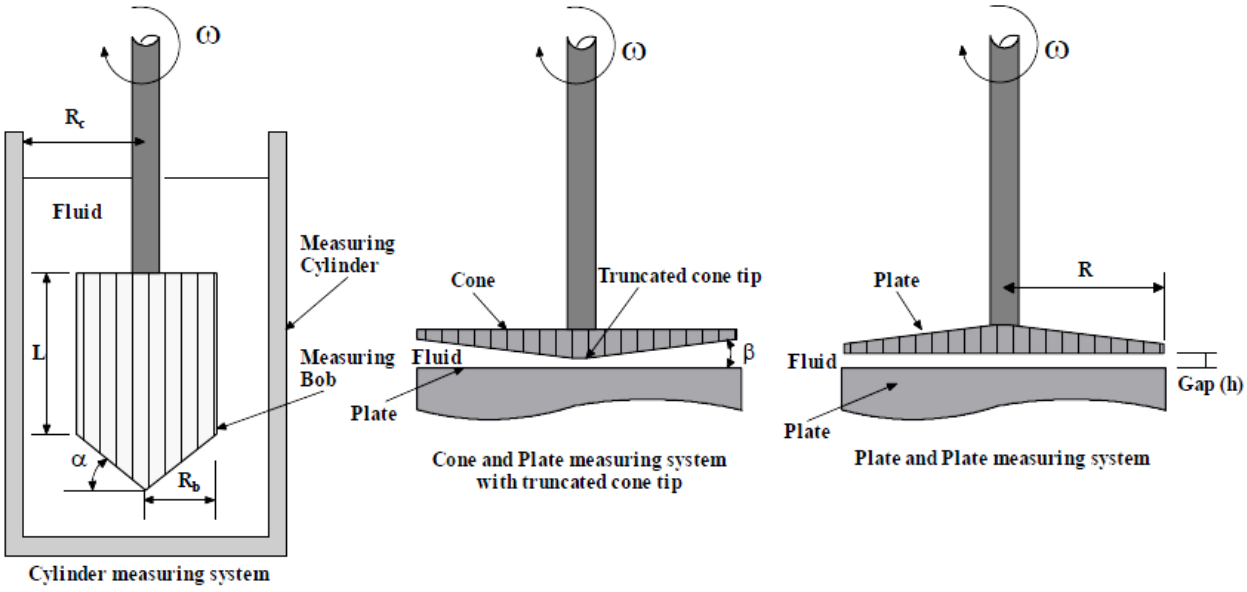

Figure 2.8: Types of rotational viscometer measuring systems (Haldenwang, 2003)

The equations which describe the resulting shear stress and shear rate from the concentric cylinder type measuring system are given below according to Metzger (2002). The equations are in terms of the torque *T*, gap β, radial velocity ω and radii (R_c *and* R_b) from Figure 2.8.

$$\tau = \left(\frac{\partial^2}{2\partial^2}\right)\frac{T}{2\pi L(R_b)^2 c_L} \text{ and } \dot{\gamma} = \omega\left(\frac{\partial^2}{(\beta^2 - 1)}\right), \quad (2.11)$$

Where $\delta = R_c/R_b$ and c_L is the resistance coefficient for the frontal area correction. Rotational rheometers are widely accepted instruments for fluid characterisation and provide reliable and accurate rheometric properties. However the shearing geometries provided by these instruments do not always resemble the true flow conditions which are experienced in line for example in a process pipe line thus the need for other techniques such as tube viscometry and PUV+PD (Roberts, 2001).

2.2.5.2. Tube Viscometry

Tube or capillary viscometers are the most commonly used instruments for the measurement of viscosity due to their relative simplicity and low cost. Their working principle relies on multiple measurements of the volumetric flow rate within fully developed laminar flow. A typical tube viscometry setup is illustrated in Figure 2.9.

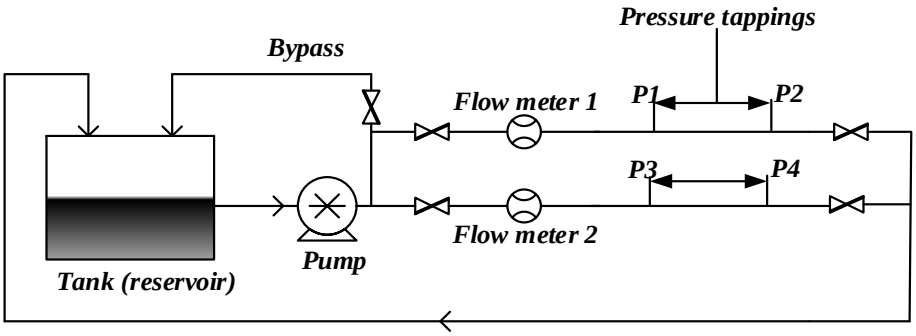

Figure 2.9: Typical tube viscometry test setup

These flow rate measurements are then used in a mathematical relationship to arrive at rheological parameters such as the shear-stress and shear-rate distribution. For fully developed flow, Equation (2.12) shows such a relationship:

$$\frac{Q}{\pi R^3} = \frac{1}{\tau_w^3}\int_0^{\tau_w} \tau^2 f(\tau) d\tau\,, \quad (2.12)$$

Where the wall shear-stress is $\tau_w = (R/2)/(-\Delta P/L)$ and $(-\Delta P/L)$ is the pressure drop per unit length of the pipe (Chhabra & Richardson, 1999). Usually, several pipe test sections with different pipe diameters are used, and the raw pressure and flow rate data is then used to obtain the true

rheogram after applying the Rabinowitsch–Mooney procedure. The procedure is described under Appendix C.1.

2.2.5.3. On-line and in-line viscometry

Conventionally most rheological characterisation tests are carried out offline, which means test samples are periodically taken from the process line for laboratory tests to examine whether the final or intermediate product still meets the desired specification (Barnes, 2000). Evidently this approach is inadequate and is prone to several inaccuracies especially for complex non-Newtonian fluids, particularly those which exhibit time-dependency. Nowadays the trend is to actually measure rheological parameters in-line or on-line (by-pass stream) so as reduce alterations in the rheology of the test sample. It is preferable to use an in-line rheometer that is non-invasive and does not interrupt with process dynamics. Articles such as (Cullen et al., 2000 ; Powell, 2008) describe several possible on-line techniques based on ultrasound technology. Cullen et al. (2000) then highlights the prerequisites for an ideal industrial standard in-line viscometer for the food industry, as that which is: non-intrusive, easy to clean-in-place, provides a quick response time and good sample renewal to ensure that any measurement obtained is representative of the actual fluid under process conditions. Additionally such a sensor must meet standard sanitary requirements. A typical in-line viscometer which meets most of these specifications, the Flow-Viz™ system, is discussed in detail in Sections 2.4.2 and 3.1.1. The newly developed Flow-Viz^{TM} system which operates based on the PUV+PD technique is an in-line technique, and thus validating its performance would also require a method such as tube viscometry which will also be able to characterise fluids within the same test conditions i.e. flow loop pipe geometry, temperature conditions, flow and pressure conditions.

2.3. PULSED ULTRASOUND VELOCIMETRY (PUV)

This section presents the principles of ultrasound theory and ultrasound technology. The PUV and PUV+PD techniques are then described in detail. A literature review of past works on both PUV and PUV+PD methods is then presented, and highlights the current trends and the research gap which this thesis work addresses.

2.3.1. Ultrasound physics

Ultrasound is basically sound which is out of the acoustic range of humans because of its high frequency. Typically the frequency range of ultrasound is of magnitudes greater than 20 kHz. The term acoustics is derived from the Greek word *akuin* which means to *hear* (Blauert & Xiang, 2008). Table 2.1 shows different sound frequency ranges.

Table 2.1: Sound categories by frequency range (Blauert & Xiang, 2008)

Sound category	Frequency range
Audible sound	16Hz – 16 kHz
Ultrasound	> 16 kHz
Infrasound	< 16 Hz
Hypersound	> 1 GHz

2.3.1.1. Characteristic properties of ultrasound

Sound is a wave phenomenon which propagates mechanical vibrations through matter in the form of longitudinal and shear waves. Figure 2.10 is presented to illustrate some important characteristics of ultrasound which include some wave theory. The sinusoidal wave shows an exponential decay in amplitude as it propagates further within the fluid medium. As a basis for pulsed ultrasound, Shutilov (1980) describes continuous wave attenuation within a fluid medium and mentions that it can be related to the distance of propagation using the spatial attenuation coefficient α_0 as follows:

$$\alpha_0 = \left(\frac{-1}{A_{MAX}}\right)\left(\frac{dA_{MAX}}{dx}\right) \tag{2.13}$$

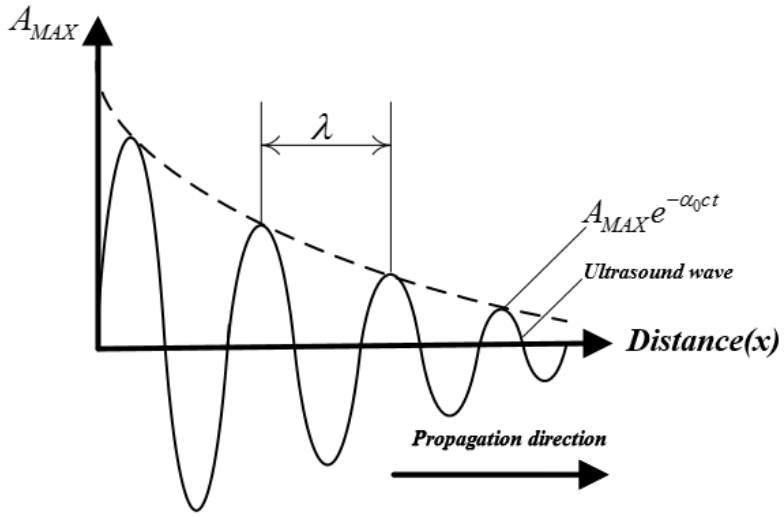

Figure 2.10: Ultrasound wave propagation showing attenuation adapted from (Ouriev, 2000)

By substituting $x = ct$, in Equation (2.13) where c is the speed of sound within the fluid medium, gives an equation which describes ultrasound wave attenuation in a sample fluid. This general equation which governs ultrasound wave motion in relation to attenuation is represented by the following mathematical relationship:

$$A_{MAX} = A_{max}e^{-\alpha_0 ct} \tag{2.14}$$

The damping constant τ_0 is a time related coefficient and is given by

$$\tau_0 = (\alpha_0 c)^{-1} \tag{2.15}$$

$$A_{MAX} = A_{\max}e^{-\frac{t}{\tau_0}} \tag{2.16}$$

The attenuation coefficient is dependent on the ultrasound frequency of the material, temperature and other parameters.

2.3.1.2. Ultrasound propagation at material boundary layers

Before an in depth discussion of ultrasound propagation in boundary layers is presented a brief electrical analogy is used to explain the underlying principles. *Electrical impedance* is defined as the ratio of the voltage to the current which is a measure of the resistance or restriction to the flow of current. Similarly *acoustic impedance* is defined as the ratio of the acoustic excess pressure Δp_0 to the particle velocity ξ' which is simply a measure of how a specific material opposes longitudinal wave motion resulting in a certain degree of reflection (Povey, 1997).

In general acoustic impedance *Z* is a complex quantity and in the acoustic case:

$$Z = \frac{\Delta p}{\xi'} = \rho \frac{\omega}{k} \approx \rho c \tag{2.17}$$

where ω is the wavelength and k is the magnitude of the wave vector or number. The common term used for $Z = \rho c$ is the characteristic impedance. In order to get the desired response when ultrasound propagates through materials, the acoustic properties of the material have to be known especially the acoustic impedance. This leads to the concept of impedance matching. Matching the impedance of the transducer to both the electrical circuitry and the target sample is important to the successful transference of acoustic energy. If there is a mismatch power transfer from electrical form will not be transferred into the sample. An impedance mismatch causes reflection of the wave. This concept is further explained by the illustration in Figure 2.11.

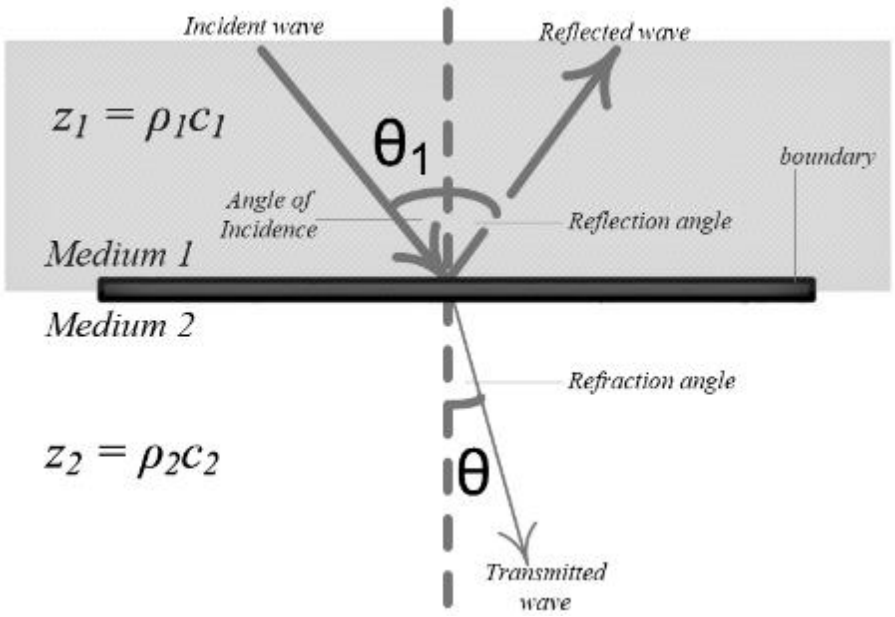

Figure 2.11: Ultrasound wave propagating obliquely between two mediums

Based on the description in Shutilov (1980), if medium 1, which has the incident ultrasonic wave, has a specific acoustic impedance $Z_1 = \rho_1 c_1$, where ρ_1 is a material layer density and c_1 is the sound velocity (subscript 1 denotes parameters related to medium 1). Similarly, medium 2 is defined as a bounding layer with the specific acoustic impedance $Z_2 = \rho_2 c_2$. The ultrasound wave propagates in layer 1 with the incident angle θ_1. At each boundary layer the ultrasound wave be subjected to refraction and reflection. The following law which is known as Snell's law in optics, describes the relationship between the refraction and reflection angles of boundary layers and the respective speed of sound values for the two layers:

$$\frac{\sin\theta}{\sin\theta_1} = \frac{c_2}{c_1} \tag{2.18}$$

For pulsed Doppler velocimetry measurements (see Section 2.3.2), a correct interpretation of the velocity distribution measured along the beam axis depends on the angle θ. Figure 2.11 above shows that the angle θ changes at the interface between two different materials. Thus, it is important to make sure that the choice of the interface layer materials results in a desired beam with correct properties, such as the angle of refraction. Analysis of different couplants and their effects was also considered as a major part of the experimental work and some basics on acoustic couplants are covered under Section 2.3.3.

With reference to Equation 2.18 it can be concluded that: a higher sound velocity in material layer 2 will result in a corresponding increase in the beam angle θ. To calculate the loss of the acoustic energy of the ultrasound beam that propagates through three layers, the following analysis is performed. By considering the incident ultrasound wave from layer 1 to layer 2, at the interface between the two layers the intensity I_1 of the initial ultrasound wave is written as:

$$I_1 = I_1' + I_2, \tag{2.19}$$

where I_1' is the intensity of the reflected ultrasound wave and I_2 is the intensity of the refracted ultrasound wave transmitted into the boundary layer 2. The acoustic energy reflection coefficient can be written as:

$$r_1 = \frac{I_1'}{I_2}, \tag{2.20}$$

and the transmission coefficient can be written as:

$$\kappa_1 = \frac{I_2}{I_1} \tag{2.21}$$

Thus, the balance of acoustic energy at the interface between two different materials is defined as:

$$r_1 + \kappa_1 = 1. \tag{2.22}$$

The energy reflection coefficient can also be described by the relationship in Equation 2.23.

$$r_1 = \left(\frac{z_1 - z_2}{z_1 + z_2} \right)^2 = \left(\frac{c_1\rho_1 - c_2\rho_2}{c_1\rho_1 + c_2\rho_2} \right)^2, \tag{2.23}$$

Alternatively according to Equation 2.21, the reflection coefficient can be expressed as:

$$r_1 = 1 - \kappa_1 = \frac{4z_1 z_2}{z_1 + z_2}. \tag{2.24}$$

Since reflection and refraction of the ultrasound beam have been discussed it is also necessary to highlight the phenomenon of total internal reflection, which can occur at boundary layers. Using Equation 2.18, $\sin\theta/\sin\theta_1 = c_2/c_1$ where θ is the refracted wave angle and θ_1 is the reflected angle it is evident that when θ_1 is 90° total internal reflection occurs. This means there is no transmission into the second medium. If $c_2 > c_1$, then the refraction angle will be greater than the angle of incidence. Since the refraction angle can never exceed 90° there is a maximum angle of incidence θ_1, defined by:

$$\theta_1 = \arcsin\left(\frac{c_2}{c_1}\right) \tag{2.25}$$

This maximum angle of incidence is known as the critical angle.

2.3.1.3. Ultrasound propagation in fluids

The above discussion (section 2.3.2.2) was more inclined to the general propagation of ultrasound waves across material layer boundaries. Since fluid characterisation based on ultrasonic techniques is paramount in this research work it is therefore necessary to look at the different critical parameters which affect ultrasound propagation in fluids.

The velocity of sound is highly dependent of the properties of the material though which it propagates (Povey, 1997). Since ultrasound wave motion can be described by a series of compressions and rarefactions as it passes through the material as shown in Figure 2.12, it is the nature of these mechanical movements within a specific material which determine how fast the wave propagates. Hence, the physical properties of the material are major parameters to be considered for ultrasound propagation.

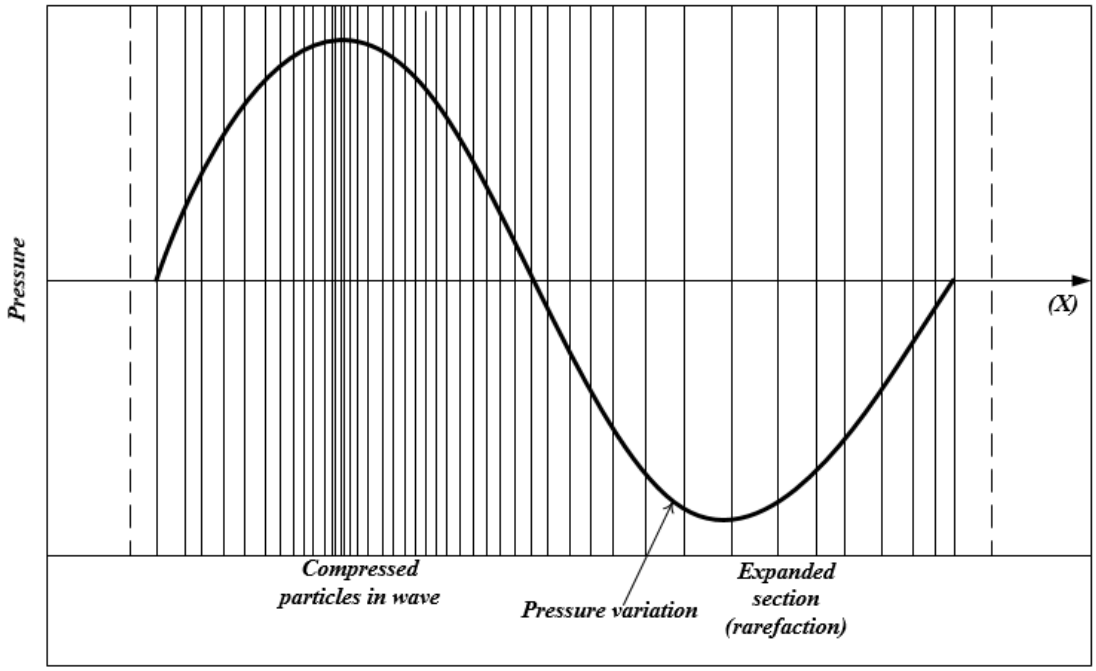

Figure 2.12: Illustration of rarefactions, compressions and spatial pressure variation of sinusoidal, plane wave in fluid medium adapted from (Povey, 1997).

Wood (1941) reviews the physical properties of a medium which influence sound velocity. Density and elasticity are mentioned as the major properties which affect sound velocity and these properties correspond to the mass and stiffness of a particle vibrating in a sound field. Now, as the wave of rarefactions and compressions passes through the medium the volume and density fluctuate locally about the normal values. Thus the important variations can be described as:

$$s = \frac{\delta\rho}{\rho_0} \text{ and } \Delta = \frac{\delta V}{V_0}, \tag{2.26}$$

where (*s* = condensation, ρ = instantaneous density and ρ_0 = original density) and (Δ = dilation, V = instantaneous volume, V_0 = original volume). For practical setups with small displacements s = $-\Delta$ to a very good approximation and this is the linear region (Povey, 1997). The bulk modulus of elasticity is, $B = -\delta p/\Delta = -\delta p/s$, where *p* is the instantaneous pressure drop, δp the stress and δV the corresponding strain. In short the bulk modulus B measured in (Pa) is the ratio of the stress to the strain, multiplied by the volume of the material under strain. The adiabatic compressibility κ, is then defined by: $\kappa = 1/B$. To summarise the discussion of sound propagation in homogenous fluid mediums, the Wood equation is given below:

$$v = \sqrt{\frac{B}{\rho}} = \sqrt{\frac{1}{\kappa\rho}}\,, \tag{2.27}$$

The Wood equation (Equation 2.27) shows that the velocity of sound is solely determined by the elasticity and density of the material through which the sound travels.

Propagation of ultrasound in water

Since water is a common fluid and exhibits unique acoustic properties with variation of temperature, it is necessary to discuss in brief these peculiarities within the context of this research work. At temperatures of approximately 74°C the temperature coefficient of the velocity of sound in pure water is positive. This is not the same for most other liquids. An equation to describe this temperature dependence with the addition of a pressure dependence term is given as:

$$\begin{aligned} v = {} & 1402.39 + 5.03711T + 0.0580852T^2 + 3.33420\times10^{-4}T^3 \\ & -1.47800\times10^{-6}T^4 + 3.14643\times10^{-9}T^5 + 1.6\times10^{-6}(p_0 - 10^5), \end{aligned} \tag{2.28}$$

where v is the velocity of sound m/s; T is temperature in °C; and p_0 is the absolute pressure in Pascals.

Equation (2.28) is accurate to within 0.015 m/s between 0.0001°C and 95.126°C and when p_0 = 10^5 Pa. The ready availability of water and the existence of proven accurate speed of sound data in water provide a convenient method for calibrating ultrasound apparatus for the velocity of sound measurement (Wood, 1941 and Povey, 1997).

The discussion of the velocity of sound in water, clearly shows that small fluctuations in temperature affect the velocity of sound. Therefore, if the velocity of sound used in the calculation of velocity vectors is inaccurate then the magnitude of the velocity profile is incorrect. Thus, it is important to ensure that temperature fluctuations are noted and proper instrumentation is attached to the measuring system to correct for temperature dependency of the important velocity of sound parameter in PUV measurements. The in-line measurement of the velocity of sound value is also recommended as a way to improve the overall accuracy of PUV systems.

2.3.2. Pulsed (Doppler) Ultrasound Velocimetry (PUV) operating principle

2.3.2.1. Introduction

In 1997 Povey indicated that the development of ultrasonic velocimetry had reached a stage of development that was comparable to that of nuclear magnetic resonance a decade before. The superiority of the technique over other flow visualisation methods stems from the fact that it can penetrate optically opaque materials, it is relatively cheap and provides detailed fluid properties in a rapid and non-invasive manner (Povey, 1997).

The technique originated from its use in the medical field around the 1950s (Satomura, 1957). One of the first people to explore with the technique outside the medical field was (Takeda, 1986; Takeda, 1999). A detailed review of these works on PUV is discussed Section 2.4.2.

To date the technique was exploited in a number of industrial applications because of its low-cost, reliability, accuracy and great potential to be incorporated in industrial process monitoring (Kotzé, et al., 2014a) and (Kotzé, et al., 2014b).

2.3.2.2. The Doppler effect

The Doppler Effect was first proposed in 1842 by Austrian physicist Christian Andreas Doppler who first noticed it in sound waves (Jensen, 1996). The phenomenon which is described by the Doppler effect is that a change in the observed frequency of a sound wave occurring when the source and observer are in motion relative to each other, with the frequency increasing when the source and observer approach each other and decreasing when they move apart. The motion of the source causes a real shift in frequency of the wave, while the motion of the observer produces only an apparent shift in frequency, this shift is also known as the Doppler shift (Jensen, 1996).

Similarly, this principle can be used for ultrasonic transducers which emit sound bursts of wavelength λ into a fluid medium which contains target particles. The emitted sound waves are echoed and received. If these scattering target particles also known as reflectors are in motion with a non-zero velocity component into the acoustic beam axis and the transducer (*source*) is stationary with respect to a particle, the Doppler shift takes place and the received signal becomes

'Doppler shifted' by a frequency f_d. Thus using the Doppler formula and having an emitted ultrasound wave of frequency $f_d = c/\lambda$ the received signal has a frequency f_r written as:

$$f_r = f_e \frac{c - V_{Tr}}{c + V_{Tr}} \tag{2.29}$$

The equation which then relates the velocities of the target particles in the medium of interest is then given by:

$$v = \frac{c f_d}{2 f_e \cos\theta}, \tag{2.30}$$

where θ is the Doppler angle and the Doppler shift frequency is $f_d = f_e - f_r$. Jensen (1996) highlights that the classical Doppler effect is only an artefect in PUV systems. This is due to the fact that the time-shift or delay is of particular interest and not the Doppler shift. Figure 2.13 then shows the significance of the Doppler angle and the velocity components.

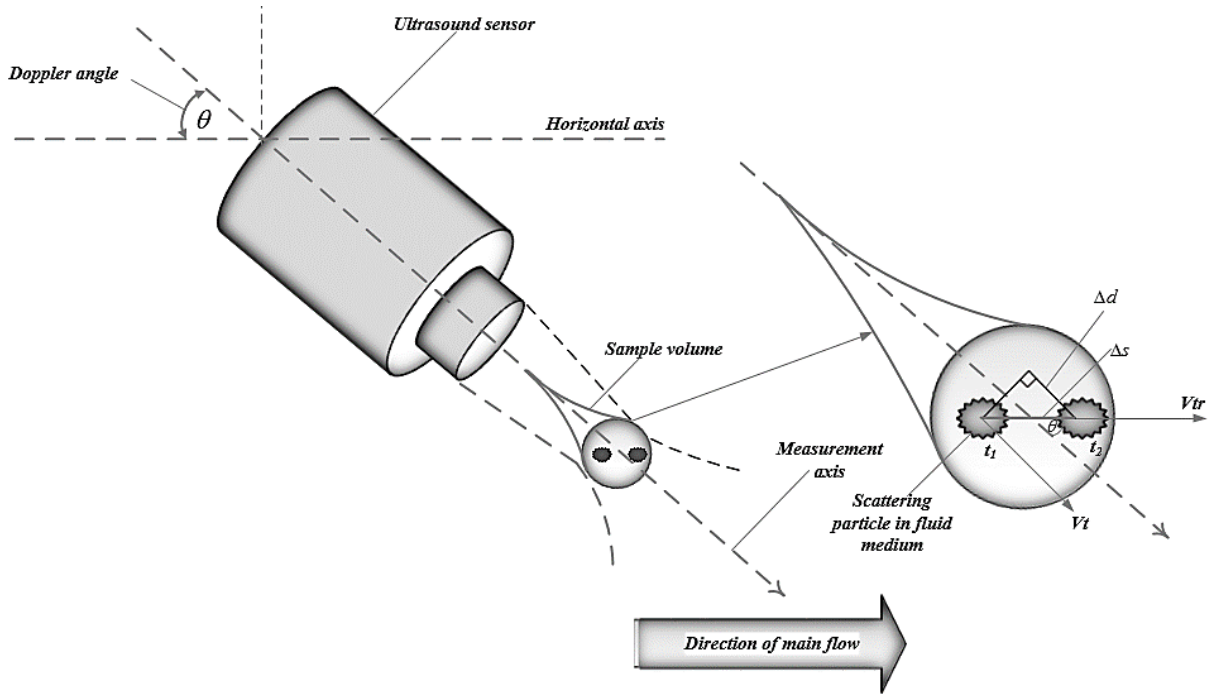

Figure 2.13: Moving target particle within a sample volume (gate) adapted from (Birkhofer, 2007)

As shown in Figure 2.13, the target particle has moved a distance Δs along the direction of flow and a distance Δd in the direction of the ultrasound beam within a time delay $\Delta t = t_2 - t_1$. With a value of the speed of sound in the fluid of interest the distance along the beam axis can be written as:

$$\Delta d = \frac{(t_2 - t_1)c}{2}, \tag{2.31}$$

where *c* is the speed of sound in the fluid. To calculate the component of a particle velocity in the direction of fluid flow Equation 2.33 is used to resolve the velocity component to the direction of the main flow by making use of the Doppler angle *θ*:

$$\Delta s = \frac{\Delta d}{\cos\theta} = \frac{(t_2 - t_1)c}{2\cos\theta}, \tag{2.32}$$

$$V_{Tr} = \frac{\Delta d}{T_{prf}} = \frac{(t_2 - t)c}{2T_{prf}\cos(\theta)} = \frac{V_t}{\cos(\theta)}, \tag{2.33}$$

V_{Tr} is the resulting velocity component in the direction of the main flow and V_t is the velocity component along the ultrasound beam axis.

2.3.2.3. Working principle of PUV systems

Figure 2.14 shows the main parameters contained within a PUV measurement. The transmitted ultrasound beam is divided into a number of segments known as gates or channels. Each of these gates returns an echo signal from a target signal at a certain depth along the ultrasonic beam axis. Hence, each gate is in fact a measuring volume by which the velocity of vector of a target particle is calculated.

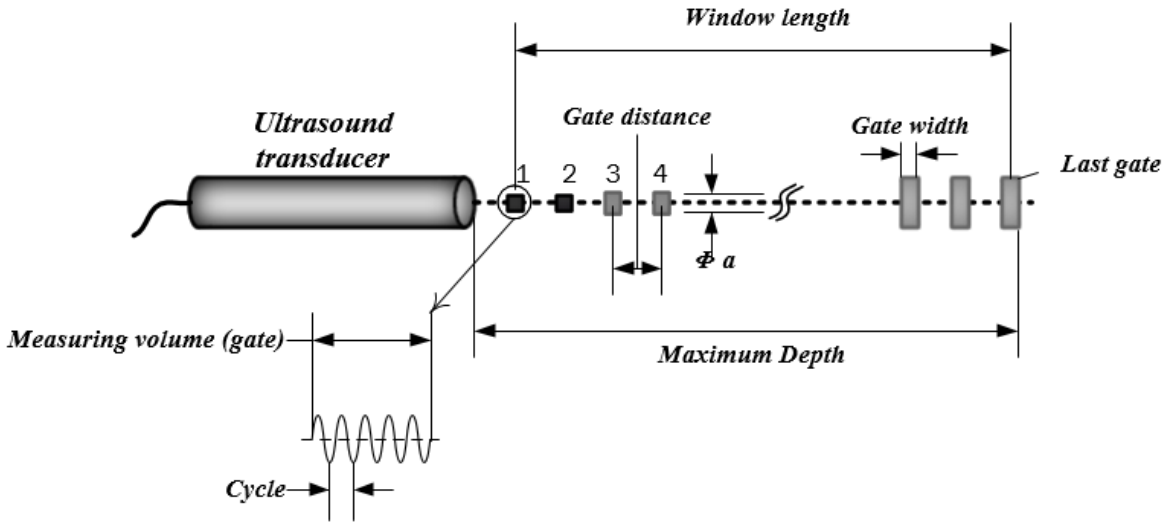

Figure 2.14: Schematic of an ultrasound beam showing beam divergence, divergence and gate distances (Kotzé, 2007)

The gate width in time units is determined by the number of cycles in the measuring volume. The gate width is then defined as ($n\lambda_0$), where n is the number of cycles per sample volume, a is the diameter of the diverging beam and λ_0 is the wavelength of ultrasound in the medium.

The accuracy of the measured profiles is dependent on a number of factors such as the instrumentation used within the measurement setup including the ultrasonic transducers and acoustic couplants. Regardless of the transducers used, certain adjustable parameters such as the gate width are of great importance in enhancing the radial accuracy and resolution of measured results. The smaller the gate distance, the higher the spatial resolution. Section 2.3.4 discusses some fundamentals of signal processing and velocity estimation techniques which are used in practice.

2.3.3. Ultrasonic transducers

Within a PUV measurement setup, the ultrasonic transducer plays an important role in acquiring and emitting ultrasound pulses into the fluid medium. It accomplishes this by sending ultrasonic energy into the fluid medium and then listens for echo data which contains the necessary time-shift information required for velocity estimation. Takeda (2012) describes the three main components of an ultrasound transducer as: the active element, the backing and the wear plate. The generated ultrasonic burst goes through each of these elements before travelling to the outer

environment. An impedance mismatch between any of these inner elements and also with the outer medium results in loss of beam energy.

A typical ultrasonic transducer is presented below in Figure 2.15:

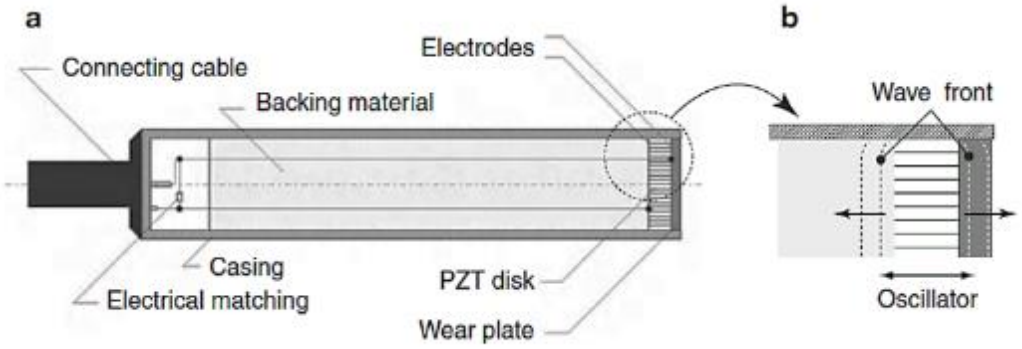

Figure 2.15: Typical single active element transducer (Takeda, 2012)

The active element is made up of a piezoelectric crystal which converts electrical energy to acoustic energy and vice versa. The thickness of the piezo crystal is designed to be half of the wavelength, making the resonant frequency equal to:

$$f_{res} = \frac{c}{2L_c}, \tag{2.34}$$

where L_c is the thickness of the crystal and c is the sound propagation speed in the material (Jensen, 1996). The backing or damping layer is specifically inserted to lower (dampen) the vibrations of the piezo crystal and prevent them from radiating back to the face of the crystal or active element. Heavy damping ensures a short, broad band pulse. In pulsed ultrasound systems, the time it takes to switch the transducer from receiving mode to transmission mode as well as the spatial resolution across the measuring axis are of great importance and thus impedance matched backing materials are required for enhanced dynamic characteristics (Jensen, 1996).

2.3.3.1. Characteristics of emitted ultrasonic beams

The emitted ultrasound beam can be better described in terms of the pressure variance starting from the face of the transducer radiating outwardly as shown in Figure 2.16 below:

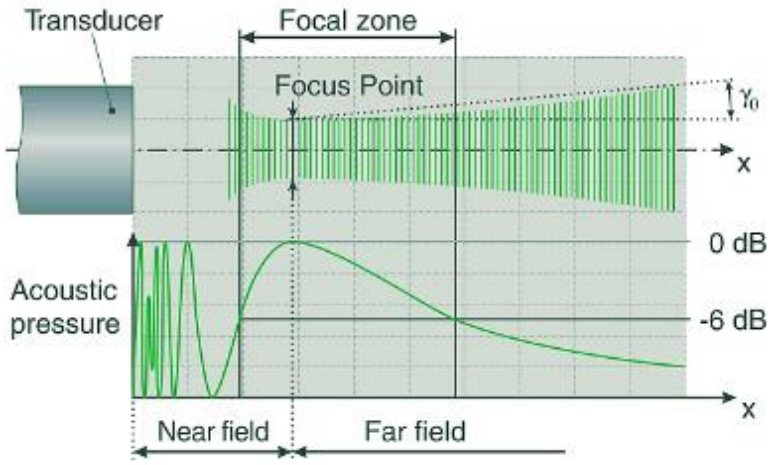

Figure 2.16: Variation of acoustic pressure from transducer front (Met-Flow SA, 2002)

The generated beam can be subdivided into the near-field and the far-field. The near field consists of a non-linear pressure variation which is undesirable for most practical measurement setups and is usually avoided by deep-setting the transducers within a depth equal to the near-field as described by Kuttruff (1991). This near-field distance is described as:

$$N = \frac{D^2 f_0}{4c}, \tag{2.35}$$

where N is the near-field distance, D is the diameter of the active element, f_0 is the ultrasound frequency and c is the sound velocity in the test medium. Most non-invasive sensor setups for pipe flow measurements eliminate the undesirable fluctuations of the near field zone by positioning it before the wall interface, so that the far-field zone is positioned at the fluid flow region.

2.3.3.2. Fundamentals of transducer characterisation and evaluation

Within practical PUV systems the ideal ultrasound transducer is one that focuses the total acoustic energy radiated from the transducer front (usually circular front) into a narrow band of high intensity throughout the measurement depth, especially within the far field region (Bechtold, 2006). Work by Kotzé et al. (2013) also shows the relevance of accurately determining the resultant beam properties e.g. the Doppler angle, from the emitted ultrasound beam as this greatly influences the calculation of correct velocity profiles.

Generally the beam divergence from a circular front transducer can be described by:

$$\gamma_0 = \sin^{-1}\left(\frac{0.51\lambda}{D}\right), \tag{2.36}$$

where γ_0 is the beam divergence half angle for a (-6dB drop).

Aside from the main beam or lobe emitted into the medium under study a number of side lobes can also be realised. The side lobes represent energy lost from the main beam, which is highly undesirable (David & Cheeke, 2002). If the side lobes are wide enough, they can interfere with information obtained from the main beam. Thus, the need for ultrasonic transducer characterisation becomes evident in-order to facilitate the design of advanced sensor technology, which mitigates side lobes and focuses the acoustic energy throughout the measurement depth.

Figure 2.17 highlights the typical shape of a measuring volume from an ultrasound sensor and the variation of intensity as it propagates through the fluid medium:

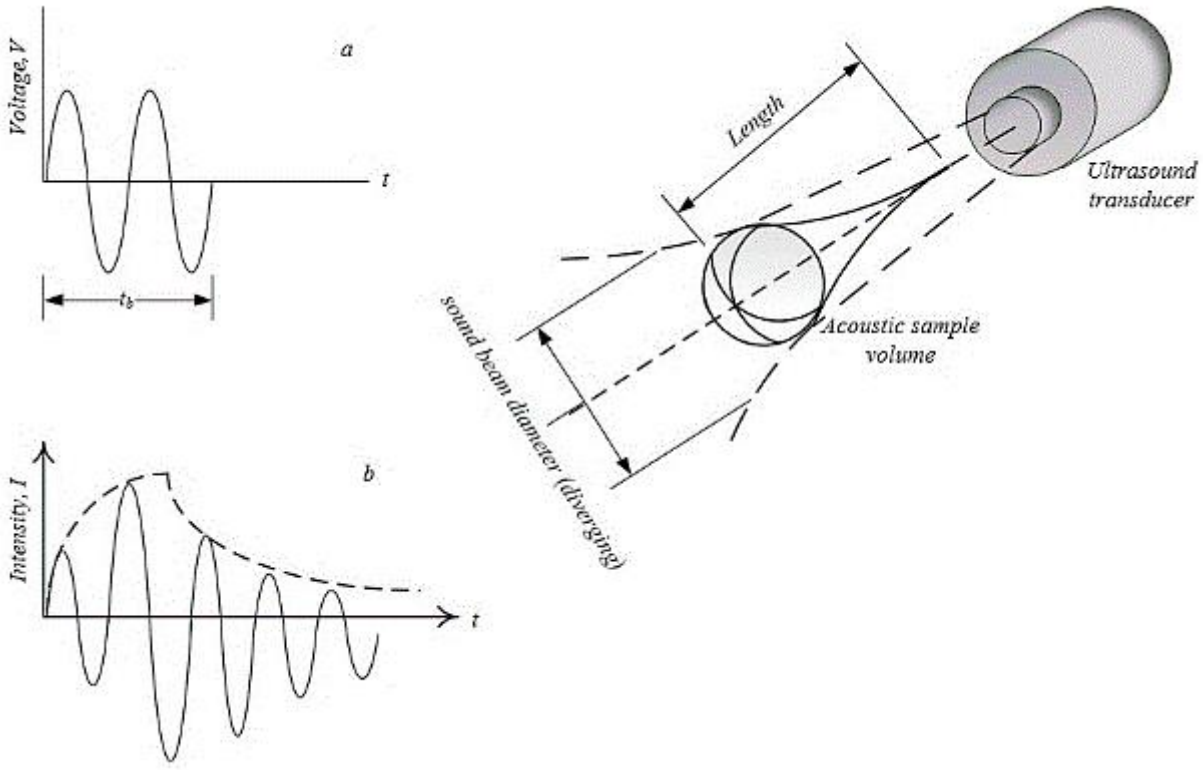

Figure 2.17: Transducer response and sample volume geometry adapted from (Jorgensen et.al, 1973)

Figure 2.17 illustrates that the sample volume actually has a drop shaped geometry as opposed to a cylindrical measuring volume. This shape is due to beam divergence with increase in

propagation distance. The intensity of the ultrasound beam initially increases in the near field and then decays exponentially.

- **Acoustic couplants and their effects on ultrasound beam properties**

As mentioned in Sections 2.3.1.2, the effect of impedance matching at material boundary layers is paramount as it determines the properties (e.g. focal zone geometry and angle of incidence) of the resultant ultrasound beams. Determining the resultant beam properties from ultrasound sensors especially for Doppler velocimetry measurements becomes even more important as small errors in parameters such as the Doppler angle translate to significant errors in the determined velocities. Work by Kotzé et al. (2013) in which different ultrasound transducers were acoustically characterised using an advanced needle hydrophone setup showed that, the location of the focal zone also affects the accuracy of the measured velocity profile in the near wall region. In addition the lateral dispersion of the ultrasound beam also needs to be measured as it is a critical determinant of the lateral resolution of a PUV system. By performing acoustic characterisation tests which show detailed information about the beam shape, informed design improvements can be implemented for the development of more accurate sensors with narrower and high intensity beams. A typical acoustic (intensity distribution) colour map from a transducer acoustic characterisation test, illustrating important beam properties such as the shape and location of the focal zone, is shown in Figure 2.18.

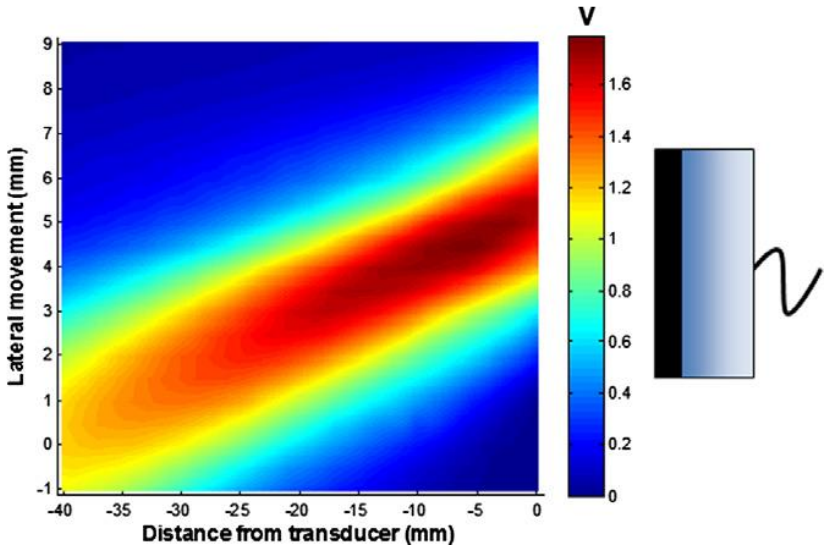

Figure 2.18: Acoustic map illustrating important beam properties such as focal zone geometry and intensity distribution (Kotzé et al., 2013)

Acoustic tests to determine ultrasound intensity distributions of highly focused ultrasound field (HIFU) transducers were also presented by Zhou et al. (2006). The researchers used a 3-dimensional positioning system to facilitate the accurate measurement of the acoustic intensity field at different spatial locations. Similar methods to those used by Kotzé et al. (2013) were also presented in Umchid (2014). The work by Umchid (2014) describes acoustic characterisation tests to measure the variation of acoustic pressure in the focal region of the beam produced by HIFU type transducers. The focal zone geometry was illustrated by using colour and contour plots similar to Figure 2.18.

Figure 2.19 illustrates how the incidence angle emitted from the transducer changes from an initial value α to the final angle θ which is then used as a parameter in PUV measurements.

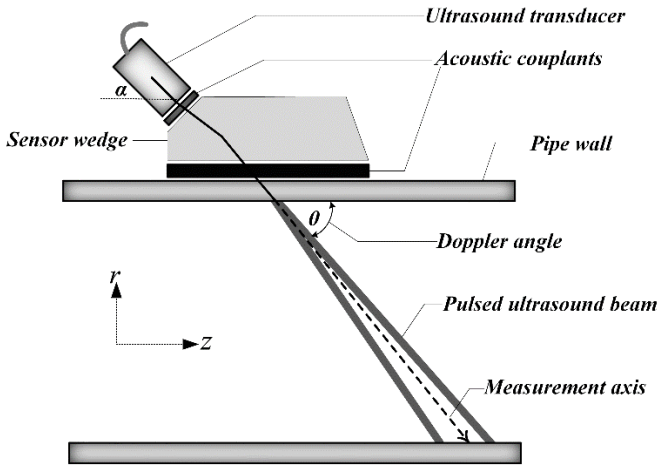

Figure 2.19: Non-invasive ultrasound sensor setup showing beam incidence angle at boundary layers

As seen from Figure 2.19, the actual measurement angle θ is influenced by materials of different acoustic impedances which lie between the transducer and the test fluid. The acoustic couplants used at the different interfaces should be chosen correctly, so as to maintain a known Doppler angle and desirable focal zone properties, which are consistent for the different sensor setups. For example, Szebeszczyk (1994) and Sanderson & Yeung (2002) describe the necessary guidelines for non-invasive sensor installations. Factors such as proper preparation and cleaning of the mounting surface greatly improve the measurements if procedures are adhered to.

Krautkramer & Krautkramer (1990) further point out that the effective function of acoustic couplants in facilitating optimum transmission of the ultrasound beam through boundary layers is highly influenced by the test conditions. Acoustic properties of couplants are greatly dependant

on temperature, and thus proper care has to be taken in considering a specific couplant for temperature extensive industrial applications, especially if a longer couplant replacement time is required. The effect of couplants on critical beam properties (e.g. Doppler angle, intensity distribution) for industrial stainless steel pipe coupling is further discussed in Chapter 3, as it formed part of this research work.

2.3.4. Fundamental Signal processing and velocity estimation techniques

Advanced signal processing plays a major role in the accurate determination of the measured velocity profiles. Currently the main techniques for velocity estimation are based on the Fast Fourier Transform (FFT) and the time domain equations. This is due to the fact that the velocities which are being extracted from the echo data are essentially frequency shifts, hence the analysis in the frequency domain. In addition, frequency domain techniques result in satisfactory results over a wide range of applications. However, time domain signal processing algorithms have been found to work well in a wide range of signal-to-noise ratios as compared to the standard FFT approach (Barber et al., 1985). There are basically two types of time domain algorithms for velocity estimation:

(i) phase-shift estimators that employ autocorrelation techniques of the baseband signal and
(ii) time shift estimators that use frequently cross-correlation of the RF signal to track movement of scatterer in the fluid medium

As for Fourier based signal processing, the basic technique involves the extraction of the Doppler shifts in the ultrasonic signal back-scattered from the fluid medium. In simple terms, the estimation of average flow velocities within a sample volume involves the determination of Doppler shifts in the received ultrasound signal. The Doppler shift may be determined by quadrature demodulation and spectral analysis. The block diagram in Figure 2.20 summarises the key steps in the demodulation of the acquired signal.

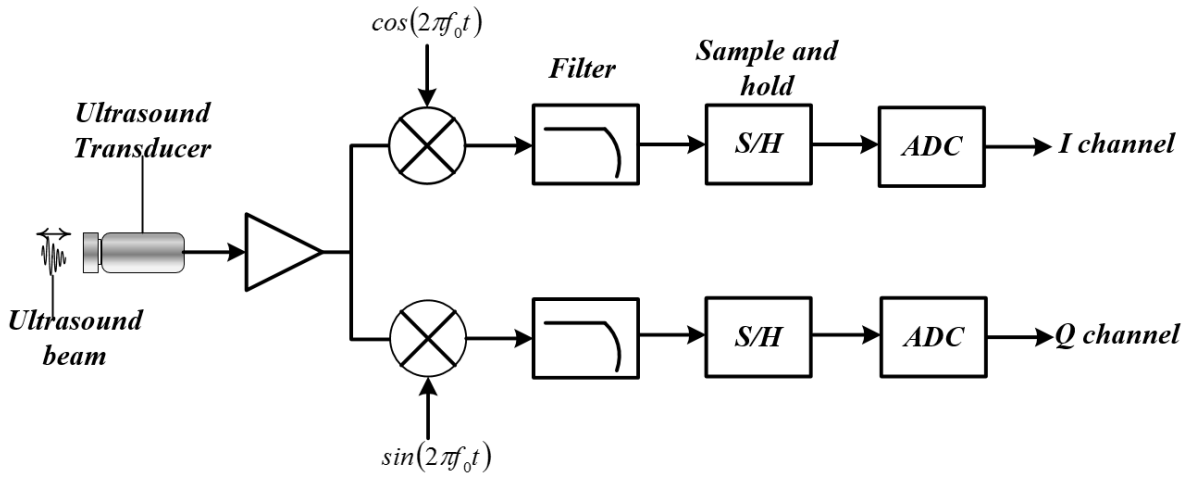

Figure 2.20: Conventional analogue demodulation (adapted from Jensen, 1996))

The block diagram presents the conventional method of processing the received echo data from the transducer in order to obtain the gate velocities required to reconstruct the velocity profile. Firstly, the received signal is multiplied by cosine and sine signals which are at the ultrasound transmission frequency. The noise signal is then removed from the in-phase and co-phase signals before digitising. After the digitisation process, several velocity estimation techniques are then applied to obtain the velocity profile.

According to work done by Barber et al. (1985), the velocity estimation can be understood by viewing the Doppler signal as:

$$f(t) = I(t) + iQ(t), \tag{2.37}$$

where $I(t)$ and $Q(t)$ are the in-phase and co-phase signal components, respectively. The Fourier transform of the Doppler Signal is calculated as follows:

$$\hat{f}(\omega) = \int_{-\infty}^{\infty} f(t) e^{-i\omega t} dt, \tag{2.38}$$

and the power spectrum $S(\omega)$ is given by:

$$S(\omega) = \hat{f}^*(\omega)\hat{f}(\omega). \tag{2.39}$$

The above frequency domain algorithm uses the Burg algorithm. The Burg algorithm used enables the estimation of the power spectrum in-phase and co-phase Demodulated Echo Amplitude (DMEA data). The Doppler frequency used for velocity estimation is the one which is viewed as a maximum power point within the spectrum (Kotzé, 2011). As for the time-domain algorithm, the velocity estimation is based on the measured $I(t)$ and $Q(t)$ data (Barber et al., 1985). Equation 2.40 below, represents this estimation:

$$f_d = \frac{1}{2\pi f_{PRF}} \tan^{-1}\left(\frac{\sum_{i=1}^{M} \left(Q_i * I_{i-1} - Q_{i-1} * I_i \right)}{\sum_{i=1}^{M} \left(I_i * I_{i-1} + Q_{i-1} * Q_i \right)} \right). \tag{2.40}$$

Detailed information regarding the above mentioned velocity estimation techniques and mathematical equations which describe them is given in Birkhofer (2007) and Jensen (1996). The diagrammatical representation of how the Doppler frequency shift f_d is calculated is shown in Figure 2.21. The Doppler frequency f_d is of great importance since it is one of the main parameters used to estimate the velocity vectors.

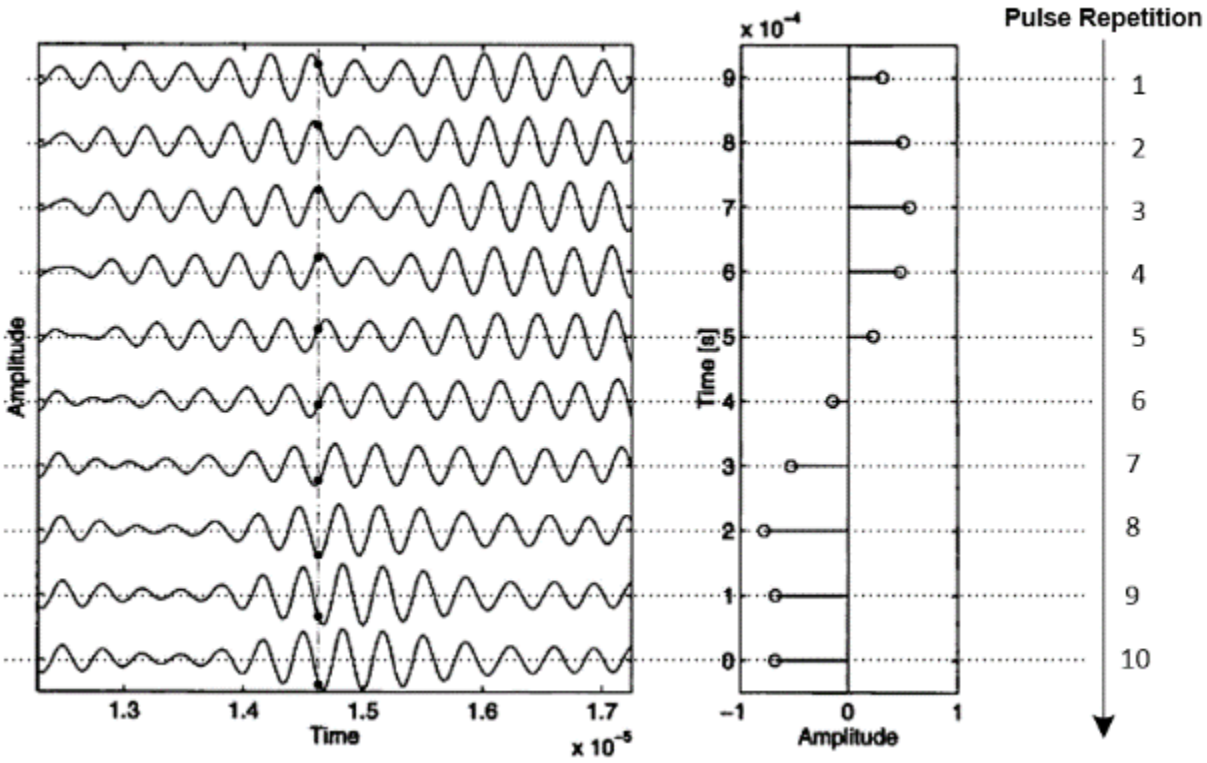

Figure 2.21: Detection of the Doppler shift frequency by sampling multiple acquired echo signals adapted from (Jensen, 1996)

Basically in pulsed ultrasound systems (as shown in Figure 2.21), several acquired pulses numbered from top to bottom (1 – 10), are sampled at the same point (which corresponds to the depth or a specific gate). The corresponding sample points are also shown in the Figure 2.21 with the dashed vertical line drawn through all of them. The amplitudes of the samples are then plotted on a separate graph against time. The frequency of this secondary waveform, which was plotted from the sampled values gives the required Doppler frequency. This frequency, obtained from the secondary waveform of sampled points is much lower compared to the emitting frequency (which is typically in the MHz range). The obtained Doppler frequency f_d at that instant, gives the velocity at that depth as $V = cf_d / 2f_0$.

It has to be mentioned that there are depth limitations and maximum velocity limitations with pulsed ultrasound. These limiting conditions are dependent on the pulse repetition frequency which can be related to the time for a pulse to be echoed back to the ultrasound sensor. The relationships which describe these constraints are given below:

The maximum velocity V_{max} is:

$$f_d = \frac{f_{prf}}{2} \Rightarrow V_{max} = \frac{cf_{prf}}{4f_0} \tag{2.41}$$

The maximum depth P_{max} is then given as:

$$P_{\max} = \frac{c}{2f_{prf}} \tag{2.42}$$

In combined form the measurement constraint is described as:

$$V_{\max} \cdot P_{\max} = \frac{c^2}{8f_0}. \tag{2.43}$$

Therefore by appropriately adjusting these measurement parameters, accurate flow velocities can be extracted from the fluid medium. Undesirable artefacts such as velocity aliasing can be eliminated or used to an advantage when the measurement constraints are well defined for the specific test (Takeda, 2012).

2.3.5. Summary of ultrasound physics and PUV

Pulsed Ultrasound Velocimetry (PUV) was discussed in detail from its basic theory up to its operating principles. Ultrasound waves were described in terms of transverse and longitudinal wave motion. Attenuation of ultrasound which is related to the fluid's (propagation medium's) properties was also discussed since it affects PUV measurements. The pulse repetition frequency was noted as a major parameter which determines the measuring constraints (*maximum flow depth and the maximum flow velocity*) of the technique. Other important factors which influence the quality of PUV measurements, such as ultrasound transducer characteristics and beam divergence were also discussed, highlighting aspects such as the near-field and far-field characteristics of the emitted beam. The ideal beam which is required for accurate measurements has to be as narrow as possible throughout the whole measurement length (pipe diameter). This requirement is still a major limiting factor on the quality of velocity profile results, especially when complex geometries are considered. The selection of appropriate acoustic couplants for a specific application was noted and it was shown that different acoustic couplants should be considered based on the measurement conditions. The resulting Doppler angle is highly dependent on the

choice of couplant used. Thus, the accuracy of measured PUV data, can be greatly improved by performing acoustic characterisation of transducers and sensor mounting setups. From these ultrasound characterisation tests, input parameters for PUV measurements such as the Doppler angle, location of focal zone and beam intensity can be known and used appropriately for optimum test results.

2.4. THE PUV+PD METHOD FOR RHEOLOGICAL CHARACTERISATION OF FLUIDS

The PUV+PD in-line rheometric method was developed in Erlangen, Germany by Steger, (1994). Since then the technique has been improved by a number of research groups until the recent development of the latest rheometric system, Flow-Viz™ (Wiklund, et al., 2014). Information regarding research work that has been done on the PUV+PD methodology is presented in Section 2.4.2. A typical PUV+PD setup is shown in Figure 2.22.

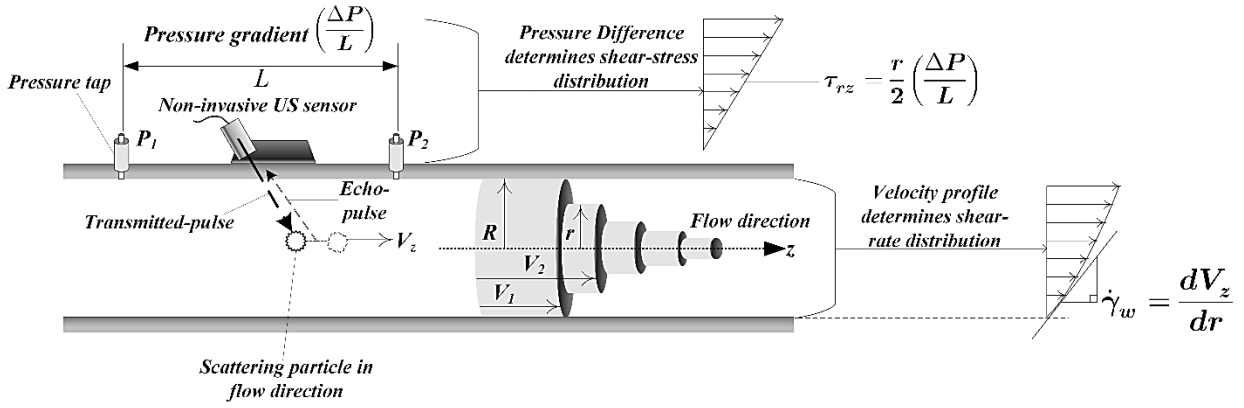

Figure 2.22: Typical PUV+PD methodology

Basically the PUV+PD system combines pulsed ultrasound Doppler velocimetry with a pressure difference technique in-order to determine the rheological parameters of the fluid under test. The influence of the shear rate-dependent viscosity on the shape of the laminar pipe flow velocity profile is exploited in order to obtain the shear rate distribution from the measured velocity profile. Flow calculations which combine rheological models are used to determine the viscous properties of the fluid using a curve fitting approach. Several methods have been used for estimating the proper rheological model to 'curve-fit' the flow data. Wiklund et al. (2006) explains the use of the integrated form of the Power-law model which is used in curve fitting calculations to get the

rheological parameters (*n* = flow behaviour index *(Power-law)* and *K* = fluid consistency coefficient *(Power-law)*).

Besides the curve fitting procedure for obtaining the rheological parameters, the direct gradient method may also be used (Wiklund & Stading, 2008). The shear-stress distribution is derived from the differential pressure measurement, whilst the gradient of velocity profile is used for shear-rate calculations. The velocity profile is differentiated, that is the rate of change in velocity against spatial position along the pipe radius. This is illustrated in Figure 2.22. This approach is superior to curve fitting in that it requires no prerequisite knowledge of the flow behaviour of the fluids under test.

2.4.1. Post-processing of PUV+PD data

With the PUV+PD system (Flow-Viz^{TM}) which was used for this work, all acquisition data is conveniently saved in a SQL database file. The file contains pressure drop, rheometry and velocity profile IQ-data which can be extracted and post-processed

The rheology of the fluid (i.e., *K, n* and τ_y) is often calculated based on a curve fitting approach or a direct gradient method (differentiating the profile across the pipe radius to obtain point shear-rates, also referred to as non-model approach). Velocity profiles are usually integrated across the pipe radius to determine the volumetric flow rate (Furuichi, 2013). Figure 2.23 illustrates the parameters used in the integration method.

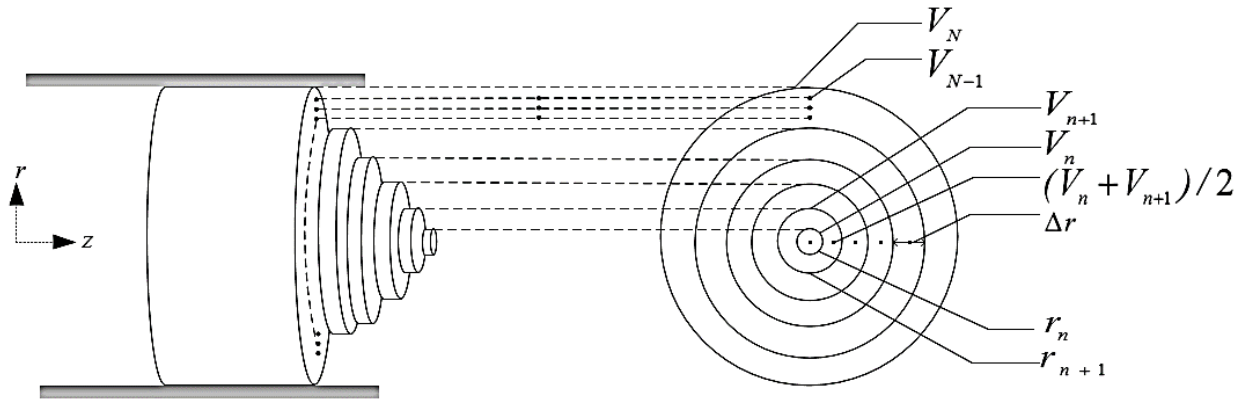

Figure 2.23: Model used for volumetric flow calculations from velocity profile adapted from (Furuichi, 2013)

The formula used to calculate the flow rate is given as Equation 2.44.

$$Q = \frac{\pi}{2}\sum_{n=1}^{N}(r_{n+1}^2 - r_n^2)(V_{n+1} + V_n) \tag{2.44}$$

where *N* are the number of gates across the pipe radius. The increments in the radial point are based on the set channel distance Δr. Thus, at each radial point a velocity vector V_n is defined. The actual velocity value used for each concentric area is the average value of two successive points V_n and V_{n+1}. Typical velocity profiles in wastewater sludge are shown before and after processing (Figure 2.24).

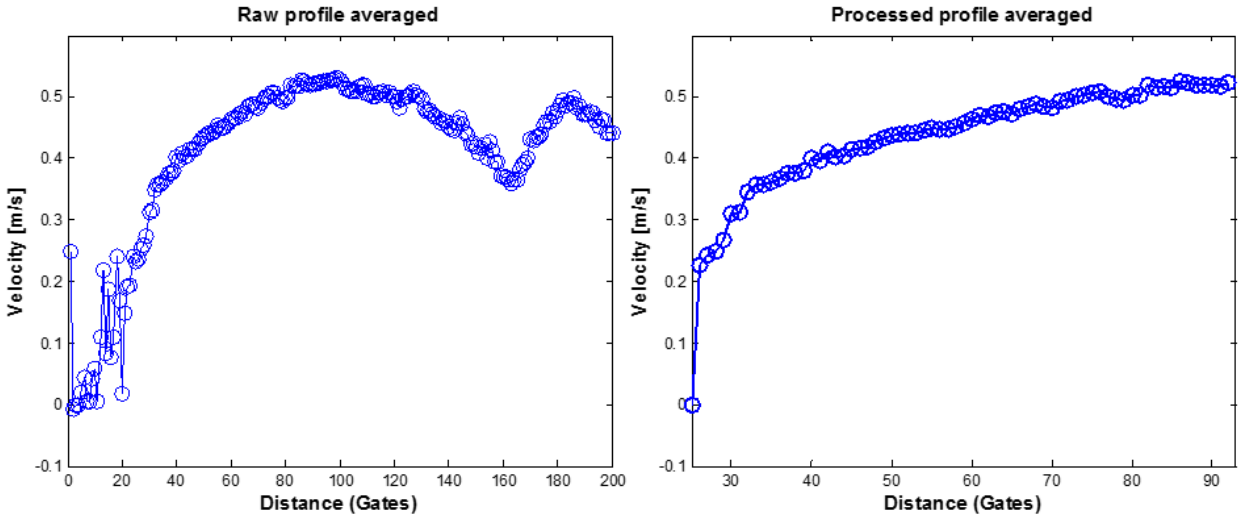

Figure 2.24: Typical velocity profiles as shown from post-processing (left) raw profile (right) processed profile

The raw profile shows distortion in the near wall region due to the sample volume overlapping the pipe wall interface. Algorithms within the PUV+PD system software correct for this by estimating the wall position. After removal of such artefacts by wall estimation, the processed velocity profile shown in Figure 2.24 (right) is obtained, and is then used for flow rate and rheometric calculations. Work still needs to be done in order to improve the existing wall detection techniques. Wiklund et al. (2007) mentions that a change in wall position by a few gates result in completely different rheological parameters in a given test fluid and thus wall detection accuracy is paramount if constitutive model based fitting is used for in-line rheological characterisation.

2.4.2. A review of PUV+PD

This section gives a brief history of the development and optimisation of the PUV+PD rheometric technique. The current problems which still persist in the use of the PUV+PD method are also presented.

2.4.2.1. Origins of the PUV technique

The earliest use of ultrasonic techniques for fluid measurement dates back to the 1960s, where it was originally developed for cardiovascular measurements in the human body by Japanese researchers in medical engineering (Satomura, 1957). Further advancements of the technique were done by (Takeda, 1986) whilst developing a PUV instrument for measuring the flow of opaque liquid metal. More information can be found in Takeda (1999); Takeda (1986). Takeda (1986) discusses the application of the PUV technique of Doppler shift methods for ultrasonic velocity profiling in water with suspended Al_2O_3 powder. This work was a stepping stone to the currently used PUV methods for flow measurements in general fluids.

2.4.2.2. Development of the PUV+PD rheometric method

Steger (1994) then combined the PUV technique with a pressure difference measurement, thus forming the basis of the PUV+PD rheometric methodology. Since then, the PUV+PD method has been continually under development in a number of research institutes. Ouriev & Windhab (2003); Windhab & Ouriev (2002); Ouriev & Windhab (1999) presented an improved in-line, rheological measuring technique which was developed and tested in opaque fluids and concentrated suspensions. The PUV equipment used was based on the PUV profiler by Met-Flow SA (UVP-monitor). These early works demonstrated how PUV+PD could be a powerful tool for in-line rheological characterisation of industrial suspensions.

Wiklund et al. (2001), presented work on in-line rheometry based on the PUV+PD method. The PUV equipment was based on a similar Met Flow SA (UVP-DUO monitor) as presented by Ouriev & Windhab (1999). The paper focused on the basic principles of PUV+PD, which include the integration of velocity profiles with the pressure difference measurements to determine the flow-curve. Standard flow-curve models such as the Herschel-Bulkley and Power-law models were then used in non-linear regression calculations to approximate the correct rheological parameters

(such as the Power-law exponent *n*) of the fluid under test. Conventional rotational rheometers, Bohlin CS-50, ARES and Physica MCR-300 were used for validating the results. On comparison, the in-line results obtained using the PUV+PD technique closely matched those from conventional rotational rheometers. Similar works were done by Wiklund et al. (2002) and Wiklund et al. (2006) in which they further tested the capabilities and limitations of the in-line PUV+PD technique in the rheological characterisation of industrial suspensions. The former showed that the rheological behaviour of cellulose fibre suspensions could not be measured using the off-line rheometers due to compression and drainage of the sample, thus showing the importance of PUV+PD as the only alternative method to characterise such complex suspensions.

In a laboratory setup to study the shear crystallisation process of cocoa butter, Birkhofer et al. (2004) also made use of the Met Flow SA UVP-DUO monitor. The PUV+PD methodology was used to rheologically characterise the cocoa butter suspensions. Whilst working on a related study, Birkhofer et al. (2008) highlighted the linear dependence of the decrease in velocity of sound to the formation of crystalline fat in the cocoa butter process. This work proved that it was possible to characterise the shear crystallisation of cocoa butter in line, using the PUV+PD method. These studies together with Wiklund et al. (2007) also resulted in the development of improved application software which integrates the velocity profile data and sensor data (temperature and pressure) into one interface thus offering convenience and easier automatic monitoring of processes. The developed software made use of the ActiveX library provided by Met-Flow SA to communicate with the UVP-DUO monitor. The aim was to directly obtain the Demodulated Echo Amplitude (DMEA) data from the UVP-DUO to enhance signal processing using alternative algorithms. The developed software application was then exploited in successive works which used the commercial Met Flow SA monitor.

Wiklund & Stading (2008) provides essential information, regarding the use of PUV combined with pressure difference (PUV+PD) method within the constraints of different industrial suspensions and industrial conditions. They addressed issues related to pulsed ultrasound velocimetry and rheological characterisation using the Met-Flow SA, UVP-DUO equipment within a miniaturized flow loop in a laboratory setup. The flow loop consisted of conventional flow-meters to validate measured results from the PUV+PD method. They also tested a variety of industrial suspensions and were able to characterise most of the fluids. The research work describes the PUV+PD method as an invaluable tool for process monitoring, since rapid changes in rheology during processing could be monitored in real-time, in line. In addition, results presented from in-line measurements of strawberry yoghurt, vegetable sauce, cellulose pulp and seafood chowder

further show that PUV (and the PUV+PD method) can be applied to industrial suspensions containing both soft and hard particles. In conclusion, Wiklund & Stading (2008) pointed out that, improved transducers, flow adapter cell design and more sophisticated signal processing should improve velocity profile measurements also in suspensions with much higher concentration of particles.

In relation to Wiklund & Stading (2008), Kotzé, et al. (2008) evaluated the in-line PUV+PD rheometric method against in-line tube viscometry and off-line rotary viscometry for model mining suspensions. They used the same UVP monitor (METFLOW SA, UVP-DUO) as Wiklund & Stading (2008). A custom tube viscometer rig which consisted of three poly vinyl chloride (PVC) pipes and one stainless steel pipe was used. An in-line mass-flow meter was installed on the rig and two different pressure transducers with different measuring ranges were attached to each pipe. The flow adaptor housing the ultrasonic transducers for the UVP measurements was installed on the stainless steel pipe. Bentonite and Kaolin were used as the test fluids. The off-line and in-line tests were in close agreement (within 15%). This showed the potential for development of new in-line rheometers for process control within the mining and minerals industry. Despite the extensive and evaluative work a commercial PUV+PD system was not realised at this point due to outstanding issues such as the need for improved velocity gradient measurements close to pipe wall interfaces as well as characterised ultrasonic sensor technology for improved measurement accuracy across the pipe diameter.

The previously discussed work based on the PUV+PD methodology, made use of ultrasonic sensors installed in flow adaptors which included cavities to cater for the elimination of the near field distance during velocity profile measurements. The flow adaptor design sufficed for a time but it was evident that the cavities got clogged with the process fluid which compromised the accuracy of the results. To address this problem, Kotzé, et al. (2012 & 2013) presented improvements and optimisations in the PUV+PD rheometric technique by introducing a new ultrasonic transducer based on a delay line material. The improved transducer was compared to standard commercially available ones and significant reductions in previous problems were noted. With the addition of improved signal processing techniques, the work further advanced the PUV+PD technique towards the main goal of realising a compact and robust in-line rheometric system for use in industrial applications. Acoustic characterisation of ultrasonic transducers was also carried out. This was done in-order done to gain better understanding of the beam propagation and to use the information to design more advanced non-invasive sensors. Despite the different approaches taken to improve the measurements, the main conclusion was that non-

invasive sensor technology would greatly reduce near wall errors and improve overall accuracy. The reason for this was that the delay line transducers were still in contact with the test fluids, which does not comply with strict hygienic requirements. The setup also presents a safety hazard when high pressures or temperatures are present during measurements. Complete non-invasive sensor technology that is capable of measuring through pipe wall materials was shown to be a great necessity for industrial use of the technique.

2.4.2.3. Development and optimisation of the Flow-Viz™ PUV+PD system

Recently a non-invasive PUV+PD industrial rheometric system, Flow-Viz™ was developed, however its capabilities and limitations have not yet been fully evaluated over a wide range of industrial fluids. The latest publications and work on the Flow-Viz™ system are presented by Kotzé, et al. (2014) and Wiklund, et al. (2014). These works form part of the ongoing collaborative research between SP and CPUT. The most recent work, resulted in a system which contained more capable pulser/receiver electronics to allow for a greater spatial resolution across the pipe diameter. The pulser/receiver electronics described in Kotzé et al. (2015b) and Wiklund et al. (2014) had faster microprocessors based on FPGA technology and were thus able to provide real-time FFT processing for improved in-line performance and velocity profile measurement.

Flow-Viz™ is still being optimised through research work which includes, accurate estimation of wall interfaces and velocity of sound measurements for successful process monitoring. Since Flow-Viz™ provides unique non-invasive Doppler velocimetry measurements through industrial grade stainless steel pipes, the drive to advance the sensor technology is by performing detailed acoustic transducer characterisation tests. Previous transducer characterisation tests by Kotzé et al. (2013) showed that, determining the focal zone shape and location as well as the correct Doppler angle is highly important as these properties have an effect on the measured velocity profile especially in the near wall region. Changes in the shape of the beam were noted along the beam axis, after the beam had propagated through the delay line material boundary (described in Section 2.3.1.2). The result of this work was the introduction of the delay line sensors which where a marked improvement from the commercially available sensors.

Similar characterisation tests in which a 3-dimensional scanner was used to navigate a hydrophone in the measurement of the acoustic intensity distribution of beams produced by high intensity focused ultrasound (HIFU) transducers were presented in Zhou et al. (2006) and Umchid

(2014). Umchid (2014) describes measurements which utilised a planar scanning technique inorder to adequately cover the focal plane of the acoustic beam along the acoustic axis.

The importance of acoustically characterising the new Flow-Viz^{TM} non-invasive sensors to determine the beam properties was taken into account and set as a major objective of this research work. The acoustic characterisation tests based on planar type measurements (described in Umchid (2014) and Kotzé et al. (2013)) were carried out at SP, Gothenburg. Several acoustic couplants were also tested and their effects on the resultant beam after propagating through stainless steel were noted. Appropriate couplants for industrial installations were also suggested based on the guidelines presented by Sanderson & Yeung (2002).

2.4.2.4. PUV+PD industrial applications

PUV+PD based in-line rheometers such as can be used in a wide range of industrial applications especially for quality control purposes. For example, Kotzé et al. (2011) presented work in which the flow behaviour of mineral suspensions was characterised. The research showed that water usage could be reduced whilst maintaining continuous flow in mineral slurries by constantly monitoring the flow using PUV+PD. This study the potential for using PUV+PD in mining applications.

A recent publication (Kotzé, et al., 2014a) of the work carried out at Zeekoeivlei wastewater treatment plant in Cape Town, also showed how PUV+PD could be used for monitoring the rheological properties of sludge in line. The on-going work is aimed at establishing a relationship between rheological parameters and polymer concentration. If this link is established, the polymer concentration can be optimised through in-line monitoring resulting in water and polymer savings. With the PUV+PD system which was used by Kotzé on a 3 wt% sludge it was shown that the rheological characteristics of the sludge could be monitored in real time. With such a setup, effective flocculation can be achieved by implementing a feedback loop which uses industrial standard signals from the PUV+PD system connected to a Programmable Logic Controller (PLC) and corresponding actuators.

Furthermore the PUV+PD technique is a desirable in-line rheometric unit in many quality control applications in the food-processing and chemical industries. A number of research articles in which the PUV+PD based systems were successfully applied to the characterisation of food products have already been published (Birkhofer et al., 2008; Wiklund et al., 2001; Wiklund et al., 2012). The non-invasive installation of PUV+PD based units such as Flow-Viz^{TM} meets the sanitary requirements of this type of industry where ease of installation and removal are also considered for cleaning purposes (Roberts, 2001).

2.5. SUMMARY OF LITERATURE REVIEW

The literature review presented past and present works on the PUV+PD methodology. The earliest works on PUV were by Satomura in the 1950s using a continuous wave system for medical diagnostics. The PUV technique was then used by Takeda (1986) during experiments with liquid metal. This was a major development as it opened up new avenues for the use of PUV besides its use in the medical field. The PUV+PD rheometric technique which combined PUV with pressure measurement, was then developed by Steger (1994) and since then it has been continuously optimised by a number of research groups for in-line rheological characterisation.

Several difficulties were faced whilst using the older PUV+PD systems. The earlier systems made use of flow adapter cells with cavities and these introduced errors related to inaccurate wall estimation and overlapping sample volumes. To address this Kotzé, et al. (2012 & 2013) presented work which dealt with acoustic characterisation of new delay line transducers and improved signal processing techniques. Recently the Flow-Viz™ system presented in Wiklund et al. (2014) and Kotzé et al. (2015b), which is a new non-invasive rheometric tool based on the PUV+PD method was developed as an in-line rheometric tool for industrial applications. The new rheometric system has not yet been fully tested in a wide range of applications to determine its reliability and effectiveness. To further advance the unique technology for industrial in-line rheometry, the non-invasive sensor technology needs to be acoustically characterised to determine important beam properties through stain less steel pipes. By understanding the ultrasound beam shape and accurately determining the Doppler angle parameter in newer sensors the overall PUV measurement accuracy is improved. Furthermore, the effect of different acoustic couplants for industrial installations is also a factor noteworthy of in depth study, since these couplants alter the shape of the propagated beam. The current work presented in this thesis adds on to the ongoing development of the Flow-Viz™ system by including acoustic characterisation of the non-invasive ultrasound sensors, since it is essential for the development of advanced ultrasound sensor technology.

CHAPTER THREE: METHODOLOGY AND APPARATUS

This chapter describes the apparatus, test materials and experimental methods that were used in order to accomplish the objectives of this research work.

Acoustic characterisation tests were carried out at SP-Technical Research Institute of Sweden, Gothenburg. Test facilities available included high precision needle hydrophones and an advanced XYZ-scanner setup which were used for these particular tests. The main objective of these tests was to determine the beam properties of different ultrasound transducers developed by Flow-Viz™. Additionally several acoustic sensor setups with different coupling media were also evaluated.

To assess the performance of the in-line rheometric Flow-Viz™ system, a portable stainless steel flow loop was used to conduct fluid characterisation tests. The flow loop was fitted with instrumentation (electromagnetic flow meters, thermocouples and differential pressures sensors) for acquiring the process variables needed for the in-line viscometric measurements. The flow-meters also served as a verification tool to the Flow-Viz™ system volumetric flow measurement. CMC, bentonite and kaolin at different concentrations were used for the tests in order to fully test the Flow-Viz™ system over a wide range of viscosities and fluid properties.

3.1. APPARATUS

3.1.1. Flow-Viz™ system

The Flow-Viz™ system (http://flow-viz.com/index.html) is an in-line rheometric unit which operates based on the PUV+PD principle, delivering real-time rheological characterisation and continuous feedback for process and quality control purposes. The system can be subdivided into three integral parts which are namely:

I. ***Flow-Viz™ operator's panel*** – which contains the industrial PC, on-board electronics for signal conditioning, pulser/receiver electronics and a multi-touch panel display for data input and visualisation.
II. ***Advanced graphical user interface (GUI)*** – Flow-Viz™ system software which controls user input and output and communication between on-board electronics and industrial PC.
III. ***Sensor unit and DAQ*** – ultrasound sensors for velocity profile measurements together with pressure transmitter for differential pressure measurements. Connections for other sensors such as the (PT100) temperature sensor are also included.

Figure 3.1 gives a system overview of the above described components.

(a) **(b)**

(c)

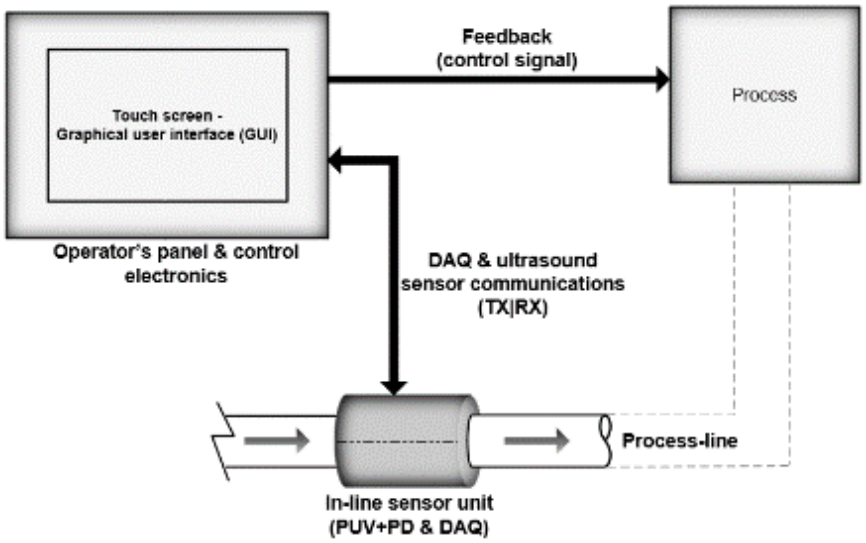

Figure 3.1: Flow-Viz™ system (a) Flow-Viz™ operator's panel (b) integrated in-line sensor unit and (c) schematic block diagram

3.1.1.1. Flow-Viz™ operator's panel and advanced GUI software

The V3 electronics platform is at the heart of the Flow-Viz™ system. It consists of the world's only fully digital and integrated electronics for combined ultrasound velocity profiling with pressure difference measurements plus additional data acquisition (DAQ) and signal output modules. All

electronics boards and modules are housed in the Flow-Viz^{TM} operator's panel which is shown in Figure 3.1(a).

The first set of electronic modules is made up of an industrial PC which is connected to a multi-touch screen. Signal conditioning and data transfer modules are connected to the industrial PC via an internal Peripheral Component Interconnect (PCI) connection. The industrial computer performs computational algorithms to determine the rheology of the fluid under test. The other set of electronics is made up of a central Field Programmable Gate Array (FPGA) for most of the ultrasound calculations for sound speed and velocity vector calculations. The V3 platform and the industrial PC are then integrated via Ethernet communications for inter-module data transfer.

- **Industrial PC unit with 19" multi-touch operator's panel**

The primary role of the industrial PC is to run the Flow-Viz™ Graphical User interface (GUI) application software and to communicate with the on-board V3 electronics (motherboard). The software also enables the display of real time data (instantaneous values of the process variables). The output and input of user information is done through a 19" multi-touch panel. The GUI software allows friendly user interaction with the optimised multi-touch gesture screen to set different measurement parameters associated with the PUV, temperature and pressure measurements. The technical specifications of the industrial PC unit in this work are: A >2.5 GHz Intel® Core™ i7 quad-core CPU with CFast and SSD memory cards, up to 8GB RAM, USB 3.0 ports and 2 independent Gbit Ethernet interfaces for remote control (Wiklund et al., 2014; Kotzé et al., 2015b). All datasets are saved into a SQL database and can be exported to Excel and PDF file formats if necessary.

- **V3 Embedded electronics platform (including the baseboard, communications and data-acquisition board)**

The main function of this set of electronics is to acquire signals from the flow loop sensors (ultrasound, pressure and temperature) and to send data to the host industrial PC. An integrated motherboard contains the pulser/receiver and communication electronics. The three main parts of the motherboard are described as follows:

Baseboard – The baseboard provides filtering and stabilization of the power. It contains 8 analogue and digital input and output channels as well as 4–20 mA, 0–10 V, +/-5 V; 16bit, 4 PT100 circuits and serial ports.

The pulser/receiver electronics – The pulser/receiver electronics described in Kotze et al. (2015b) transmit pre-programmed bursts using an Arbitrary Waveform Generator (AWG) with up to 80 $V_{pk\text{-}pk}$ voltage amplitude. The weak received echoes are then processed by the Low Noise Amplifier (LNA) and a Programmable Gain Amplifier (PGA) that applies a gain between 7 and 55 dB with a 0.7–7 MHz bandwidth. The received echo data from different radial positions is sampled at 100 MSample/s with 16 bit resolution, and is then sent to the FPGA for demodulation and storage in the Synchronous Dynamic Random Access Memory (SDRAM). Repeated samples stored on the SDRAM for each radial positions/depths are read back in the FPGA, where a block floating point Fast Fourier Transform (FFT) performs spectral analysis. All the necessary acquisition and processing parameters such as the Pulse Repetition Frequency (PRF) and ultrasound transmission are conveniently programmed on the FPGA module by the host PC.

Communication board – A National Instruments (NI) sbRIO-9606 was used as the communications module. The sbRIO board has a 400 MHz processor, a Field Programmable Gate Array (FPGA) for custom timing, in-line processing, and control; 96 Digital Input-Output (DIO) lines and provides Ethernet, RS232, Controller Area Network (CAN) and Universal Serial Bus (USB) connectivity. The inputs and outputs on the base board are controlled from the FPGA on the sbRIO. Additional multichannel sensors for temperature and pressure acquisition are easily interfaced and utilise the communications module to continuously update the industrial PC unit (Wiklund et al., 2014; Kotze et al., 2015b). A block diagram of the electronics architecture is presented in Figure 3.2.

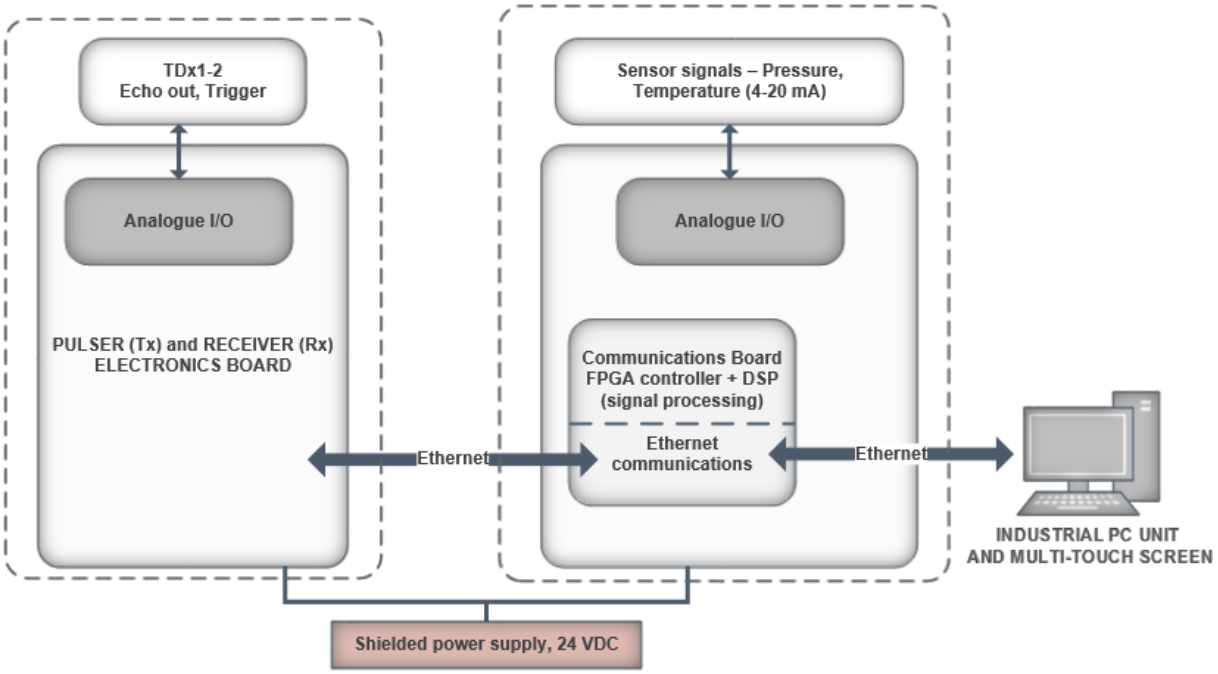

Figure 3.2: Flow-Viz™ electronics architecture

The main technical specifications related to the main-board electronics are summarised in Table 3.1.

Table 3.1: Main technical specifications for communications and data acquisition board

Attribute	Specification
Ultrasound (TX-RX)	Two channel (transducer)
Transmitter (TX)	16 bit programmable waveform, AWG
	100 MHz – 16 bit ADC
Receiver	200 kHz– 10 MHz bandwidth
	16 bit ADC
Processing	Programmable demodulation, filtering, down-sampling, ROI position and extension
Communications (PC ↔ FPGA)	Ethernet

3.1.1.2. Non-invasive ultrasound sensor unit

Specially manufactured ultrasound transducers were used for in-line tests. The ultrasound unit allows measurements through industrial stainless steel pipes with diameters ranging from as small as 10 mm internal diameter (ID) to 165 mm ID (Wiklund et al., 2014). The transducers are contained in a plastic wedge with adjustable screws, aligned at a Doppler angle of approximately 70°. This angle is optimal for the transmission of the acoustic energy through the housing wedge and stainless steel pipe wall. Acoustic liquid couplant is applied between the sensor unit's inner surface and the outer pipe wall to improve the impedance matching and hence the proper transmission of the ultrasound wave into the fluid medium. Bayonet Neill–Concelman (BNC) connectors are used to connect the sensor unit to the pulser/receiver electronics. The whole ultrasound sensor unit is shown in Figure 3.3.

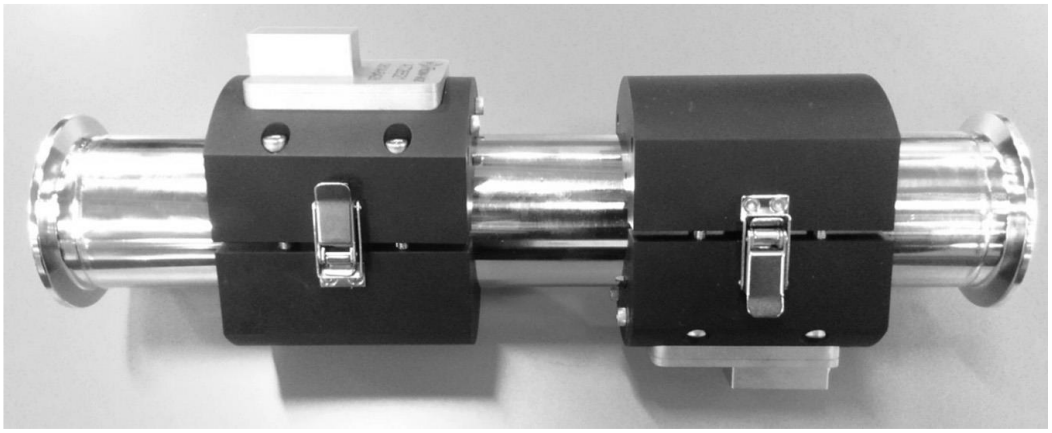

Figure 3.3: Flow-Viz™ non-invasive clamp-on ultrasound sensor units installed onto a stainless steel pipe

3.1.2. Stainless-steel (316L) flow loop

The stainless-steel (316L) flow loop was used for the in-line PUV+PD and tube viscometry tests. Three pipe test sections were used with the following inner diameters (ID) and corresponding outer pipe diameters (OD): (22.4 mm ID, 25.1 mm OD), (35.1 mm ID, 38.1 mm OD), (47.8 mm ID, 50.8 mm OD). A *SPX* rotary lobe pump with non-shearing pumping action was connected to the mixing tank. The loop consisted of several instruments to measure the process variables and test parameters. Three *Wika* PT-100 resistance temperature devices (RTD) were attached to the flow loop at different points. One for each of the pipes that is in the 22.4 mm and 47.8 mm inner diameter pipes and one for the mixing tank. Volumetric flow rates were measured using electromagnetic flow meters. An *Endress and Hauser Promag H* rated at 300 L/min was used to measure flows in the 47.8 mm pipe whilst a *Krohne Optiflux 4000* was used in the 22.4 mm pipe. The differential pressure was monitored by ABB pressure transmitters with remote seals. The *ABB 266 MRT* pressure transmitter rated at 100 bar maximum pressure was utilised in the 22.4 mm pipe whilst the *ABB 265 DR* transmitter with a lower pressure rating of 2.5 bar was used in the 47 mm pipe.

The complete tube viscometry setup was calibrated using water and the Colebrook-White equation was used in the procedure which is described in Section 3.2.4. After the water test and calibration procedures were completed, water was mixed with powders of bentonite, kaolin and Carboxymethyl cellulose (CMC) to form different concentrations of fluids which were then used for the in-line experimental tests. The non-invasive ultrasound sensors were attached to the 47.8 mm (ID) pipe for velocity profile measurements. A glass window was installed on the 47.8 mm pipe after the pressure drop test section. This window was used to inspect the level of the suspensions during tests and also to determine whether no air bubbles were present in the system Figure 3.4 shows an image of the stainless steel flow loop with the corresponding schematic in Figure 3.5.

Figure 3.4: Stainless steel (316L) flow loop at the FPRC

All sensor data were logged into a PC for further processing. The schematic in Figure 3.5 shows the interconnections between the instrumentation and the Flow-Viz™ unit. The post-processing PC unit has a NI-PCIe 6251 installed for logging the sensor data into the LabVIEW™ based program.

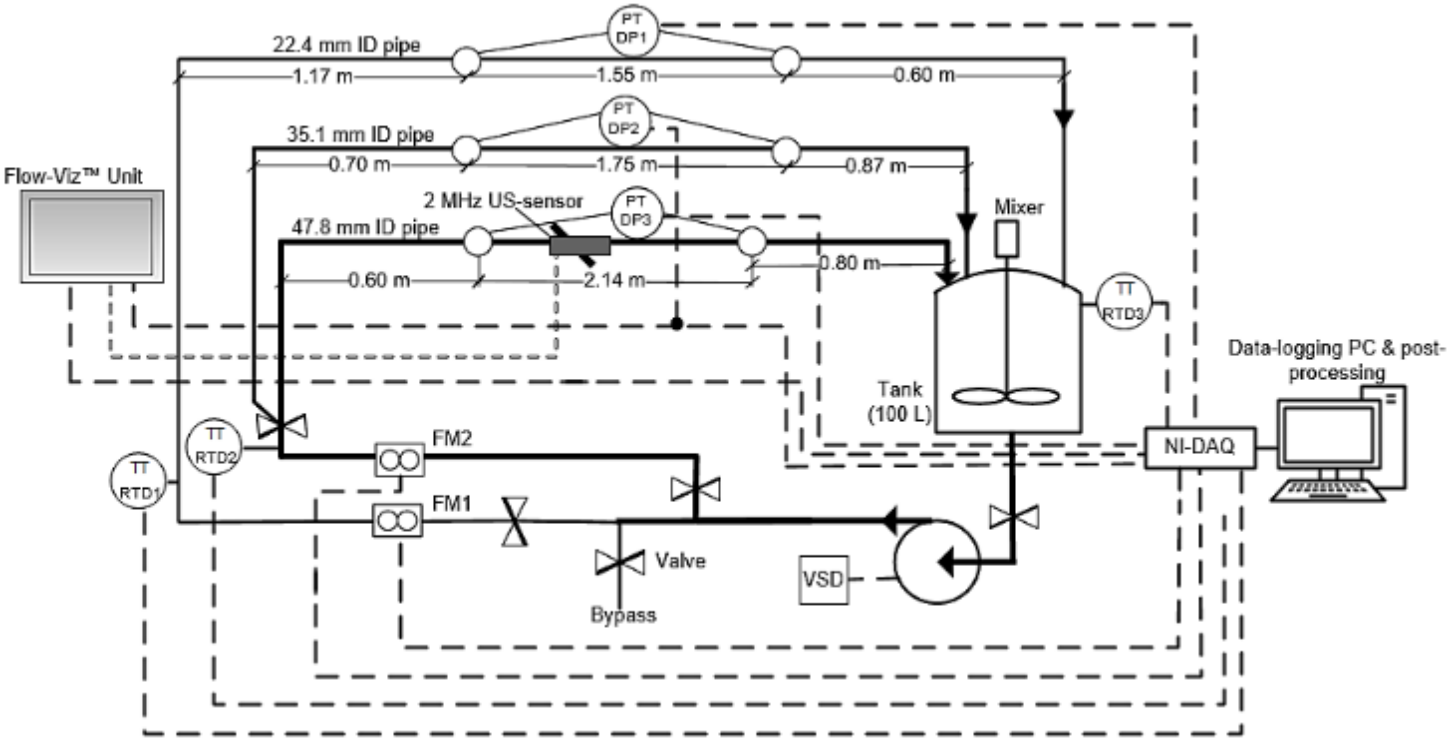

Instrument/Equipment type	Identifier	Flow loop location
Wika PT-100 resistance temperature device 1	RTD1	22.4 mm ID pipe
Wika PT-100 resistance temperature device 2	RTD2	47.8 & 35.1 mm ID pipe
Wika PT-100 resistance temperature device 3	RTD4	Mixing tank
Krohne Optiflux 400 magnetic flow meter	FM1	22.4 mm ID pipe
Endress + Hauser Promag H magnetic flowmeter	FM2	47.8 mm ID pipe
ABB 266 MRT differential pressure transmitter	DP1	22.4 mm ID pipe
ABB 265 DR differential pressure transmitter	DP2	47.8 mm ID pipe
SPX Rotary Lobe pump	-	Mixing tank
SC-2345 NI-data acquisition board	NI-DAQ	Data logging PC

Figure 3.5: Stainless steel flow loop schematic diagram

3.1.2.1. Rotary Lobe pump

A 3 kW SPX rotary lobe pump was used to drive the test fluids through the pipe system. The pump was chosen because of its non-shearing pumping action. The pump draws in fluid as the rotors disengage, forming cavities. The liquid is transported inside the cavity of the rotors around the inner walls of the rotor case. Liquid is then pressured out from the pump as the rotors engage, closing the cavities. Figure 3.6 illustrates the operating principle.

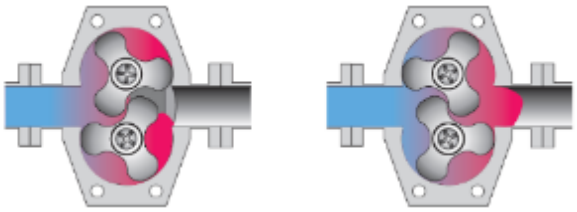

Figure 3.6: Flow loop rotary lobe pump with non-shearing action.

The main operating parameters for the pump are rated as: Displacement of 0.301 dm^3/rev, nominal internal diameter of connection (inlet/outlet) 50 mm, maximum working pressure 7 bar, maximum speed 950 rpm and a maximum torque of 108 Nm.

3.1.2.2. Differential pressure sensors

Two differential pressure transmitters manufactured by ABB were installed onto the stainless steel flow loop. The *266 MRT* pressure transmitter with a maximum span of 10 MPa was installed on the smaller diameter pipe (22.4 mm) whilst the *265 DR* pressure transmitter (250 kPa span) was installed onto the 47.8 mm pipe. The pressure measurements were used for determining the shear stress values required for in-line rheology using the Flow-Viz™ system and conventional tube viscometry.

The pressure transmitters make use of remote seal technology. Pressure applied from within the pipe is transferred to the transmitter's pressure transducer by means of a transfer fluid within the capillaries. The remote seal technology is appropriate for complex industrial suspensions and applications since it completely isolates the transmitter from the process fluid.

Figure 3.7 shows a single remote seal from the pressure transmitter attached to the pipe section.

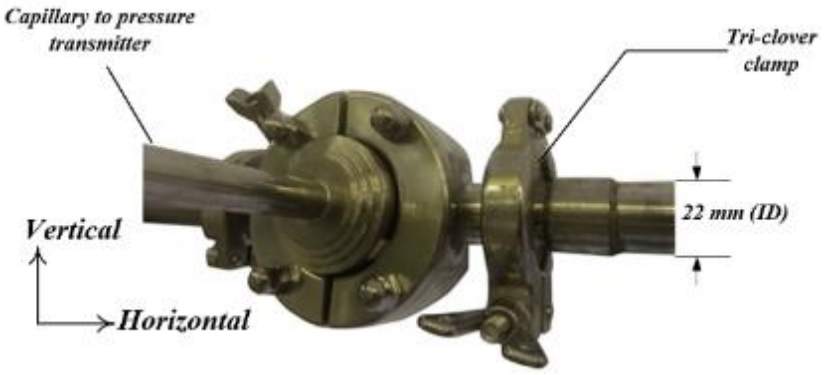

Figure 3.7: Remote seal connection for pressure transmitters

3.1.2.3. Temperature sensors

Three PT-100 resistance temperature devices (RTDs) by *Wika* were used for acquiring temperature from the loop. The four wire sensors with compensation leads were directly connected to the analogue temperature input of the Flow-Viz™ unit. The same sensors were also connected to the National-Instruments (NI) SC-2345 signal conditioning modules which were then connected to the NI-PCIe 6251 data acquisition device for real-time computer based logging. One sensor was connected to each pipe section in direct contact with the pipe wall in order to increase the accuracy of the readings.

3.1.2.4. Flow-Meters

The *Krohne Optiflux 4000* flowmeter (FM1) was shared between the 35.1 mm and 22.4 mm pipes. The *Endress+Hauser* magnetic flow meter was used within the 47.8 mm line. The respective ratings for the two flow meters are as follows:

- *Krohne Optiflux 4000* – according to the technical datasheet the maximum volumetric flow rate is (Q_{max} of 5.9 L/s) with an accuracy of ± 0.4% of the measured value.
- *Endress+Hauser Promag H* – according to the technical datasheet the recommended use range of use is within [35 to 1100 dm^3 /min], with a full scale value of current output for a volumetric flow rate of (Q_{max} ~ 5.5L/s). The accuracy is ± 0.5%.

3.1.2.5. Data acquisition and post processing

LabVIEW™ software was used to acquire the measured variables together with National-Instruments™ data acquisition hardware. The SC-2345 data acquisition board with current to voltage converters was used to acquire the 4-20 mA current signals and convert them to corresponding 1-5 V voltage signals before logging. The data-logging program included the conversion calibration constants to represent the absolute measured values. Signal averaging and optimised sampling were carried out in software for improved accuracy. This setup was only used for the tube viscometer measurements.

The NI-PCIe 6251 data acquisition device used to transfer the sampled data into LabVIEW™ had the following specifications: 16 bit ADC resolution, 2.8 MS/s, ±10 V input range per channel with analogue and digital triggering. For pressure, flow-meter and temperature acquisition a sampling rate of 1 kS/s.

3.1.3. Fluids used for experiments

The materials used for the rheological characterisation tests were mainly fluids which exhibit a wide variety of rheological characteristics. CMC, bentonite and kaolin powders (http://www.proteachemicals.co.za) were mixed with water to form different suspensions and solutions. The diversity of the test fluids is seen for example in bentonite and kaolin clay which both exhibit a yield-stress however the curvature of their flow-curves varies with increase in shear-rate. On the other hand, CMC was characterised using the Power-law model. Two concentrations of each model fluid were tested, that is, one high and a low one. A relative density test (Section 3.2.6) was carried out in order to calculate the concentrations of the suspensions used for the tests.

3.1.3.1. Water

Clean water was used for calibration purposes using the procedure described in Haldenwang (2003). The whole flow loop was first cleaned and flushed with several runs of water before the actual volume of water for calibration was stored in the tank. The calibration by water was done by comparing the measured pressure and flow-rate data, with the predicted ones from the theoretical Colebrook-White equation for the different test pipe sections. The water calibration test

was also used to show the validity of the velocity profiles from the Flow-Viz^{TM} instrument, by comparing the non-dimensionalised velocity profiles measured using the Flow-Viz^{TM} system with the theoretically predicted values. For the ultrasound tests with water, a few seeding particles were mixed in the tank so as to obtain good echo/backscatter for velocity profile measurements as suggested in Takeda (2012).

3.1.3.2. Carboxymethyl cellulose (CMC)

Two concentrations of CMC in water solutions were used. A high concentration of ~7.7 %w/w was chosen and the lower having a concentration of about ~5.16 %w/w. The two concentrations were chosen as they allow reliable testing of the measurement capabilities of tube viscometry and PUV+PD within the same fluid. By using a dilute and more concentrated mixture of the same fluid, disparities in the measurement capabilities of each characterisation technique with varying concentration can be readily noticed. The CMC was first tested using the tube viscometry methodology. After the tube viscometry, PUV+PD testing was then carried out. The final ultrasound tests were conducted using the Flow-Viz™ system.

3.1.3.3. Bentonite

A high concentration of 7.48% w/w and lower concentration of 5.4 %w/w were used. Bentonite was chosen for the tests as it is a common drilling mud used in mining applications and also offers good backscatter for the PUV measurements. Similarly with CMC, two concentrations of dilute bentonite where selected used for testing inorder to obtain reliable and acceptable data. The lower concentration of 5.4 %w/w was made low enough to obtain a more dilute suspension which still shows the yield stress characteristic. Hydration of bentonite suspensions took about 2-3 days after thorough mixing in the mixing tank.

3.1.3.4. Kaolin

Like bentonite, kaolin powder mixed with water required thorough mixing. Suspensions were agitated by the mixer and then left for about a day before running in-line tests on the flow loop. Concentrations of 38.4 %w/w and 30.79 % w/w were used. The same procedures and sets of tests as done for bentonite and CMC were carried out for kaolin.

3.1.4. XYZ-scanner and needle hydrophone experimental setup

An XYZ-scanner setup with a spatial resolution of 1 micrometer at SP-Technical Institute, in Gothenburg Sweden, was used for the acoustic characterisation tests. The setup consisted of a robotic XYZ-scanner mounted on top of a transparent water tank. The submersible needle hydrophone and the different acoustic sensors where immersed in the water tank at room temperature. The XYZ-scanner was used to navigate the needle hydrophone probe across a predefined scanning grid i.e. to cover the area where the beam was located. Figure 3.8 shows the XYZ-scanner setup.

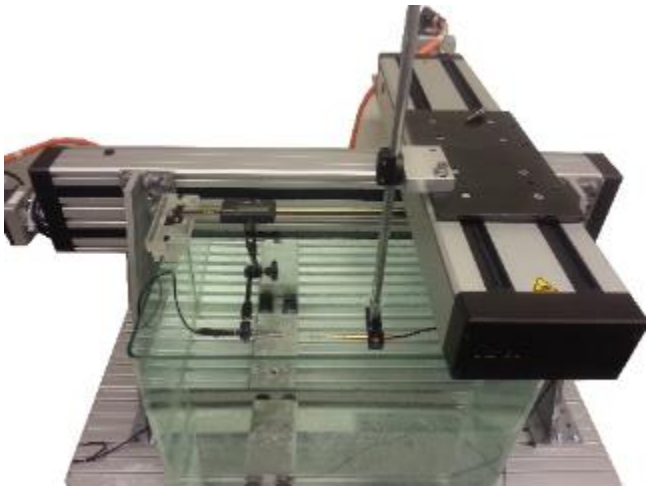

Figure 3.8: XYZ-scanner used for acoustic characterisation tests

The schematic of the XYZ-scanner is shown in Figure 3.9 with a top view perspective of the water tank scanning area.

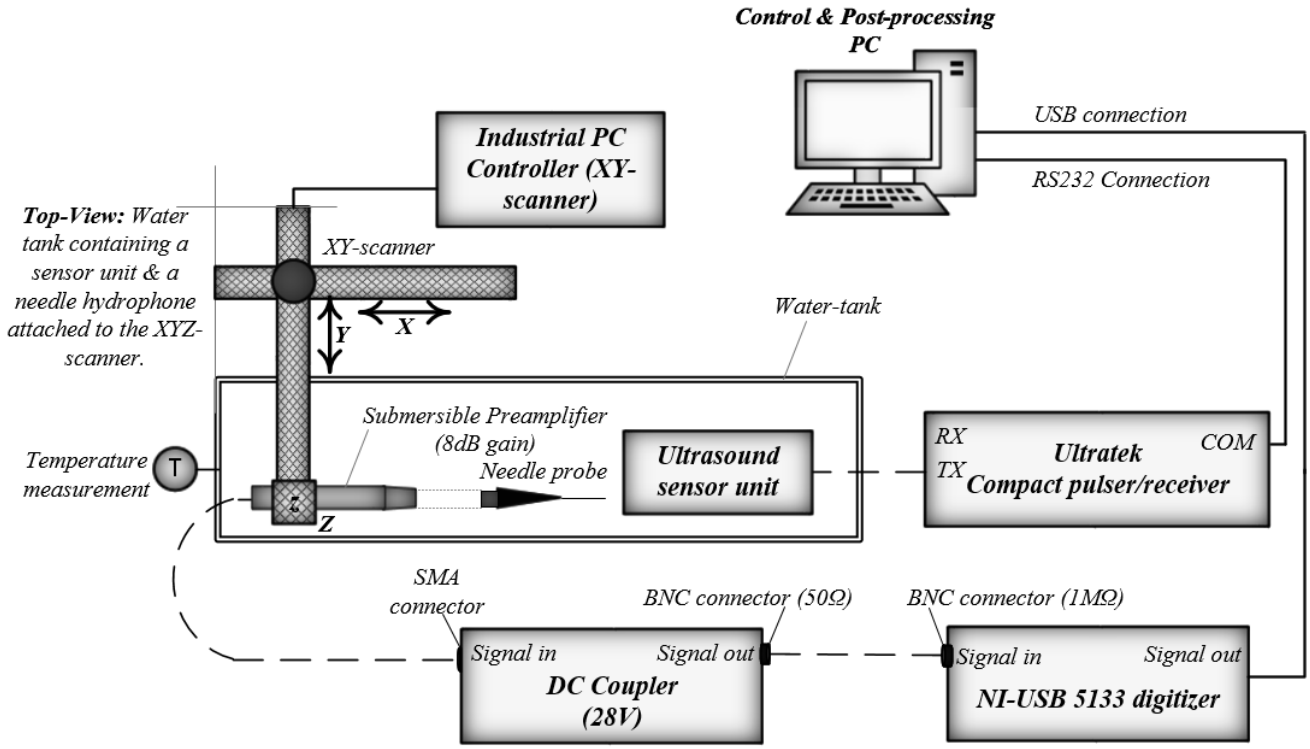

Figure 3.9: XYZ-scanner experimental setup showing data acquisition system components

The 1 mm needle hydrophone probe was connected to a submersible preamplifier with a gain of 8 dB. Temperature readings within the water tank fluctuated between 21-23 °C for the duration of the tests. The technical specifications of the pulser are shown in Table 3.2.

Table 3.2: Specifications of the Ultratek compact pulser/receiver

Parameter	Value
Pulse Voltage [V]	40-300
Pulse Width [ns]	20-484
Damping resistor [Ω]	8.4, 8.5, 9.9, 10.1, 48, 52, 375 & 750
Low Pass Filter [MHz]	48, 2, 1, 8.8, 7.5, 6.7, or 5.9
High Pass Filter [MHz]	4.8, 1.8, 0.8, or 0.6

Ultratek compact pulser/receiver

An Ultratek compact pulser/receiver was used to excite the ultrasound transducers. The pulser/receiver was controlled from the host computer via RS232 serial (9600 baud-rate, 8 bit data) communications. The pulser/receiver was chosen as it offered a simple interface for lower

cost and it is often used in industry for Non-destructive Testing (NDT). The pulser/receiver also allowed continuous pulsing throughout the characterisation tests and this was the main reason for selecting this pulser/receiver unit.

DC-Coupler and needle hydrophone

The needle hydrophone system (www.precision-acoustics.com/) used was made up of a combined needle probe and preamplifier with a voltage gain of 8 dB. The pre-amplifier was linked to the 28 V supplied DC-Coupler using a coaxial connection with a Sub-Miniature type A (SMA) connector. Figure 3.9 shows that the output impedance of the system was 50 Ω and the unit was connected to a National-Instruments (NI-5133) digitiser with an input impedance of 1 MΩ. A correction factor of 1.953 was applied for impedance mismatch. The value of the correction factor was determined by comparing several voltages measured throughout the measuring grid using an impedance matched Agilent oscilloscope (DSO-X-3024A) with those from the NI-digitiser. The digitiser acquired the hydrophone measurement signal for each point within the scanning grid at set times, which were determined by the Matlab based application. All the measured voltages from the different grid points were then combined during post processing in Matlab to form the acoustic map of voltages, which shows the beam intensity. A sampling frequency of 100 MHz was used for the tests.

3.2. MEASURED VARIABLES AND CALIBRATION PROCEDURES

The calibration of the test sensors was done in order to ensure accurate readings. The data acquisition device (SC-2345) enabled convenient calibration since it converts the current loop (4-20) mA signals from the sensors to corresponding voltage signals which can be easily read from the GUI software (Measurement & Automation Explorer™).

3.2.1. Internal pipe diameter measurement

Callipers where then used to measure the internal diameter (ID) of both ends of each pipe. The average value of the two ends was taken as the diameter of the pipe. Taking the accuracy of the callipers, the ID values for the pipe lines used in the flow loop (tube viscometry, PUV+PD), can be expressed as: 22.4 mm ± 0.02 mm, 35.1 mm ± 0.02 mm and 47.8 mm ± 0.02mm.

3.2.2. Calibration of flow and pressure transmitters

The NI-data acquisition device combined with the Measurement & Automation Explorer were used to obtain real time voltage measurements from the sensors thus eliminating the need for manual digital multi-meter readings and extra wiring. The measured variable (pressure, volume-flow rate) against the measured voltage value were used to plot linear curves to describe the calibration coefficients for the sensors. Based on the manufacturer technical specifications for the flow and pressure instruments, a linear relationship is expected between the measured variable and the output voltage, over the measurement range.

The graphs showing the coefficient of determination (R^2), are presented in Figure 3.10 and Figure 3.11.

3.2.2.1. Magnetic flow meters

The calibration graphs for the flow meters are shown in Figure 3.9 with the calibration constants.

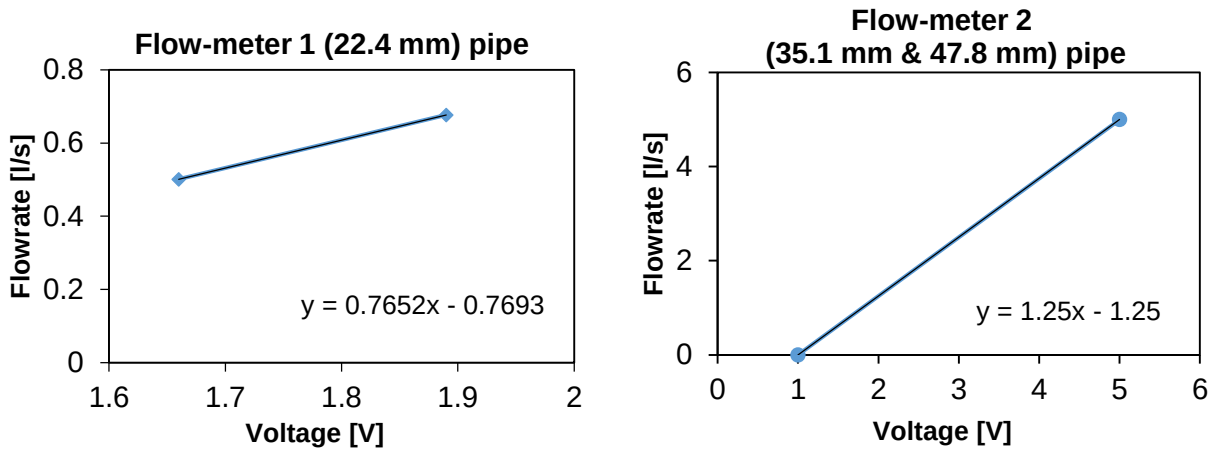

Figure 3.10: Calibration curves for the flow-meters.

3.2.2.2. Pressure transmitters

The ABB 265 DR pressure transmitter (DP2) rated at 250 kPa was used for pressure measurements in the 35.1 and 47.8 mm pipes, whilst the high pressure transmitter ABB 266 MRT rated at 10 000 kPa was used in the smaller (22.4 mm ID pipe) pipe, where higher pressures were experienced. The ABB transmitters used allowed user adjustable ranging to sustain the accuracy of the sensors at lower measuring spans. For each test fluid, the maximum pressure reading was determined by running the pump at maximum speed and then adjusting the span setting accordingly. The calibration plots are shown in Figure 3.11.

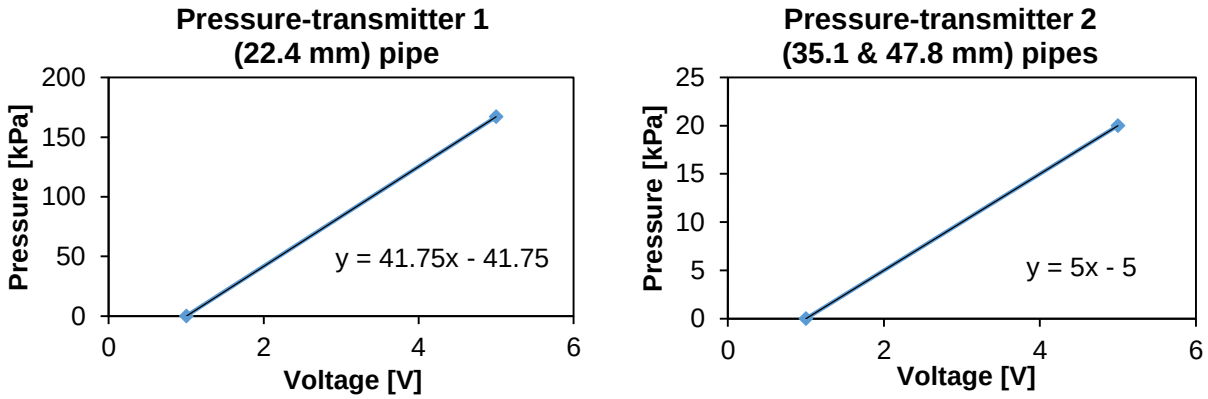

Figure 3.11: Calibration constants for differential pressure transmitters.

3.2.3. Temperature of test fluids

The temperature of the fluids was measured using Wika PT-100 RTD devices. The RTDs were connected to a RTD voltage signal conditioner card which was then connected to the main acquisition board (NI-PCIe 6251). The overall conditioning modules amplify the primary RTD voltage by a factor of 25.

Four wire RTDs were used in order to improve the accuracy of the measured temperature by using the compensation leads. The RTD measured values were also compared to a standard mercury thermometer which was immersed at different points in the flow loop. The comparison showed that the calibration was correct, and the constants were closer to the true value. The calibration constants used for the RTDs are shown in Figure 3.12.

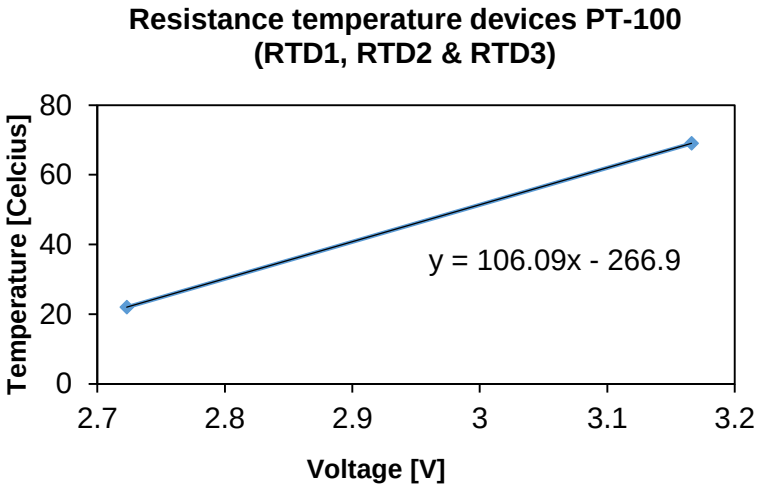

Figure 3.12: Calibration curve for RTDs

Temperature is also important for the in-line measurement of sound velocity. If temperature has a distribution in the flow field, sound velocity also changes. Wang et al. (2004) gives an in depth description on the effect of temperature variations on ultrasonic velocity measurements in pipe flow. The dependency of sound velocity on temperature is described under Section 2.2.7.3 with water as the specific example.

3.2.4. Calibration of tube-viscometer using water

The Colebrook White equation was utilised in the calibration of the flow rig using water by comparing the measured velocities with the theoretically predicted ones. This calibration procedure was carried out as a datum to determine whether the tube viscometry setup was correct and suitable for testing other fluids (model suspensions). The water test is carried out after the calibration of all flow loop instrumentation has been completed.

The turbulent flow of fluids in pipes is given by:

$$\frac{1}{\sqrt{4f}} = -2\log\left(\frac{k}{3.7D} + \frac{2.51}{\mathrm{Re}\sqrt{4f}}\right) \tag{3.1}$$

The friction factor f obtained from numerical iteration is the used to calculate the head-loss based on the Darcy-Weisbach equation:

$$h_f = \frac{4fLV^2}{2gD} \tag{3.2}$$

The Darcy-friction factor is 4 times the fanning friction factor. The wall shear stress as calculated from the head loss is given as:

$$\tau_w = \frac{f\rho V^2}{2}, \tag{3.3}$$

where V is the bulk velocity and ρ is the fluid density.

The procedure for the water test as given by Haldenwang (2003) is as follows:

- The flow-transmitters measure the flow in each pipe and the average velocity is calculated.
- The differential pressure gradient $\Delta P/L$ is measured for all three pipes.
- The average wall shear stress is calculated by using $\tau_w = D\Delta P/4L$ (Equation 2.5).

- A range of theoretical values of τ_w are calculated for a range of average flow velocities by using the Colebrook-White formula. The theoretical range is the same as the experimental range covered in the pipe test.
- This is done by optimising the Colebrook-White equation in an iterative calculation which assumes a pipe roughness of k and a calculated value of the Reynolds number to obtain the friction factor f.
- The theoretical value for the wall shear stress is obtained by using the friction factor in Equation 3.6. Deviations from the theoretical values by margins of approximately ±10% are also calculated to show how well the experimental values agree with the theoretical plots.

The theoretical and experimental curves are then plotted on linear axes as shown in Figure 3.13.

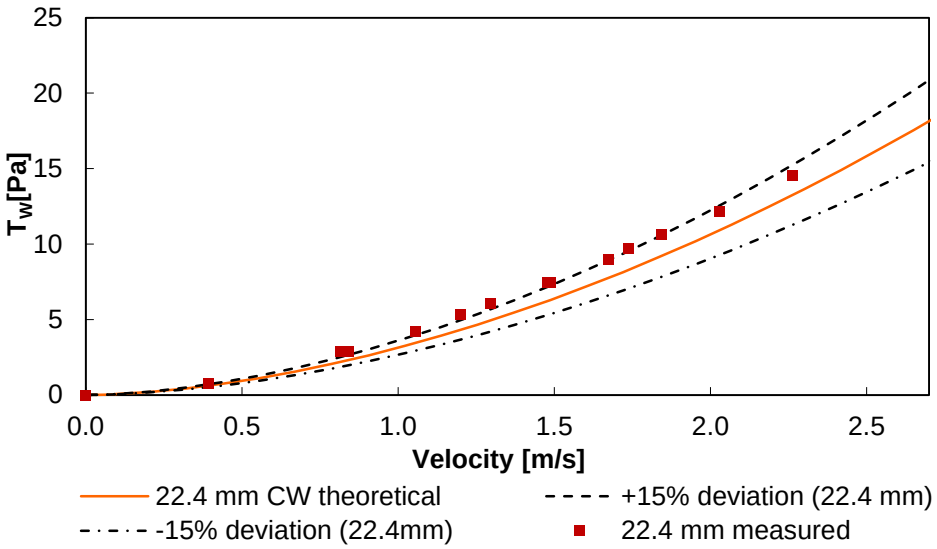

Figure 3.13: Water test data in (22.4 mm pipe) compared to theoretical Colebrook-White curves

Generally good agreement was observed between the theoretical and measured data for the water calibration test. The deviation from the theoretical prediction was close to the +15% deviation line. The difference can be attributed to some disturbances in the test conditions (pressure, temperature).

The test was repeated for the 35.1 mm and 47.8 mm pipe sections. The measurement results are presented in Figure 3.14 and Figure 3.15.

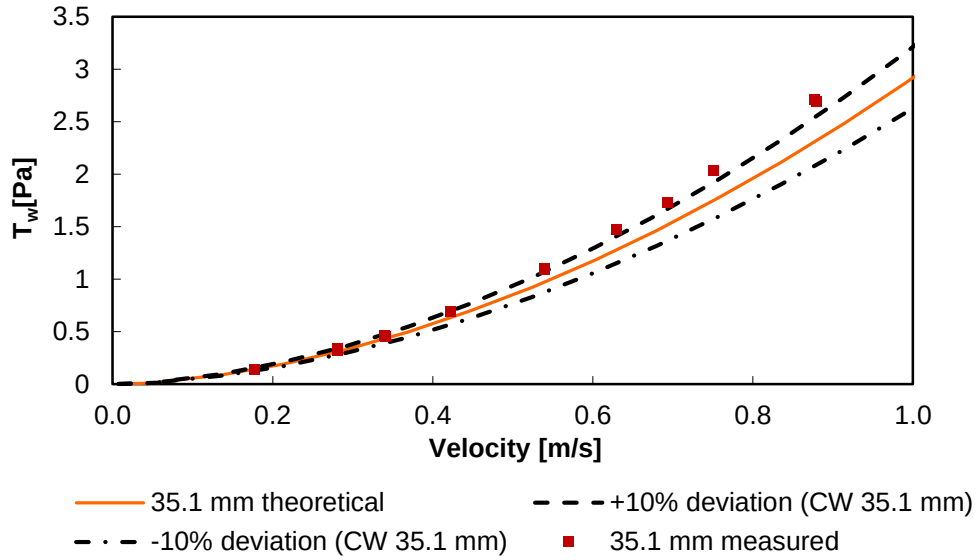

Figure 3.14: Water test measured data (35.1 mm pipe) compared to theoretical Colebrook-White

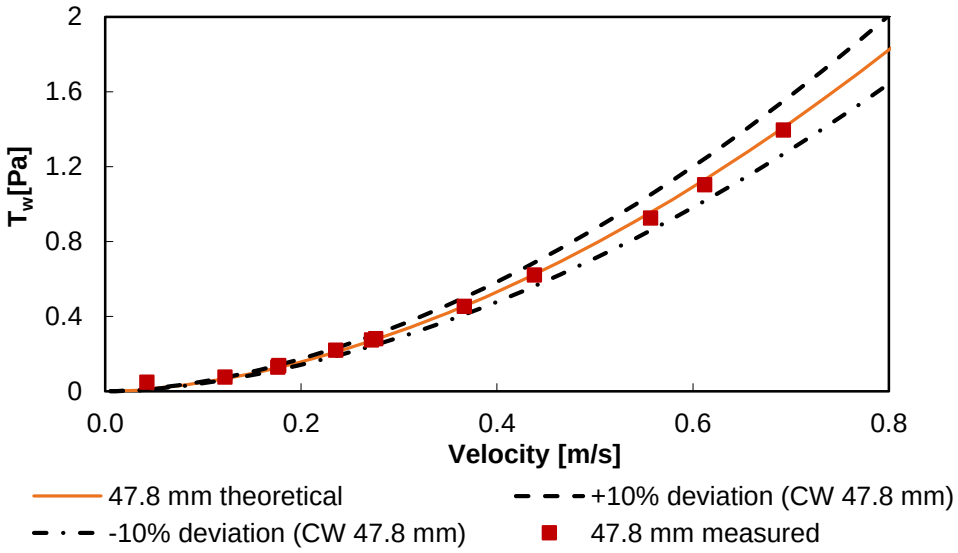

Figure 3.15: Water test measured data (47.8 mm pipe) compared to theoretical Colebrook-White

The 47.8 mm ID pipe showed good agreement with the Colebrook-White data. Most of the experimental points were well within ±10%. The Colebrook-White water test showed that the flow loop design is suitable for tube viscometry tests. The parameters which were used for the tests are shown in Table 3.3

Table 3.3: Colebrook-White test parameters

Pipe diameter (ID) [mm]	Average Temperature[°C]	Pipe roughness *k* [*μ*m]
22.4	24.	0
35.1	26	0
47.8	25	0

3.2.5. Water test with PUV+PD system (Flow-Viz™)

A water test was also performed using the Flow-Viz™ system. Water at 22-23°C was added to the flow loop (47.8 mm ID pipe) in Figure 3.5 with a few seeding particles in order to obtain good velocity profiles. The water test served to validate the Flow-Viz™ velocity measurements against theoretically predicted values. Theoretical profiles (Colebrook-White and Darcy, Equations 3.4 and 3.5 respectively) for pipe flow were compared to the measured velocity profile. The pipe roughness for the stainless steel pipe was taken to be (*k = 0 μ*m) in Figure 3.16 and Figure 3.17 is the FFT-based power-spectrum image.

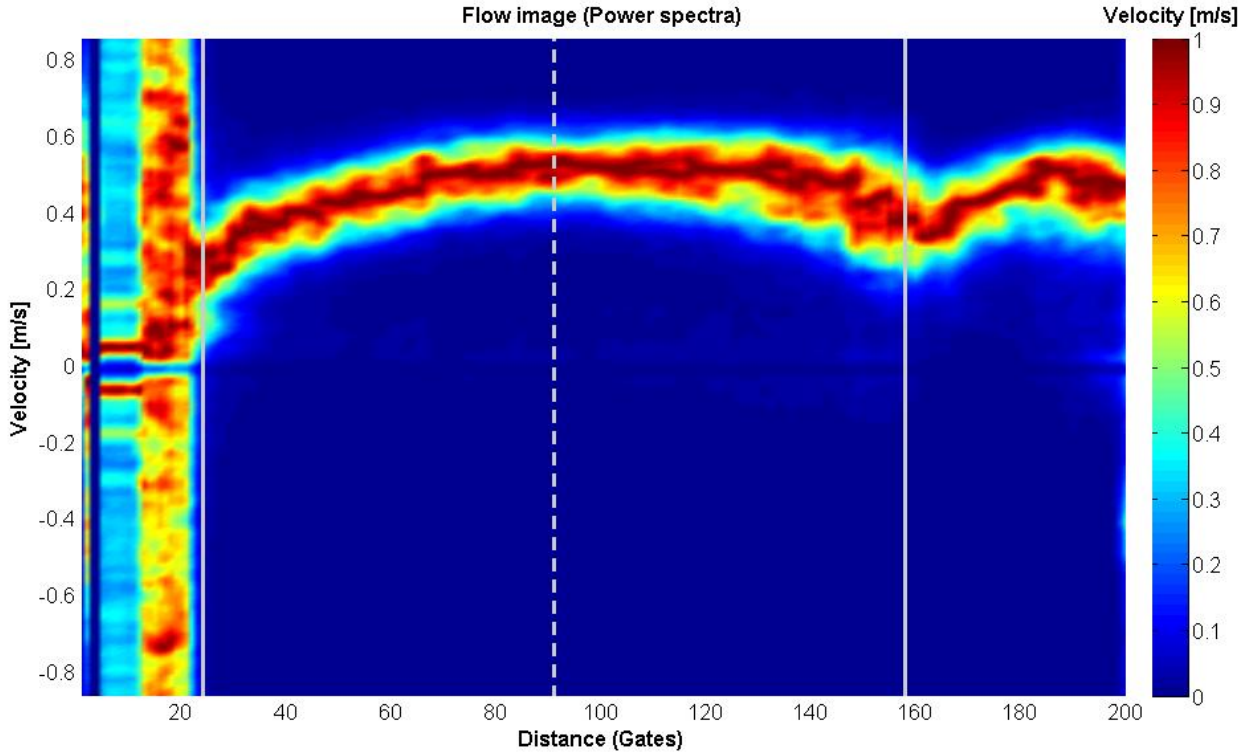

Figure 3.16: Doppler spectrum of the velocity profile measurement in water (47.8 mm pipe)

Before gate 25 in Figure 3.16 , a low SNR was measured due to the near pipe wall interface. The first solid vertical line (gate 25) on the spectrum image shows the near wall close to the ultrasound sensor, with the corresponding opposite wall shown by a similar a solid line at gate160. The centre of the pipe is depicted by the dashed vertical line. The SNR for the whole measurement was good as the power spectrum shows even distribution of energy throughout the whole profile.

Figure 3.17 shows the averaged velocity profile obtained from the water test together with the theoretical prediction. The 22 profile repetitions, were also plotted to show the fluctuations in velocities. The velocity measurement shows a typical turbulent profile shape, the Reynolds number at this flow rate (0.65 l/min) was *Re* = 18 281.

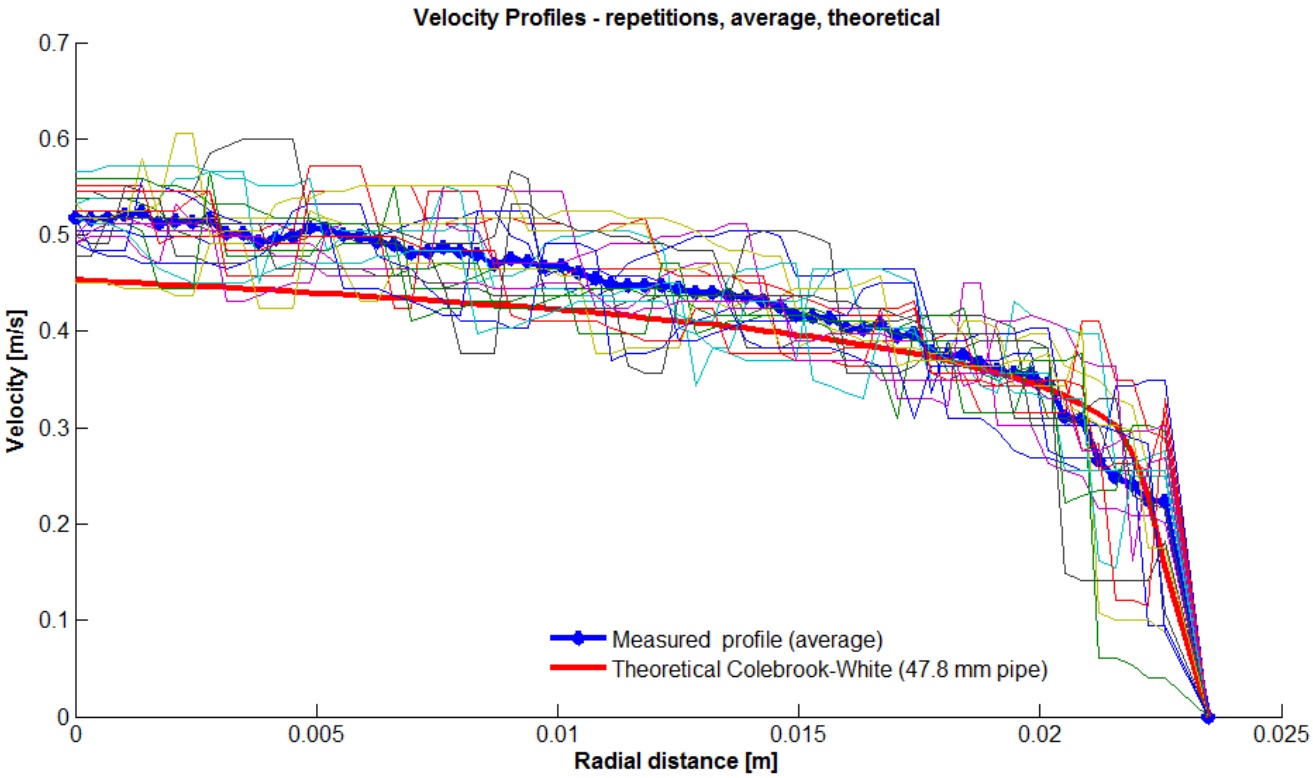

Figure 3.17: Flow-Viz^{TM} water test velocity profile in 47.8 mm ID stainless steel pipe

Figure 3.18 shows the velocity profiles plotted in non-dimensionalised form, with ±10% theoretical deviations.

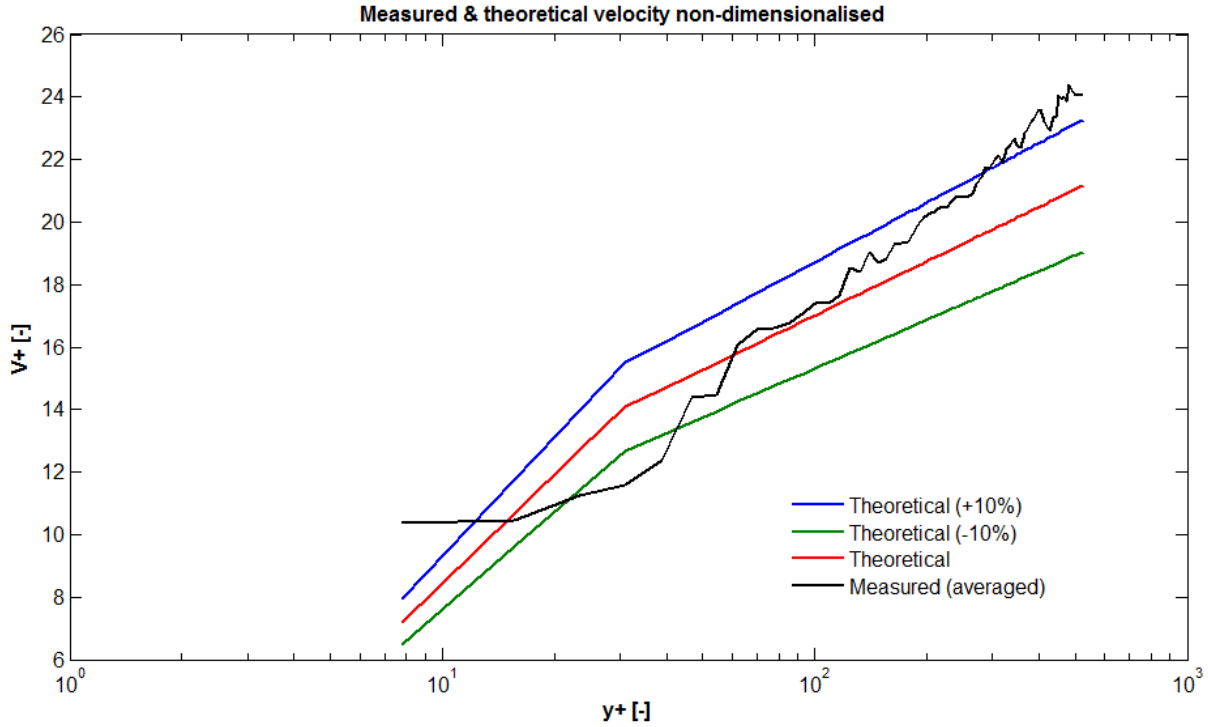

Figure 3.18: Non-dimensionalised plot for water test velocity profile

The theoretical deviation curves show good agreement (±10%) with the measured data for most of the profile. Major differences were recorded at the inner pipe wall, possibly due to the sample volume overlapping the wall interface. The volumetric flow rate from the electromagnetic flow meter was 40.5 l/min whilst the PUV measurement recorded an average of 38.9 l/min (determined by integration of the velocity profile), resulting in a difference of 4 % for the two readings. Velocity profiles were measured and compared to theory at different flow rates (13.8 l/min, 21 l/min, 30.5 l/min and 40 l/min) and similar results were found. Similar comparisons with turbulent pipe flow theory were also done in (Rudman et al., 2004), however the work used Direct Numerical Simulations (DNS). This close agreement with theoretical predictions shows that the Flow-Viz^{TM} system can accurately measure Doppler profiles even in turbulent pipe flow.

3.2.6. Relative density test

The relative densities of the mineral suspensions were measured off-line. The relative density (S_m) is calculated as follows:

$$S_m = \frac{\rho}{\rho_w} \tag{3.4}$$

$$S_m = \frac{Mass\ of\ \ slurry\ sample}{Mass\ of\ \ equal\ volume\ of\ \ water\ as\ \ sample} \tag{3.5}$$

The relative density of the slurry sample is obtained by carrying out the following procedure (Haldenwang, 2003):

i. Three volumetric flasks (250 ml) of the same type and a high-precision scale that can measure to a milligram are required.

ii. Make sure the volumetric flasks are thoroughly dry and empty to obtain the mass of the flask as *(M_1).*

iii. Partially fill the flask with a well-mixed slurry sample directly obtained from the in-line mixing tank, and this will be measurement (M_2) i.e. (flask plus mass of slurry sample).

iv. Pour water into the remainder of the flask mentioned in step (iii), until the water/slurry level is at the graduated mark and weigh *(M_3).*

v. Empty the flask completely and clean it thoroughly. Fill the flask with water to the same graduated mark and weigh *(M_4)*.

vi. From Equation 3.5 the relative density can be calculated by:

$$S_m = \frac{M_2 - M_1}{(M_4 - M_1) - (M_3 - M_2)} \tag{3.6}$$

vii. The actual slurry density ρ_m is then calculated by using Equation 3.4

3.2.7. Velocity of sound measurement

The velocity of sound values for the different test fluids used in the PUV+PD tests were determined from the RF-data which was measured during the in-line tests. The RF-echo data stored after each in-line measurement was used to obtain the velocity of sound. For kaolin suspensions, an off-line test with two transducers configured in a pitch-catch mode (AToM) was conducted. The attenuating effects of the kaolin inhibited the accurate determination of the inline velocity of sound using a single transducer. With a single transducer the opposite wall echo from the RF-data could not be determined, thus the use of the offline test. However, the latest Flow-Viz^{TM} electronics has two channels that can be used in pitch-catch mode, unfortunately this was not available during this work.

For the in-line velocity of sound test the correct propagation distance was calibrated using water in the 47.8 mm pipe. The temperature of the water was recorded to be ~20.5°C. The velocity of sound equation for water mentioned earlier (Equation 2.28) which is dependent on temperature was used to determine the speed of sound during the propagation distance measurement. The velocity of sound at ~20.5°C was calculated to be 1484 m/s.

The flight time *t,* it takes the pulse to propagate from the transducer to the opposite pipe wall was determined from the single-pulse echo plot as illustrated in Figure 3.19.

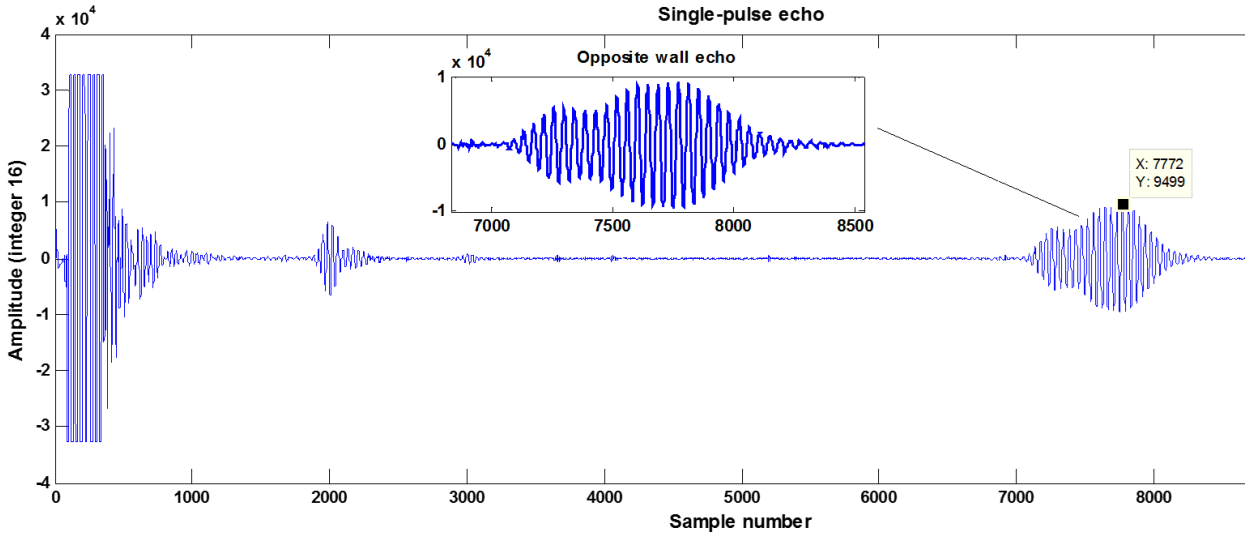

Figure 3.19: Single pulse echo plot to determine time of flight

Sample 7772 shows where the peak of the opposite wall echo was located; where each of the samples is taken after a single clock interval (74.25 MHz) of the onboard pulser/receiver.

Substituting the velocity of sound *c* and the time *t* from the samples into the time of flight, $c = d/t$ gives the distance d as 0.1555 m. The calculated propagation distance obtained from calibration procedure, was then used as a parameter in the Flow-Viz™ system to calculate the in-line speed of sound values for the different model suspensions.

The calibration for the distance d for the off-line measurement was done in a similar manner to that previously discussed for the in-line measurement. The velocity of sound obtained for the suspensions and CMC solutions used for the tube viscometry tests are summarised below in Table 3.4.

Table 3.4: Velocity of sound values for the different fluids

Fluid under test	Relative Density	Concentration	Velocity of sound [m/s]
CMC 1	1.044	7.7 %w/w	1513.0
CMC 2	1.029	5.16 %w/w	1538.2
Bentonite 1	1.048	7.48 %w/w	1584.7
Bentonite 2	1.037	5.4 %w/w	1497.5
Kaolin 1	1.314	38.4 %w/w	1711.2
Kaolin 2	1.237	30.79 %w/w	1620.6

3.3. EXPERIMENTAL TEST PROCEDURES

Standard measurement procedures for tube viscometry and PUV+PD were adhered to in order to conduct the in-line rheometric tests. Averaging and multiple sampling were taken into account in order to give a good representation of the actual measurement results. After the collection of data, analysis was carried out and these methods are discussed in Sections 3.4.1-5.

3.3.1. Tube viscometry on stainless-steel flow loop

The sequences of steps for carrying out the tube viscometry measurements was done using a procedure outlined in Haldenwang (2003). The procedure was repeated for all three pipes on the flow loop with appropriate adjustments where necessary. The procedure is outlined as follows:

- Before any fluid is tested, all necessary zeroing of pressure transmitters is done.

- Calibration of the flow loop is done by conducting water tests in the three pipe test sections and the results are compared with the theoretical curves (shear stress against shear rate) from Colebrook-White equation.

- About 100 litres of slurry are mixed in the main mixing tank until the suspension is properly hydrated and well mixed.

- An off-line relative density test is done for a representative sample.

- Flow rates are changed accordingly by using the Variable Speed Drive (VSD) control. The flow is allowed to reach steady state before any measurements are taken using the acquisition software. A settling interval of about 2-3 minutes is allowed before taking a subsequent reading.

- A LabVIEW^{TM} based program is used to log the flow and pressure data to an Excel spreadsheet whilst simultaneously displaying the measurement data on a graph in real time. The visual display of the data on a real time chart allows for the quick detection of random measurement errors.

- This process is repeated with a range of flow rates until sufficient data points are recorded over the desired pseudo shear rate range.

- Having taken all measurement data wall slip effects are noted when laminar flow pseudo shear diagrams for the different pipes do not overlap, i.e., the magnitude of shear stress in different diameter pipes should overlap when there is no slip.

After recording the tube viscometry data the Rabinowitsch-Mooney transformation (Appendix C.1) is done in post-processing to determine the appropriate shear rate from the measured flowrates. After applying the transformation, the rheological parameters of the test fluids are then found by curve fitting procedures on the rheogram.

3.3.2. In-line rheometry PUV+PD with Flow-Viz™

In-line rheometry using the PUV+PD methodology was conducted in the 47.8 mm pipe. The following procedure was adhered to in order to obtain optimised velocity profiles in the fluid under test. The PUV+PD tests were conducted soon after the tube viscometry tests in the 47.8 mm pipe. The mounting of the ultrasound sensor and set-up of Flow-Viz™ was carried out as follows:

- The stainless steel pipe to which the non-invasive ultrasound sensor is clamped is first cleaned thoroughly with a dry cloth to remove any excess dirt of fluids by following guidelines outlined in Sanderson & Yeung (2002). This is done to prevent any non-uninform acoustic impedance layers between the ultrasound transducer and the pipe-wall.
- Ultrasound sensor couplant is then applied to the mounting surface of the non-invasive sensor unit for acoustic impedance matching (discussed in Section 2.3.2.2). The sensor is then clamped tight with the fastening nuts to ensure no air gaps are present between the pipe wall and the sensor mounting wedge.
- The pressure transmitter is then zeroed after connecting it to the Flow-Viz™ unit.
- Within the Flow-Viz™ software there is a GUI window which allows the setting up of system measurement parameters. The main parameters which are set include:

  i. The pipe radius (half-ID), the length *L* between the differential pressure points.
  ii. Velocity of sound *c* and the Doppler angle of ~70°.
  iii. The initial estimate of the flow rate optimises the Pulse Repetition Interval (PRI). A recommended value for this would be less than the flow meter reading. With an optimised PRI the maximum magnitude of the displayed velocity profile is closer to the highest value of the velocity axis in the display window. This ensures that the full range of the Analog-to-Digital-Converter (ADC) is used.
  iv. The wall position can be adjusted after an initial velocity profile has been acquired to determine the correct wall gate. This parameter can be set manually or the Flow-Viz software can automatically select the correct wall gate.
  v. The rheology estimation algorithm and velocity estimation algorithm can be changed prior to or after acquiring data.
  vi. The input channel for the pressure transmitter is set to analogue channel 5. The correct calibration parameters are also set within the same window.

- After the device setup is completed measurements can then be taken by navigating back to the acquisition window.

3.3.3. Acoustic characterisation of non-invasive ultrasound transducers

Acoustic characterisation tests were performed with the aim of characterising and improving the ultrasound beam of the non-invasive sensor technology through industrial grade stainless steel (316L). The focus was on comparing the effectiveness of different couplants and sensor configurations. The needle hydrophone and XYZ-scanner test equipment described in Section 3.1.4 was used for the tests.

The test matrix included two ultrasound transducers. Two transducer housing cases for clamp-on mounting were used to attach the transducers under test onto the stainless steel (SS316L) pipes i.e. a solid wedge and the other being the latest Flow-Viz^{TM} black casing. The black casing is an improved design that allows easy installation of the sensor onto the pipe. It also features an integrated design between the transducer and sensor wedge technology. However, none of these configurations were acoustically characterised, which was the motivation of this particular research work.

For each test setup two main couplants i.e. a liquid couplant and a solid (solid-X, solid-Y and solid-Z) couplants were used. The purpose of the couplants was to facilitate the transmission of the acoustic energy from the transducer through the pipe wall. Before each test the needle hydrophone was soaked in water for at least 30 minutes so that the output stabilised before any measurement was taken.

All test materials and specific transducer designs used for this research work are guarded by confidentiality agreement thus schematics instead of original images will be used for some sensor setups. Actual manufacturer specifications and product names are therefore omitted from the thesis.

3.3.3.1. Acoustic test measurement setup and description of scanning areas

The sensor units that were tested are described in Table 3.5. Different configurations were exploited in order to ensure that the hydrophone measurements were accurate and that readily identifiable reference points could be established.

Table 3.5: Transducer and coupling configurations used for tests

Transducer type	**Description**
TYPE-A transducer	Higher frequency transducer in the low MHz range, optimised for 22.4 mm and 47.8 mm pipes
TYPE-B transducer	Lower frequency transducer in the high kHz range, optimised for 152.4 mm pipes
SENSOR DESCRIPTION	
Sensor	**Description**
Prototype sensor for 22.4 mm and 47.8 mm pipes	Flow-Viz™ prototype sensors, with TYPE-A transducer numbered (78, 79, 80 and 81)
Industrial commercial for 47.8 mm pipe	Flow-Viz™ commercial sensor (latest clamp-on design).
Industrial commercial for 152.4 mm pipe	Flow-Viz™ sensor with TYPE-B transducer, on prototype wedge.

The beam properties of transducers were determined from measuring a full acoustic map without using any mounting wedge or couplant material. For the subsequent test measurements, the transducers were mounted onto a stainless steel pipe spool piece cut in half. This was done so that the transmitted ultrasound beam from the near wall could be captured by the needle hydrophone. The needle hydrophone was moved within a predefined 2-dimensional (2D) grid to cover the transmitted beam accordingly. The methods followed for scanning and measurement were similar to those presented in (Kotzé et al., 2013; Umchid, 2014).

Measurement reference point description

For each test a reference (origin) point was first established in order to determine the position of the beam on the physical sensor unit. For the single transducer test with no wedge attached to a pipe, the reference was first set by scanning for the point of maximum acoustic energy. This was done by viewing the hydrophone output on an Agilent oscilloscope which was set to a high sensitivity (5 mV per division). This point was then set to as the centre of the X-axis (or centre of the acoustic beam). By knowing the centre value (maximum energy), the origin at X0 mm was set using the XYZ-scanner controller such that a symmetrical acoustic map could be obtained after a complete test run. The complete 2D acoustic grid is illustrated by Figure 3.20 and the schematic in Figure 3.21 which depicts the X0 origin point.

For the vertical grid measurements. Once the physical reference point on the transducer was established, a point of maximum acoustic energy was located along the physical reference line. This was also carried out by viewing the hydrophone output on the Agilent oscilloscope (sensitivity of 5 mV per division). This point was then set as reference point of the acoustic scanning grid using the XYZ-scanner controller.

A description of the single transducer (*Horizontal plane measurement*) and acoustic tests through stainless steel (*Vertical plane pipe measurement*) are described briefly as follows:

(i) **Horizontal plane measurement (Prototype sensors, no wedge):** The scanning area started at the reference point illustrated on and mapped a rectangular grid/plane to cover the face of the transducer at the point of maximum intensity (voltage), i.e. close to the centre of the sensor black area.

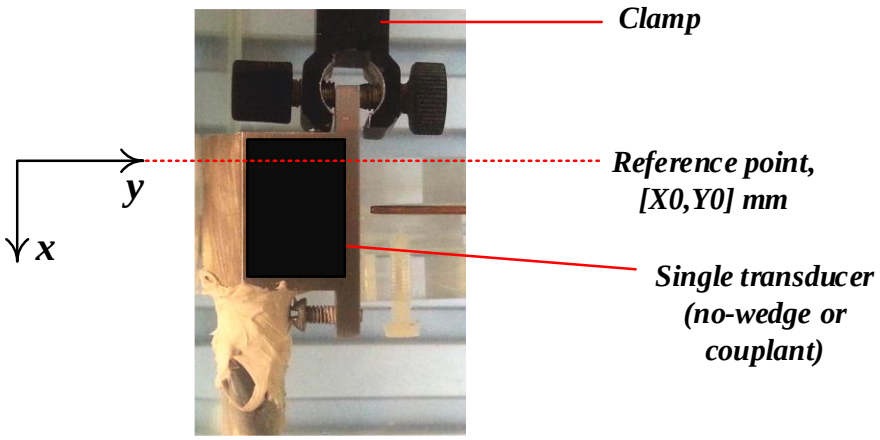

Figure 3.20: Reference point shown on transducer for prototype sensors

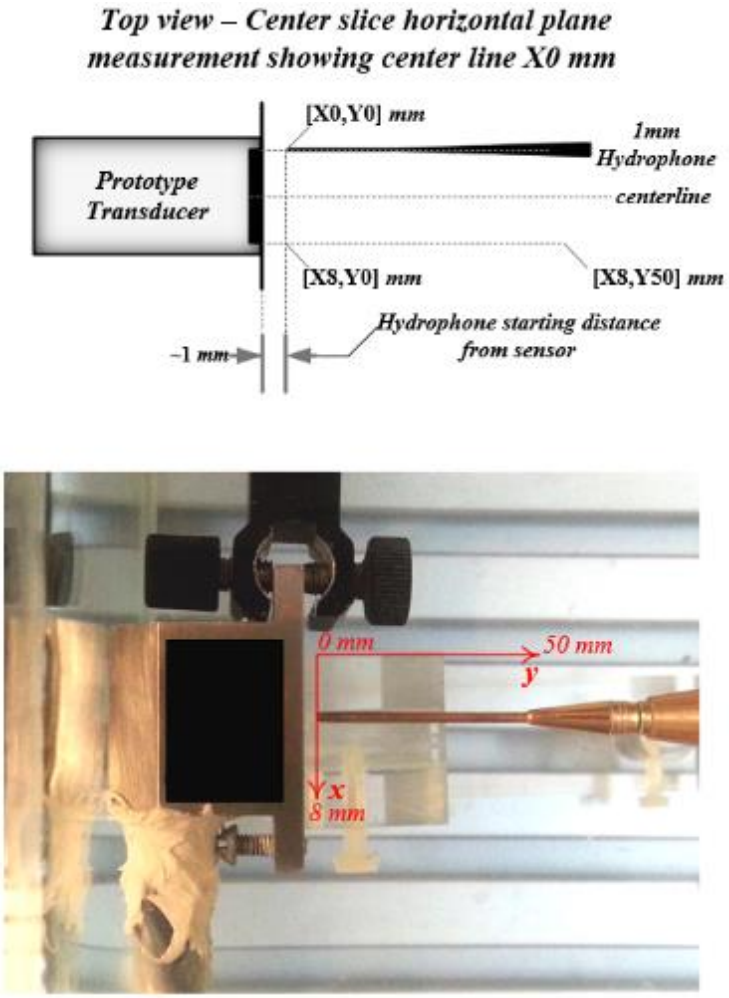

Figure 3.21: Schematic of the horizontal scanning grid for prototype transducers, without coupling wedge.

(ii) **Vertical plane pipe measurements:** The reference points for the vertical plane measurements were taken as the points at which the needle hydrophone is parallel to:

a. For the 47.8 mm prototype sensors and the industrial sensor for 152.4 mm pipes, the reference was the corner point of the diagonal line marking on the prototype wedge.

b. For the industrial commercial sensor optimised for 47.8 mm pipes, the bottom of the silver/grey edge of the sensor clamp-on housing, as shown in Figure 3.22.

The reference point was used as the origin of height measurement or as the zero height level in millimetres [Z0], in order to cover a rectangular grid which cuts across points of maximum measurable voltage, i.e. a rectangular (2D) centre slice with points of maximum measurable peak voltage; the length of the rectangle being millimetre increments from [X0 to X40] with a height defined by vertical millimetre increments from [Z0 to Zmax]. Zmax was the maximum height at which $V_{pk\text{-}pk}$ voltages could not be detected by the digital oscilloscope or NI-5133 digitizer.

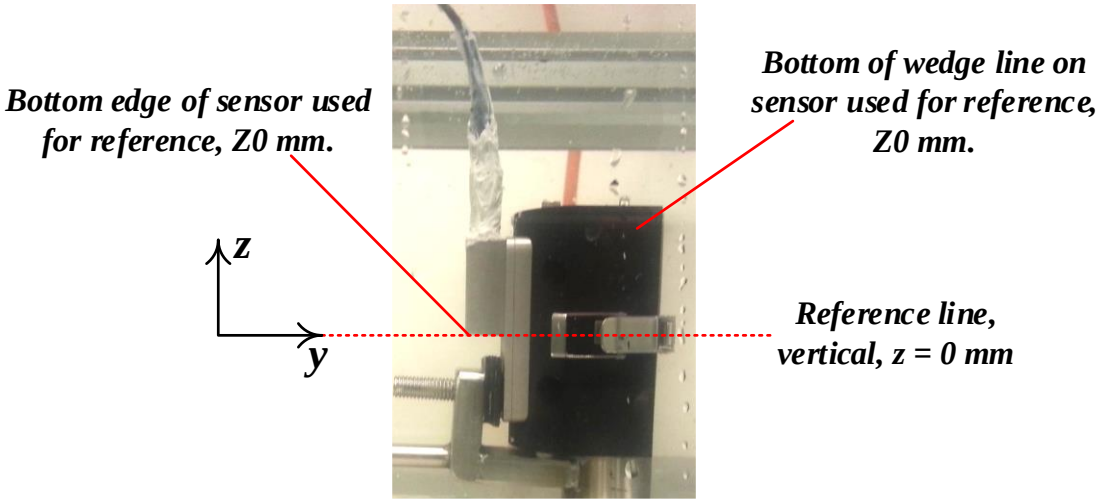

Figure 3.22: Reference point on Flow-Viz™ commercial sensor, for the vertical plane measurements.

The schematics on Figure 3.23 illustrate the different mapping grids and the corresponding reference points (X0, Y0).

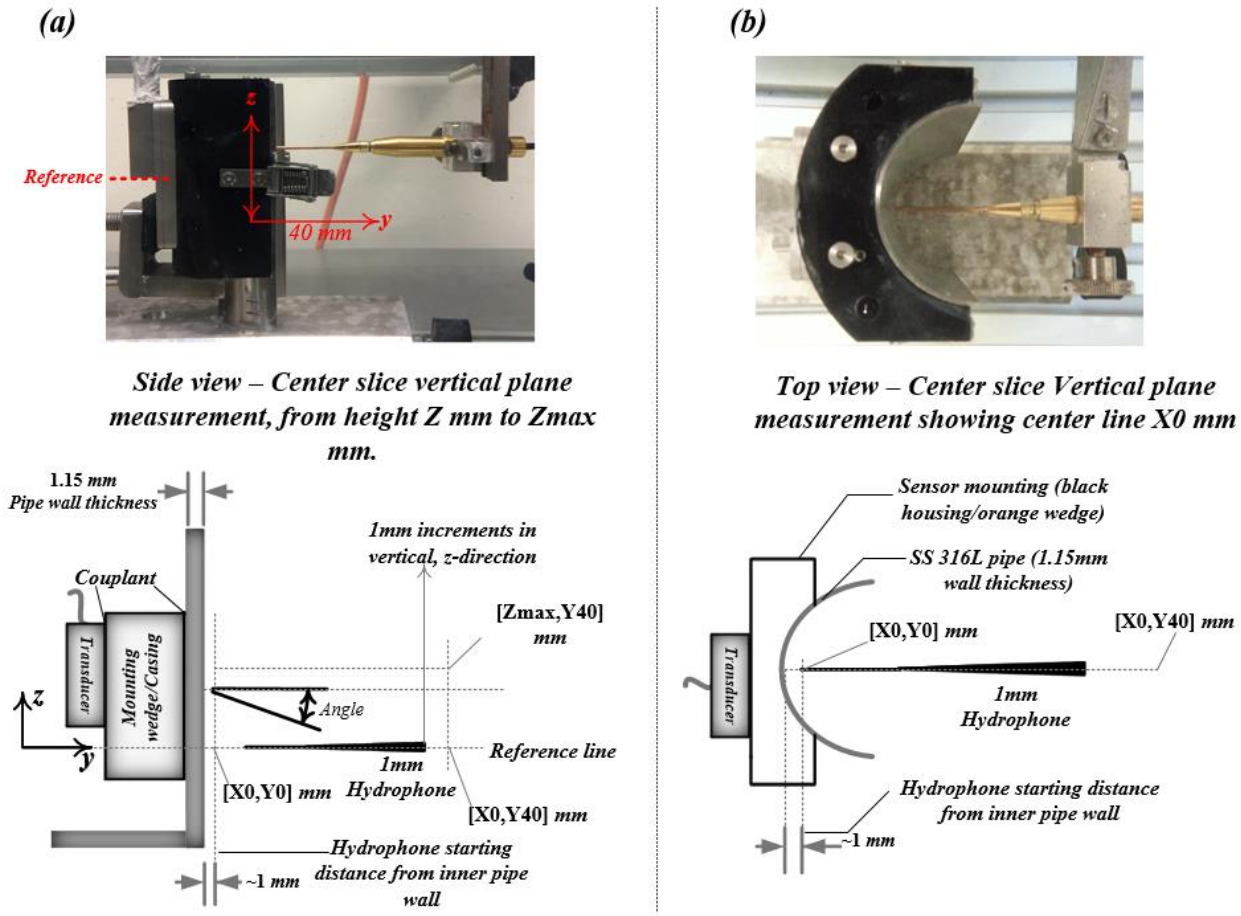

Figure 3.23: (a) Side view schematic of the vertical distance covered in the vertical direction (Z0 to Zmax). (b) top-view schematic of the lateral distance covered (X0-X40) along beam centre line (Y0)

As seen from Figure 3.23, a complete acoustic map is a rectangular grid in the Z-direction, which covers the beam accordingly with particular attention to the focal zone and Doppler angle. Table 3.6 describes the different configurations which were used for the needle hydrophone measurements in water.

Table 3.6: Acoustic characterisation test matrix

Non-invasive Sensor dimensions	Transducer type	†TDX number	Pulser/receiver settings	Couplant TDX-to-wedge	Wedge type	Couplant wedge-to-pipe	Pipe-wall thickness	XYZ-spatial resolution
47.8 mm & 22.4 mm pipe	TYPE-A	(78,79, 80,81)	Pulse length 250ns, Voltage = 100V, Gain = 20dB, PRF 1000Hz	-	-	-	-	1 mm
47.8 mm pipe	TYPE-A	-	Pulse length 484ns, Voltage = 100V, Gain = 20dB, PRF 1000Hz	-	-	-	-	1 mm
47.8 mm pipe	TYPE-A	(78)	Pulse length 250ns, Voltage = 100V, Gain = 20dB, PRF 1000Hz	liquid	prototype	liquid	1.15 mm	1 mm
47.8 mm pipe	TYPE-A	(78)	Pulse length 250ns, Voltage = 100V, Gain = 20dB, PRF 1000Hz	liquid	prototype	liquid + solid-Y + liquid	1.15 mm	1 mm
47.8 mm pipe	TYPE-A	(78)	Pulse length 250ns, Voltage = 100V, Gain = 20dB, PRF 1000Hz	liquid	prototype	liquid + solid-Z + liquid	1.15 mm	1 mm
47.8 mm pipe commercial	TYPE-A	-	Pulse length 250ns, Voltage = 100V, Gain = 20dB, PRF 1000Hz	integrated	industrial	solid-Y	1.15 mm	1 mm
47.8 mm pipe commercial (1 &2)	TYPE-A	-	Pulse length 250ns, Voltage = 100V, Gain = 20dB, PRF 1000Hz	integrated	industrial	liquid	1.15 mm	1 mm
22.4 mm pipe	TYPE-A	(79)	Pulse length 250ns, Voltage = 100V, Gain = 20dB, PRF 1000Hz	solid-X	prototype	liquid	1.38 mm	1 mm
22.4 mm pipe	TYPE-A	(79)	Pulse length 250ns, Voltage = 100V, Gain = 20dB, PRF 1000Hz	solid-X	prototype	liquid + solid-Y + liquid	1.38 mm	1 mm
22.4 mm pipe	TYPE-A	(80)	Pulse length 250ns, Voltage = 100V, Gain = 20dB, PRF 1000Hz	liquid	prototype	liquid	1.38 mm	1 mm
22.4 mm pipe	TYPE-A	(80)	Pulse length 250ns, Voltage = 100V, Gain = 20dB, PRF 1000Hz	liquid	prototype	liquid + solid-Y + liquid	1.38 mm	1 mm
152.4 mm pipe	TYPE-B	-	Pulse length 484ns, Voltage = 100V, Gain = 20dB, PRF 1000Hz	liquid	prototype	-	-	1 mm

†TDX — ultrasound transducer mounted on wedge.

Necessary alignment of the needle hydrophone with the transducer was done to ensure that the needle hydrophone was kept in parallel with the horizontal reference line. This was first done by visual alignment followed by finer adjustments with appropriate alignment instruments (level and ruler). Once the physical alignment of the transducer and needle hydrophone was completed, the test run was started from the control computer.

The pulser/receiver was set to pulse continuously for the duration of the test, whilst a specially developed Matlab® graphical user interface (GUI) program illustrated in Figure 3.24 was used to control the digitizer for acquiring and logging purposes. The Matlab® program made use of the NI-USB 5133 device driver. The acquired voltage data was sampled at 100 MHz. The Matlab® program enabled manual and automatic saving of the voltages measured for each grid point to a mat-file. Post processing code was also written in Matlab® to allow visualisation of the complete acoustic maps of $V_{pk\text{-}pk}$ voltages using appropriate plots and colour mapping to highlight the voltages present in the focal zone and the angle the beam makes with the horizontal reference line at the near-pipe wall.

Figure 3.24 shows the graphical user interface program which was designed to use the National-Instruments (NI-5133) digitizer hardware driver for acquiring the hydrophone signals. A single 2-dimensional acoustic map of the beam took ~2 hours to complete.

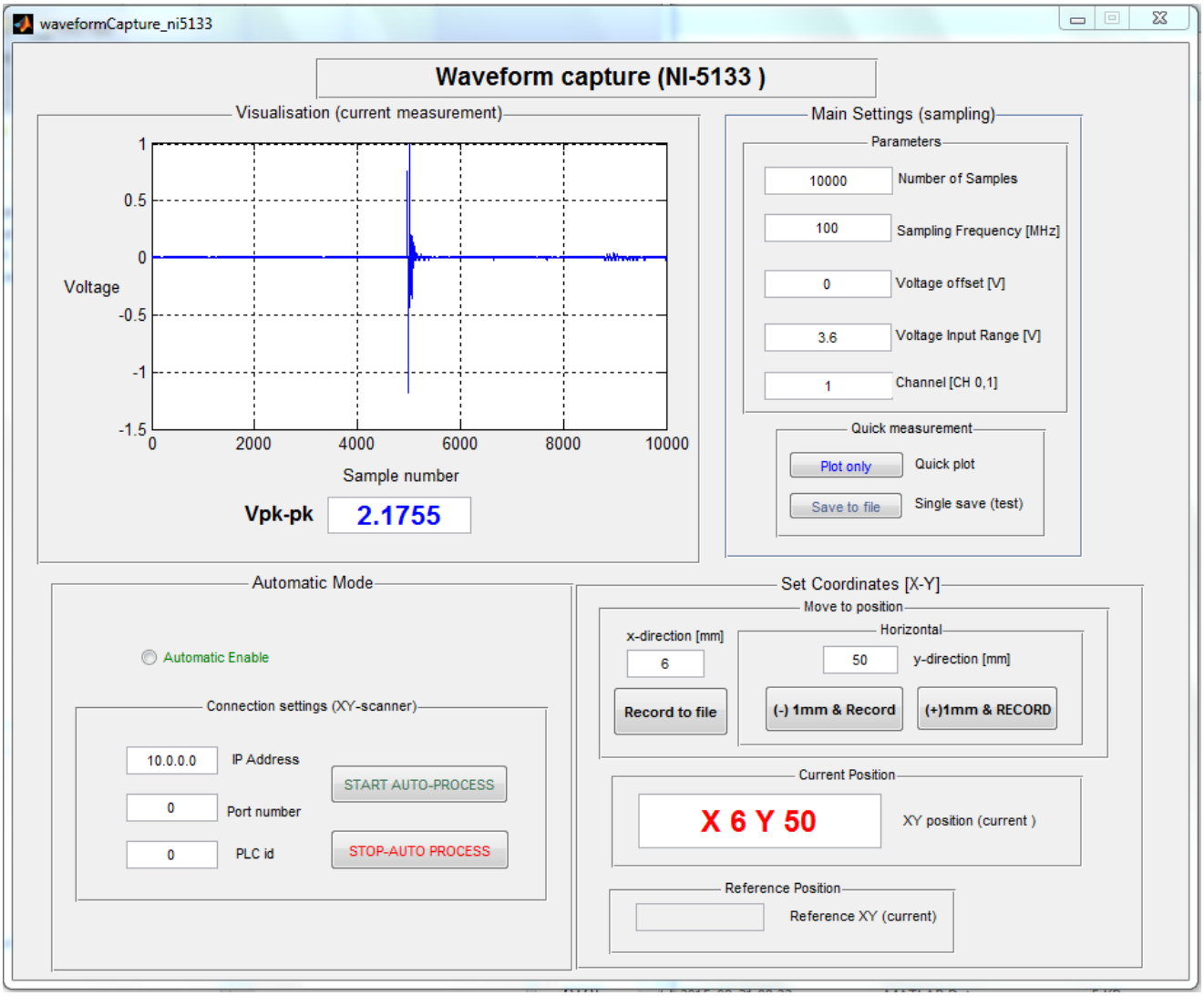

Figure 3.24: Matlab® Graphical User Interface (GUI) used for signal acquisition

3.4. MEASUREMENT UNCERTAINTY AND AGGREGATION OF ERRORS

Several measurement errors are encountered during in-line rheological tests. Errors are composed of contributions from random and systematic errors. Analysis of system errors was carried out with the intention of determining the uncertainties associated with the measured rheological data.

Since the Flow-Viz™ system rheologically characterises industrial suspensions according to a methodology (PUV+PD) which relies on the measurement accuracy of several parameters and measured variables (pressure, temperature, velocity of sound and Doppler angle), it is thus necessary to quantify some of the maximum uncertainties which are likely to arise in these measurements. The procedure for taking combined uncertainties into account can be found in Morris & Langari (2012). Statistically, the most appropriate representation of the maximum error from the addition of different system components is shown in Equation (3.11) (Morris & Langari, 2012).

$$e = \sqrt{(x^2 + y^2)} \tag{3.8}$$

3.4.1. Accuracy and error in measurement instruments

3.4.1.1. Differential pressure measurement accuracy

For the laboratory experiments carried out on the stainless-steel flow loop, the differential pressure measurements were measured using the ABB 265 DR and ABB 266 MRT pressure transmitters. The base accuracy of these sensors is ± 0.04% over the measuring range. As per manufactures datasheet, when proper device setup and operating conditions are adhered to, the maximum error which can result for a set lower range span, is given by the Equation 3.9:

$$\pm \%P_{error} = \pm(0.04 + 0.005 \cdot TD - 0.05)\% \tag{3.9}$$

where (Turn Down ratio) *TD* = *Full-range/set-span.*

For example, with a full range scale of 250 kPa for the ABB 265DR pressure transmitter a measuring span of 20 kPa was used, which corresponds to a turn down ratio of 13. By calculation the (±%P_{error}) is given as:

$$\pm 0.053\% = \pm(0.04 + 0.005(13) - 0.05)\% \quad (3.10)$$

Thus a magnitude error of 10.5 Pa is expected for the 20 kPa span.

3.4.1.2. Flow rate measurement accuracy

Two magnetic flow meters were used for the tests. From the manufacturer datasheets, the base accuracy *(%Q_{error})* of the 35.1 mm & 22.4 mm pipe flowmeter (FM1) is ±0.4% over the measuring range; whereas for the 47.8 mm pipe flowmeter (FM2) the accuracy is stated as ±0.5%.

3.4.1.3. Temperature measurement accuracy

The measuring error of the temperature readings by *Wika* (PT-100) RTDs conforms to the IEC standard (DIN/IEC 60751) (or simply IEC751) as outlined in the data sheet. The magnitude of this measuring error (*%T_{error}*) within the linear (0-600 °C) range is ±0.2%.

3.4.2. In-line tube viscometry measurement uncertainties

The uncertainties in rheological properties determined from tube viscometry are mainly dependent on the accuracy of the flow and pressure measurement instruments. Errors in pseudo shear rate and corresponding shear stress can be approximated by combining the uncertainties in the individual flow and pressure measurements. Approximations to these errors are described using Equations 3.11-3.15

- **Pseudo shear rate error**

The expression for the pseudo shear rate with error is given as shown in Equations 3.11 and 3.12:

$$\dot{\gamma}_{pseudo} = \frac{8V}{D} \pm (\%V_{error} + \%D_{error}) \quad (3.11)$$

$$Since \quad V = Q/A = 4Q/\pi D^2$$
$$\dot{\gamma}_{pseudo} = \frac{32Q}{D^3\pi} \pm (\%Q_{error} + 3(\%D_{error})) \tag{3.12}$$

where Q is the measured value of flow rate in m^3/s, $\%D_{error}$ is the percentage error in the pipe diameter and $\%Q_{error}$ is the percentage error in measured flowrate. To better understand how the individual errors propagate to the final pseudo shear rate value, an example is given.
Within the 47.8 mm ± 0.02 mm ID pipe, (Area = 0.0017945 m^2) a measured flow rate, Q of 0.0017945 m^3/s results in a pseudo shear rate with an error calculated as:

$$\dot{\gamma}_{pseudo} = \frac{32(0.0017945)}{(0.0478)^3\pi} \pm (0.4 + 3 \cdot (0.02/47.8) \cdot 100)\%$$
$$= 167.36\, s^{-1} \pm 0.53\% \tag{3.13}$$

- **Shear stress measurement error**

The shear stress measurement error is also calculated in the same manner, by combining the individual errors from the measurement components (pressure sensor, diameter and pipe length). The calculated wall shear stress with error can be expressed as:

$$\tau_w = \frac{(D \pm \%D_{error}) \cdot (\Delta P \pm \%\Delta P_{error})}{4(L \pm \%L_{error})}$$
$$= \frac{D \cdot \Delta P}{4L} \pm (\%D_{error} + \%\Delta P_{error} + \%L_{error}) \tag{3.14}$$

where ($\%D_{error}, \%\Delta P_{error}, \%L_{error}$) are the individual errors of the diameter, pressure and pipe length. By considering the 47.8 mm pipe test (47.8 mm ± 0.02 mm) section, with length (L = 2.14 m ± 0.02%) and a pressure drop reading of 5.5 kPa, the combined uncertainty in such a measurement would be given by:

$$\tau_w = \frac{0.0478 \cdot 5500}{4(2.14)} \pm (0.04 + 0.053 + 0.04)\%$$
$$= 30.71\, Pa \pm 0.13\% \tag{3.15}$$

The same expression for shear stress error (Equation 3.14) is also applied to shear stress data obtained using the in-line PUV+PD technique.

3.4.3. PUV+PD measurement uncertainties

There are different types of uncertainties which affect PUV measurements, these include the sound velocity which is dependent on temperature, the Doppler angle due to misalignment of transducers, spatial resolution of the PUV system and random errors which are introduced due to the measurement environments and test conditions. The accuracy of pulsed ultrasound velocity measurements relies mainly on two of these measurement parameters which are the Doppler angle θ and the velocity of sound c, in the medium of under test.

The influence of the variation in Doppler angle in the resulting profiles needs to be noted carefully in order to improve overall measurement accuracy. Kotzé et al. (2011) describes the errors in the Doppler angle as directly related to the estimated velocity errors. Based on the reference Doppler angle in Kotzé et al. (2011), an angle error of 30% was seen to introduce corresponding velocity errors of 5%, for a given standard Doppler angle.

The general pulsed ultrasound equations $v = cf_d / 2f_e cos\theta$ and $x = ct/2$ are used to obtain the depth information and the corresponding velocity vector information; where v is the estimated velocity vector, f_e is the emission frequency and f_d is the Doppler frequency.

Since the Flow-Viz™ pulser/receiver has a high ADC resolution and the electronics used to acquire data is reliable as described in Section 3.1.1, it can be assumed that all other errors from these sources (e.g. quantisation error) are negligible. Therefore the major sources of error in the velocities and radial points are then determined by the accuracy of velocity of sound c and Doppler angle θ parameters. In determining the error variation, a standard Doppler angle of 70° was taken as the reference value. This value of the Doppler angle is optimal for non-invasive sensor installations on pipes and is also used with Flow-Viz™ sensors. Figure 3.25 shows how these two parameters affect the radial distances.

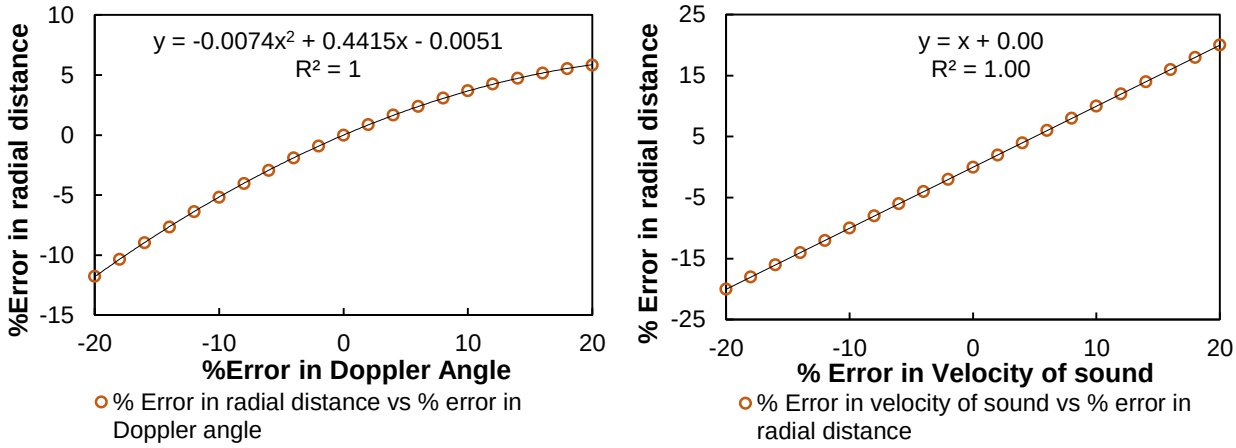

Figure 3.25: Percentage errors in radial distance due to individual errors in (left) Doppler angle and (right) velocity of sound

Figure 3.25 shows that a Doppler angle of 10% results in a ~%4 error in the radial distance and a linear relationship exists for the error in velocity of sound with error in radial distance. The combined effect of the Doppler angle and velocity of sound errors in the radial distance and calculated velocities are then depicted in Figure 3.27. The combined Doppler angle error and velocity of sound errors (e.g. 5% Doppler angle error and 5% velocity angle error) exhibit a positive linear relationship with the resultant radial distance error.

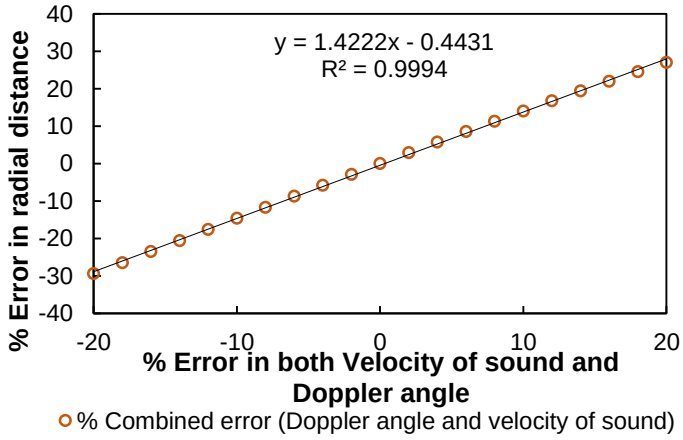

Figure 3.26: Combined effect of the Doppler angle and velocity of sound errors on the radial distance error

Figure 3.26 shows that the effect of combined error (e.g. 2% Doppler angle error and 2% velocity of sound error) has a greater impact on the measured radial velocities especially at higher values of these errors.

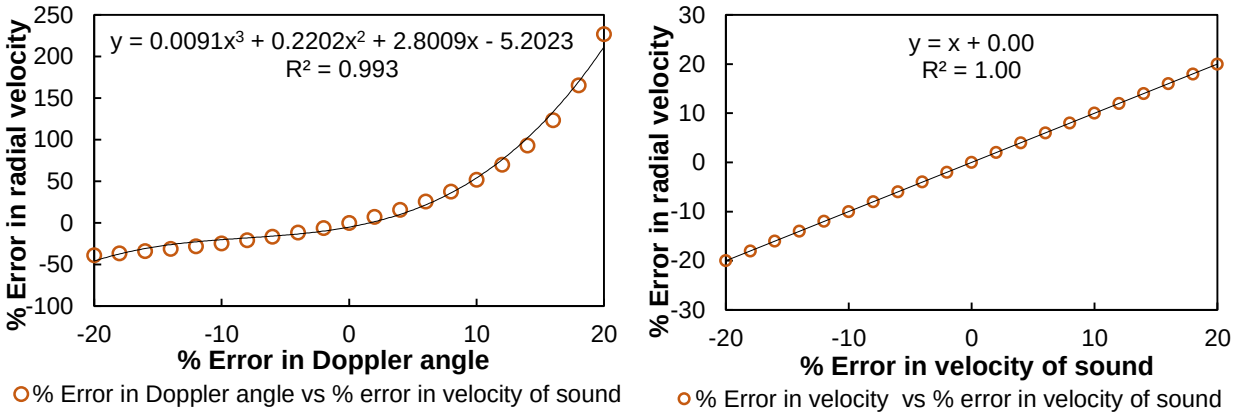

Figure 3.27: Percentage errors in radial velocity due to individual errors in (left) Doppler angle and (right) velocity of sound

Determining the error variation due to the Doppler angle around a different standard value, for example 20° would result in different margins of the velocity error. Also, it should be noted that errors of the same magnitude (e.g. 2% angle error and 2% velocity of sound error and -2% angle, -2% sound velocity error) result in different error values in the aggregated velocity error. These nonlinearities are due to the division with the cosine function in, $v = cf_d / 2f_e cos\theta$. Similar trends in velocity errors due to Doppler angle errors were also noted by (Yamamoto et al., 2006). Figure 3.28 shows the combined effect of the errors from both parameters in the final value of the radial velocity.

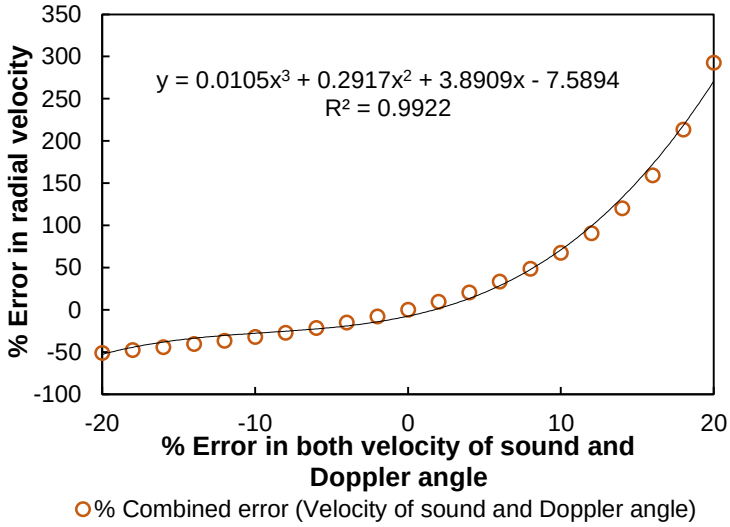

Figure 3.28: Combined effect of the Doppler angle and velocity of sound errors on the velocity error

A non-linear relationship was observed for the errors and a third order polynomial was used to approximate the trend.

- **Shear rate error (direct gradient method)**

The measured profile is used to calculate the radial shear rates of the fluid in pipe flow, by calculating the gradient between adjacent local velocity points as a function of radial distance. The resolution of the radial distance is an important parameter required to calculate the point wise gradient of the velocity profile across the pipe axis. A greater spatial resolution means that there is a more accurate representation of the measured velocity profile, since there are more velocity components defined at closely spaced radial points. However, depending on the signal-to-noise ratio the velocity variations between adjacent points are large which can result in unrealistic shear rates. Methods such as smoothing (averaging) are therefore sometimes used to improve the overall calculation. Based on the gradient method (or non-model approach), the calculation of the shear rate with error values are depicted in Figure 3.29.

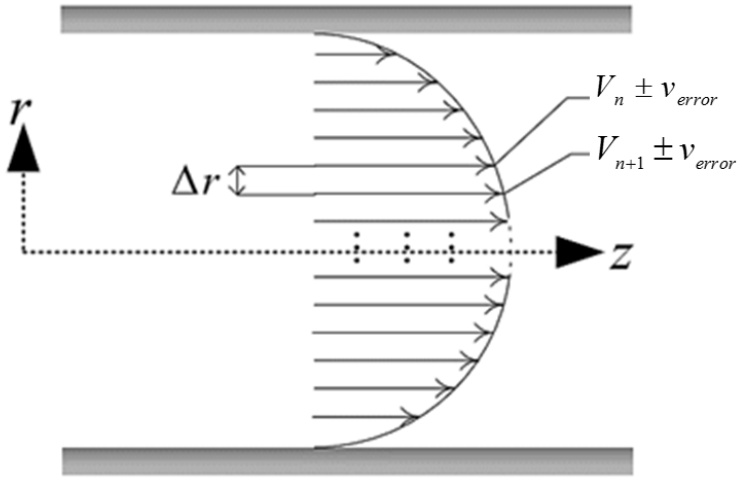

Figure 3.29: Calculation of shear rate error (gradient method)

$$\dot{\gamma}_n = \frac{dV_n}{dr_n} = \frac{\Delta V_n}{\Delta r_n} \tag{3.16}$$

$$= \frac{(V_{n+1} \pm v_{error}) - (V_n \pm v_{error})}{(r_{n+1} \pm r_{error}) - (r_n \pm r_{error})} \tag{3.17}$$

$$= \frac{(V_{n+1} - V_n)}{(r_{n+1} - r_n)} \pm \frac{\sqrt{v^2_{error} + v^2_{error}}}{\sqrt{r^2_{error} + r^2_{error}}}, \tag{3.18}$$

$$= \frac{(V_{n+1} - V_n) \pm v_{total\ error}}{(r_{n+1} - r_n) \pm r_{total\ errror}} \tag{3.19}$$

where ΔV_n is the forward difference between two consecutive is mean velocity vectors and Δr_n is the radial points at which the velocity vectors are defined. The errors v_{error} and r_{error} are assumed to be the same throughout the whole profile. Subscript *n* denotes the radial point position from the pipe-wall (zero) to the centre. An approximation to the maximum possible error in the shear rate is then given by combining the errors in the quotient $\dot{\gamma} = \Delta V / \Delta r$ as shown in Equation 3.20.

From Equation 3.18 the errors in the radial velocity, i.e. $v_{total\ error}$ and radial point $r_{total\ error}$ yield a shear rate error of:

$$\dot{\gamma}_{error\_\max} = \pm(v_{total\ error} + r_{total\ error}) \tag{3.20}$$

The relationships between the errors in velocimetry parameters (Doppler angle, velocity of sound) and errors in radial distance and velocity are described (Figure 3.25 - Figure 3.29), and their combined effect in the calculated radial shear rate is also presented in Figure 3.30.

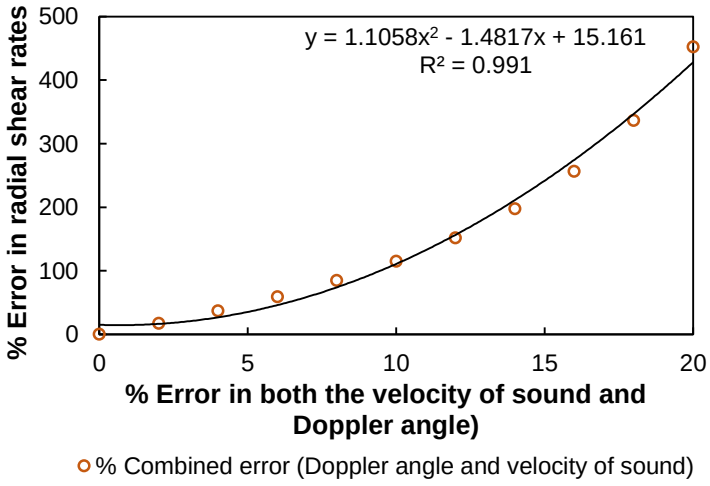

Figure 3.30: Combined effect of the Doppler angle and velocity of sound errors on the shear rate

An example to show how the velocity error and radial error due to a (2% error in Doppler angle and velocity of sound) influence the shear rate error is as follows:

With a standard Doppler angle of 70° and a velocity of sound in water of 1480 m/s, a 2% error in both the Doppler angle and velocity of sound would result in radial and velocity errors of 9.37% and 2.88% respectively (i.e. using Equation 2.30 and 2.32). Assuming the radial distance and velocity errors obtained in the calculation are constant throughout the measured velocity profile, the errors for two consecutive radial points are combined using root of sum of squares as shown in (Equation 3.21).

$$\pm \frac{v_{error}}{r_{error}} = \frac{\sqrt{{v_1}^2{}_{error} + {v_2}^2{}_{error}}}{\sqrt{{r_1}^2{}_{error} + {r_2}^2{}_{error}}} = \frac{\sqrt{2 \cdot (9.37)^2}}{\sqrt{2 \cdot (2.88)^2}} \tag{3.21}$$

By using Equation 3.20 the combined error is $\dot{\gamma}_{error\_\max} = \pm 17.33\%$.

- **Pulser settings (repetitions and pulse length)**

Other important factors which influences the measured profile is the number of repetitions which are used and the pulse length used to obtain the final profile. Adjusting the pulse length to a shorter one increases the spatial resolution, and thus the number of velocity point defined across the pipe radius. The optimum number of repetitions of pulses sent and received to obtain the final profile needs to be noted for each fluid to improve some the measurements. Birkhofer (2007) noted that increasing the number of repetitions to improve the average profile does not consistently improve the final measured profile.

- **Wall position**

With the Flow-Viz™ system the wall gate can be set automatically or manually entered by the user based on visual profile data. The location of the wall position is one major source of error in the determination of rheometric properties. Wiklund et al. (2007), showed that the by changing the wall position by one gate (less than 0.5 mm) the rheometric properties could be significantly altered. Selection of the wall gate was done by using both manual and automatic methods in order to optimise the measured profiles.

3.5. PRACTICAL CONSIDERATIONS IN EXPERIMENTAL TESTS

Some adjustments were made in order to carry out the practical tests with more accuracy and consistency.

3.5.1. Tube viscometry practical considerations

Data acquisition for all sensors on the stainless steel flow loop was carried out by averaging 10000 samples at a rate of 1000 Hz. This means the read-out time was 10 seconds. This averaging with many sample points (10000) gave a better representation of the mean values from each sensor. Additionally, logging of measurement data was carried out at least every 2-3 minutes to cater for the random fluctuations which occur especially with the pressure measurements when the steady state of the current flow/shear-rate has not been reached.

The orientation of the remote seals was that they were at ~90° to the pipe axis (sideways) as shown in Figure 3.31. This was done to prevent air bubbles from settling inside the small space close to the remote seals. Measurement difficulties with the occurrence of pressure off-sets were encountered and these were minimised by using this form of measurement configuration. For highly concentrated suspensions such as bentonite (> 7% w/w) the fluid was first circulated continuously around the pipe loop with the mixer on for at least 10 minutes to obtain a consistent mix as well as to further eliminate trapped air.

Figure 3.31: Horizontal orientation of remote seals (trapped air elimination)

A glass window was placed in line with the test pipe section. The window enabled visual inspection to ensure the pipe is filled during measurements. Figure 3.32 shows an image of the glass window next to the downstream pressure connection point.

Figure 3.32: Stainless-steel flow loop glass window for in-line visual inspection

To measure the differential pressure (high pressure port – low pressure port) of the test fluid on the flow loop, proper mounting and zeroing of the pressure transmitters was observed prior to the measurement. The following steps were taken to ensure correct zeroing of the transmitters which use remote seal technology:

i. The pressure transmitter was first fastened to the pipe using tri-clover clamps.
ii. Secondly, the pipe was then emptied of fluid by using suction (reverse pumping). This step removes any pressure applied on the seals by fluid before the actual test.
iii. The zeroing of the transmitter was then carried out as a final step to eliminate additional pressure applied whilst fastening the seals.

After the pressures transmitters were zeroed the fluid was then circulated within the pipe loop to ensure that the pipe is fully filled. In cases were the same transmitter was used in different pipes the procedure was repeated to ensure uniformity and eliminate pressure offsets in measurement data.

3.6. SUMMARY OF METHODOLOGY AND EXPERIMENTAL PROCEDURES

All measurement apparatus was discussed accordingly within the relevant sub-sections. The experimental procedures set as guidelines to facilitate optimal measurements were then outlined for both in-line techniques (PUV+PD and tube viscometry).Calibration tests were performed to ensure reliable and accurate test equipment was used. In a similar manner the acoustic characterisation test materials and setups were described in detail. Sources of error for the experimental measurements were also described. The experimental results which were obtained by implementing the procedures outlined in this chapter, are presented in Chapter 4.

CHAPTER FOUR: EXPERIMENTAL RESULTS AND ANALYSIS

4.1. INTRODUCTION

Results from the acoustic characterisation tests of non-invasive ultrasound sensor technology developed by Flow-Viz™ are presented. The aim of these experiments was to evaluate how the ultrasound beam properties change depending on different installation methods and acoustic coupling configurations used for mounting the sensors onto high grade stainless steel pipes. The results from the experiments are displayed graphically as two dimensional acoustic maps with particular attention to the location of the focal zone, length of focal zone, ultrasound beam angle and maximum intensities.

The Flow-Viz™ in-line rheometric system described in Chapter 3, Section 3.1.1 was evaluated and validated against conventional tube viscometry. Three model fluids with different concentrations were used for the in-line tests. Velocity profile measurements and rheological data for Carboxymethyl cellulose (CMC), kaolin clay and bentonite are presented. The PUV+PD measurements were carried out using the ultrasound transducer parameters (beam/Doppler angle) which were determined from the acoustic characterisation tests.

4.2. ACOUSTIC CHARACTERISATION OF NON-INVASIVE ULTRASOUND SENSOR TECHNOLOGY

The acoustic maps presented for both the vertical configuration and the single sensor characterisation tests show the peak to peak voltage ($V_{pk\text{-}pk}$) measured at each spatial point within the two-dimensional scanning area covered by the high precision XYZ-scanner.

4.2.1. Acoustic characterisation of ultrasound transducer technology

Four TYPE-A prototype transducers were characterised together with one TYPE-B transducer. The test conditions and pulser/receiver settings used are presented in Table 4.1.

Table 4.1: Test parameter for single sensor characterisation tests

Transducer type	Transducer number	Pulser Settings			
		Excitation pulse length [ns]	Voltage [V]	Gain [dB]	PRF [Hz]
TYPE-A prototypes and commercial for 47.8 mm pipe	78, 80	250	100	20	1000
TYPE-A prototypes for 22.4 mm pipe	79, 81	250	100	20	1000
TYPE-B prototypes for 152.4 mm pipe	-	484	100	20	1000

A spatial resolution of 1 mm was chosen to navigate throughout the spatial grid since it was observed through measuring that improving the resolution to 0.5 mm did not make a significant change between adjacent points for most positions across the entire grid. The same spatial resolution was used in similar tests by used by Kotzé et al. (2013). The temperature throughout the tests was ~21-22 °C.

Figure 4.1 shows the acoustic maps measured for the prototype transducers numbered 78, 79, 80 and 81. The acoustic maps for transducers with the same design i.e. (78 and 80) and (79 and 81) show major similarities especially in the shape of the focal zone.

(a)

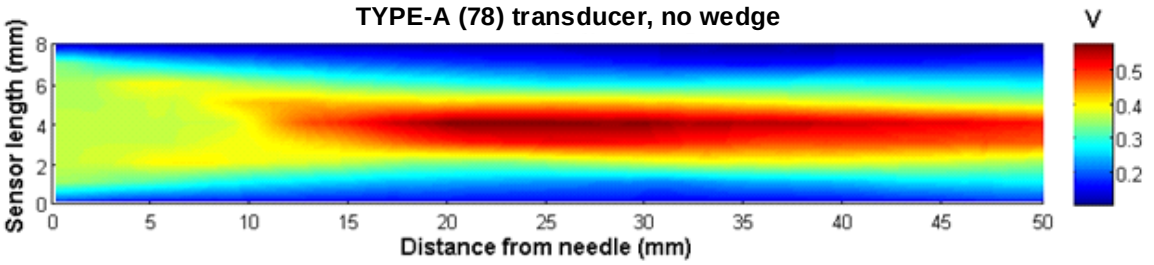

(b)

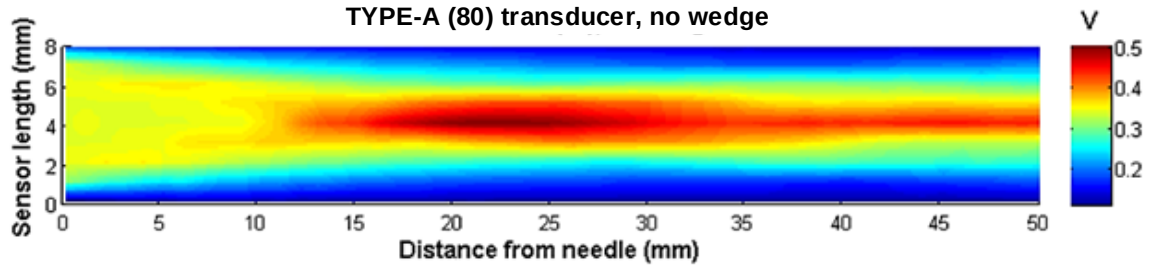

(c)

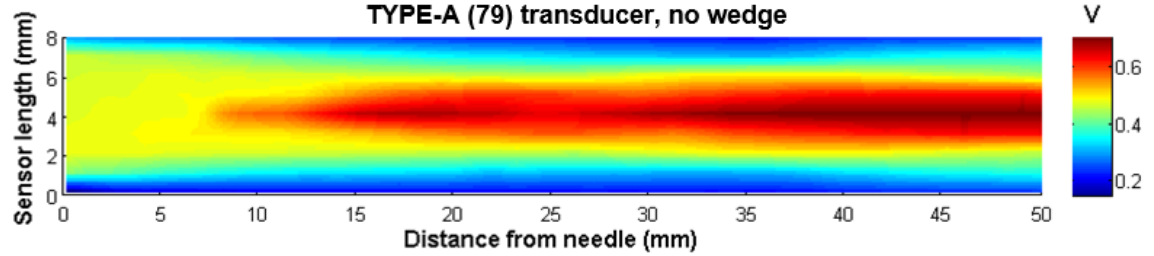

(d)

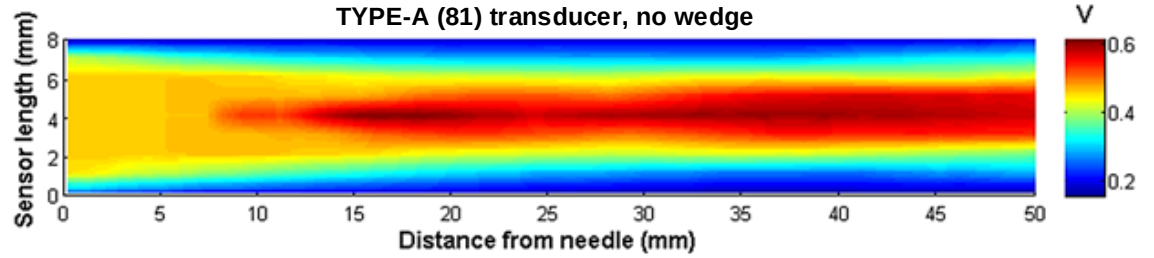

(e)

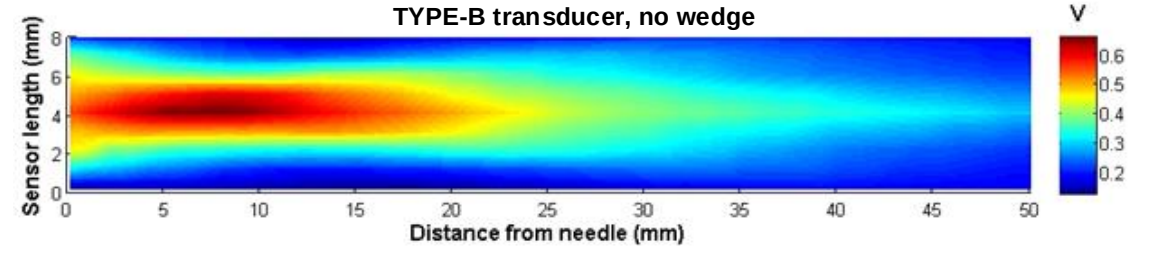

Figure 4.1: Single transducer acoustic maps for the TYPE-A transducers (a) and (b) with the same wafer design; (c) and (d) have the same design (e) TYPE-B transducer

The single transducer characterisation tests for all TYPE-A transducers show that the beam profiles are mostly centred and symmetrical across the scanning area. From
Figure 4.1 (a) and (b) the focal zone is seen to start at ~16 mm and is narrower from position ~35 mm onwards as compared to sensors 79 and 81 which show a much wider focal zone and higher energy throughout the whole acoustic map. The characteristic extended focal zone length which was seen for transducers 79 and 81 is more desirable as it allows greater penetration to provide more detailed velocity information even in highly attenuating suspensions such as kaolin.

The TYPE-B transducer (for 152.4 mm pipes) acoustic map showed a symmetrical beam over the scanning area where the maximum beam energy was located. By observing the length of the focal zone as well as the beam energy, it can be seen that these measured properties are not as expected for the TYPE-B transducer. The reduced energy and shorter focal length are due to the pulse length setting of 484 ns. This excitation pulse length was not optimised for the transducer frequency and was due to the limitations of the pulser/receiver electronics. A pulse length of 714 ns would have been the optimal setting with capable pulser/receiver electronics. Further tests are therefore required for the TYPE-B transducer.

4.2.2. Acoustic characterisation of non-invasive sensor technology

The non-invasive transducers were attached to a stainless steel pipe cut in half in order to observe the difference in the beam shape after the wall interface and also the effects of different couplants i.e. individual liquid and solid couplants, as well as their combined effect. The method of attaching the couplants and the vertical pipe tests is explained in Chapter 3, Section 3.3.3. Physical reference points on the sensor i.e. along the vertical axis of scanning grid where marked and these are shown by the zero (0 mm) point on each acoustic map. The reference points show the orientation of the beam relative to actual sensor position.

The schematic in Figure 4.2 illustrates the arrangement of the acoustic couplants used on the ultrasound transducer-to-wedge interface as well as the wedge-to-pipe mounting for all vertical pipe measurements. This schematic also shows how the beam presented in the acoustic maps for the vertical pipe tests is oriented relative to the sensor unit i.e. for all pipe tests the sensor unit position is to the left of the acoustic map; and the 0 mm marking on the *vertical movement* axis is the reference position on the physical sensor unit. The reference positions were discussed in Section 3.3.5.1.

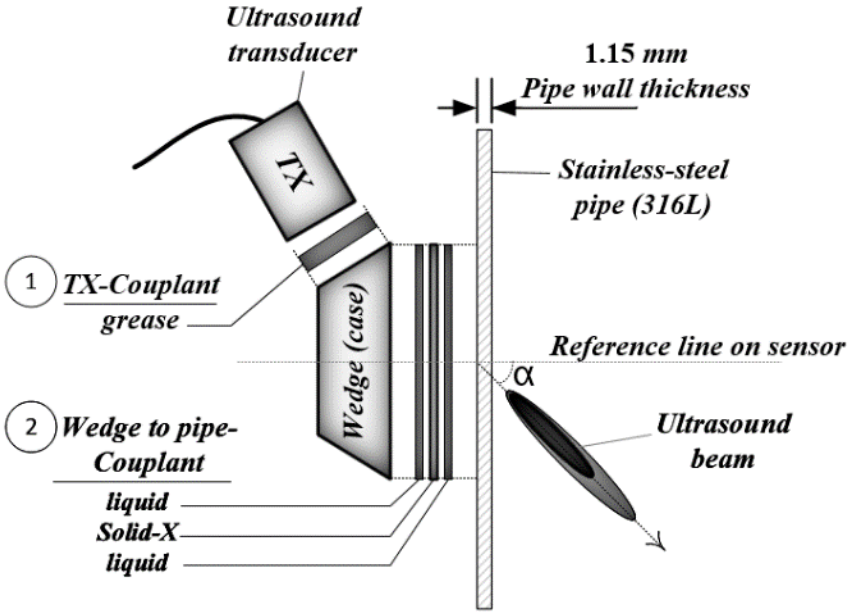

Figure 4.2: Schematic of the transducer *(TX)* and wedge to pipe couplants

The beam angle measured from the horizontal line which is parallel to the reference line is shown on each acoustic map. This angle (α) is of relevance to PUV measurements as it is used to calculate the Doppler angle (see Chapter 2, Section 2.3.3.2). The same pulser/receiver settings and test conditions shown in Table 4.1 were used for the pipe tests. Two pipes were used for the tests, with wall thicknesses of 1.15 mm for the 47.8 mm pipe and 1.38 mm for the 22.4 mm pipe. The complete test matrix which includes these dimensions is given in Section 3.3.5.

4.2.2.1. TYPE-A (78) – prototype wedge sensor configuration for 47.8 mm pipe

A liquid couplant was used for the transducer-to-wedge mounting. However, three different types of wedge-to-pipe couplants (liquid, liquid with solid-Y and liquid with solid-Z) were used. The configuration in Figure 4.2 describes the test setup, where the reference line is shown as the 0 mm mark on the vertical axis *(vertical movement (mm))*. The beam angle measured from this physical reference point (0 mm) is also shown in Figure 4.3.

(a)

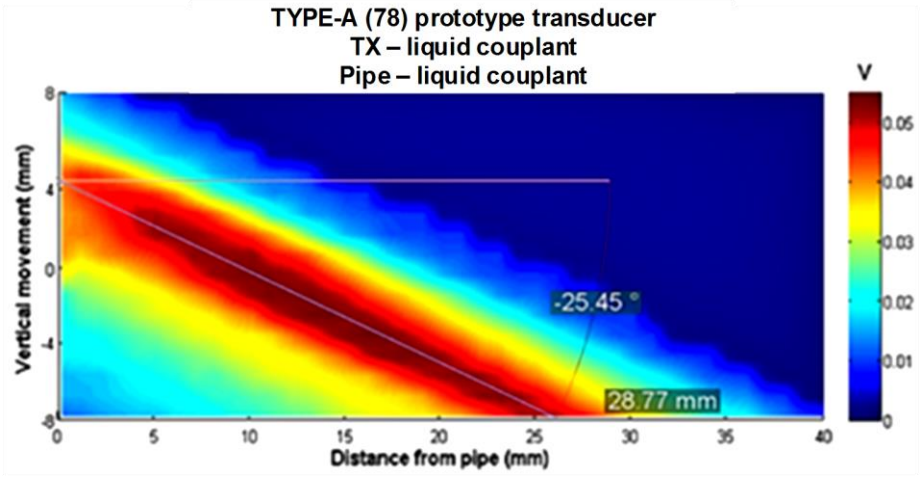

(b)

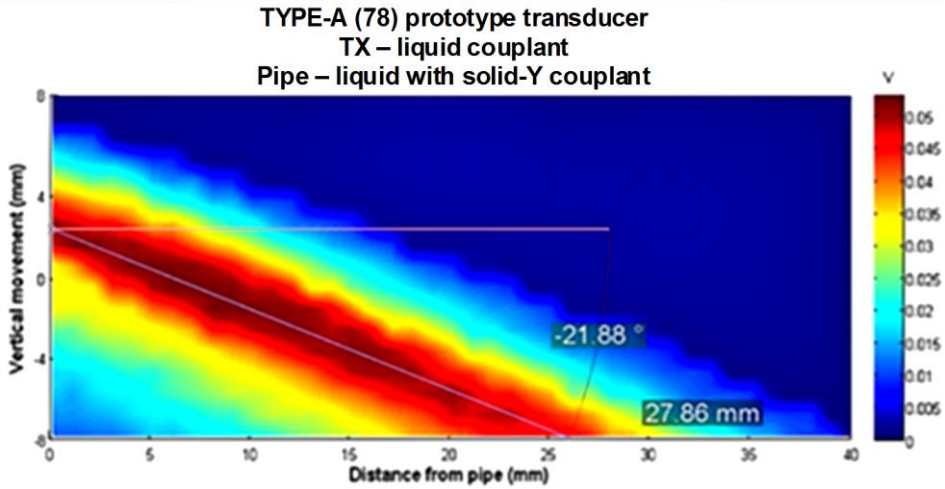

(c)

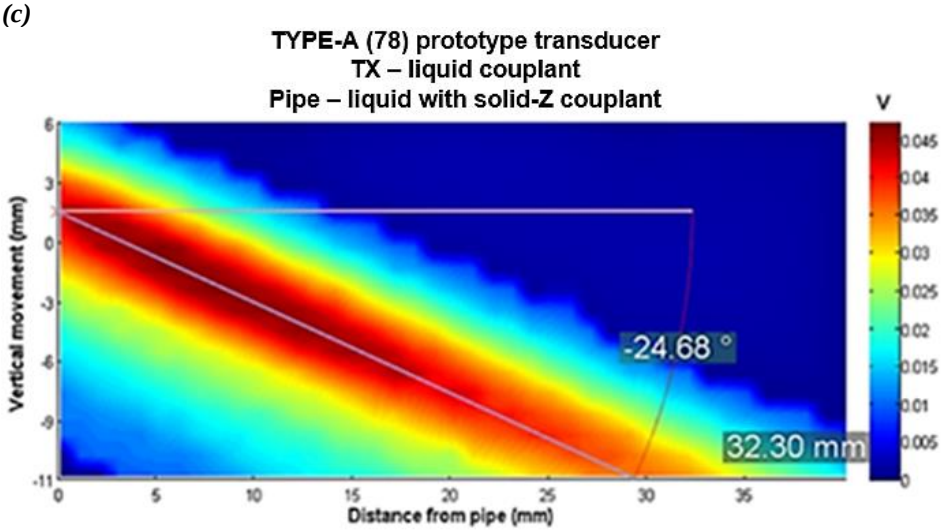

Figure 4.3: Acoustic maps for 47.8 mm (78) sensor attached to prototype wedge with (a) only liquid couplant (b) liquid and solid-X couplant (c) liquid and solid-Z couplant on pipe

Figure 4.3 (a) shows that with the liquid wedge-to-pipe couplant, the focal zone starts at a distance of approximately 5 mm from the inner pipe wall. Regarding the configurations which had the solid couplants, the focal zone was situated at the pipe liquid-wall interface. The beam angle using the liquid couplant only was ~25.45°, which was more than that of the combined solid and liquid couplants. The maximum voltages ($V_{pk\text{-}pk}$) recorded within the focal zone for (a) and (b) were 55.1 mV and 53.3 mV, respectively. The maximum voltage of 47.2 mV at the focal zone was measured with the solid-Z couplant. The acoustic map of the solid-Z couplant shows that the focal zone length covers ~17 mm which is less than the 47.8 mm ID pipe radius of 23.9 mm. The ideal focal zone from the resulting beam should be as narrow as possible and extend to cover over half of the pipe radius. The beam should also start as close as possible to the pipe inner wall, in order to improve the overall accuracy of the measured velocity profile.

By analysing the resulting acoustic maps in Figure 4.3 it can be seen that the setup with the solid-Z couplant resulted in the most undesirable beam of the three configurations since the focal zone length (~20 mm) is less than the pipe radius (23.9 mm). The most preferable beam with regards to the length and location of the focal zone is that measured from the combined liquid and solid-Y couplant. The focal zone is both close the pipe wall and extends over half the pipe radius similarly to the liquid only configuration in Figure 4.3 (a), despite having less energy than the latter.

However after taking into account the measured beam properties, the most appropriate setup for industrial application and installation is the one which utilises the liquid only couplant. The liquid only couplant is stable at high temperatures as it undergoes insignificant changes in physical properties (acoustic properties) compared to the solid couplant which cannot sustain high temperatures. Furthermore the solid couplant tends to slightly shift position during installation, which is not convenient for industrial applications where stable and less complex installations are required. This result also gives insight to the adjustments which need to be considered in the development of the next generation of non-invasive sensors. Desirable characteristics from both the liquid couplant i.e. thermal durability and from the solid-Y couplant i.e. having a focal zone which starts at the pipe wall would be effective if they are embedded in a compact sensor unit.

4.2.2.2. TYPE-A (79) – prototype wedge sensor configuration for 22.4 mm pipe

A different transducer-to-wedge couplant in the form of solid-X material was used. Solid-X couplant has a thickness which is approximately half that of solid-Y. The combined liquid and solid-Y couplants were then used for the wedge-to-pipe mounting. Figure 4.4 shows the beam properties of the two different non-invasive sensor configurations.

(a)

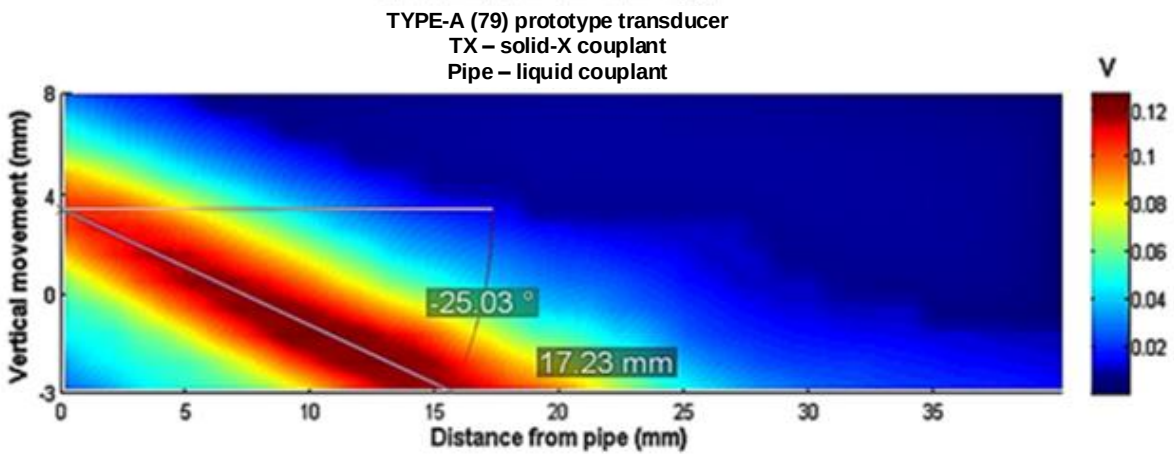

(b)

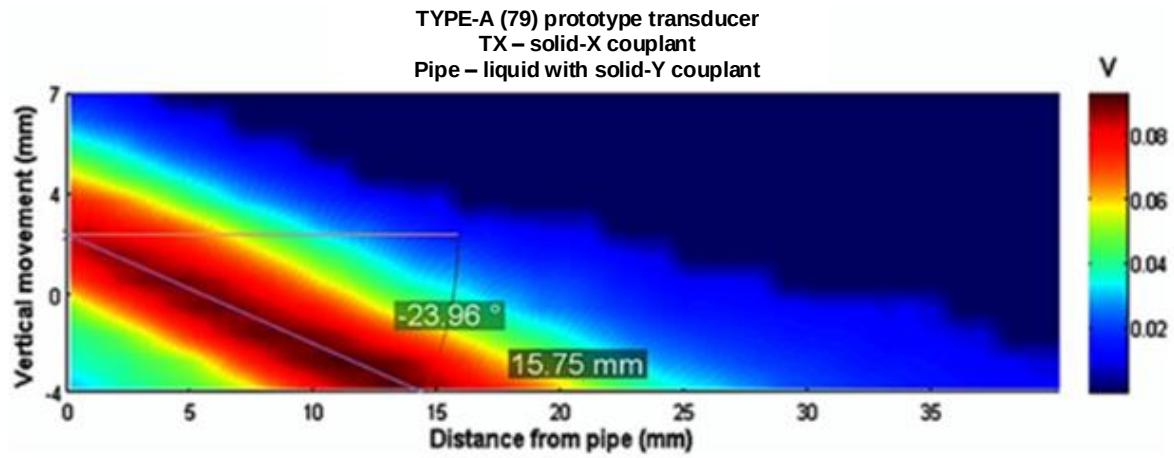

Figure 4.4: Acoustic maps for22.4 mm pipe (79) sensor attached to prototype wedge with (a) only liquid couplant (b) combined liquid and solid-Y couplant on pipe.

By comparing the current result in Figure 4.4 and that shown in Figure 4.3, the location of the focal zone in the resulting beams was similar with regards to the wedge-to-pipe couplant used. It

can be seen that with the combined solid and liquid couplant at the pipe, the focal zone is closer to the pipe wall and the beam angle is reduced compared to having the liquid couplant only.

The significant increase in energy in the vertical pipe test shown in Figure 4.4 with transducer 79 is mainly attributed to the thin solid-X couplant between the transducer and wedge interface. By comparing the maximum voltages (V_{pk-pk}) obtained with the solid-X couplant with those from the previous setup (Figure 4.3) in which the liquid couplant was used for the transducer to wedge coupling, it can be observed that the voltages are almost doubled. The maximum voltages within the focal zone for Figure 4.4 (a) and (b) were 127 mV and 93 mV, respectively, whereas those from the transducer-to-wedge liquid couplant were in the range of ~53-55 mV. Since the high energy output with solid-X was an exception when compared to the other solid couplants, it must be pointed out that the transducer (79) with the thin solid-X couplant had a different design compared to transducer 80, which could also be another contributing factor for the increased energy output (see

Figure 4.1).

Altogether, the thin solid-X couplant proved to be an effective transducer-to-wedge couplant since the resulting beams offer significantly higher energies in the focal zone across the whole pipe radius. This result also shows that alternating couplants between the wedge-to-pipe and transducer-to-wedge interfaces can significantly improve the resulting beam properties due to improved acoustic matching. Despite the notable increase in energy, the solid couplant still has the major drawback of not being suitable for use in high temperature environments as well as difficulty of installation. Thus it would be a great advancement to use this data in the development of a new coupling fixture which includes a fixed solid couplant and also improved the thermal protection to cater for high temperature industrial environments.

4.2.2.3. TYPE-A (80) – prototype wedge sensor configuration for 22.4 mm pipe

Tests with TYPE-A (80) transducer, were conducted, in order to determine whether a more optimal beam could be obtained using a liquid couplant on the transducer-to-wedge interface. The result was that, with the TYPE-A (80) transducer for 22.4 mm pipes in Figure 4.5, similar beam properties with sensor 79 in Figure 4.4 were observed. The similarity was that the wedge-to-pipe couplant with solid-Y moves the focal zone closer to the pipe wall and results in a smaller angle (24.75°) compared to the liquid couplant alone (27.16°). The acoustic maps are displayed in Figure 4.5.

(a)

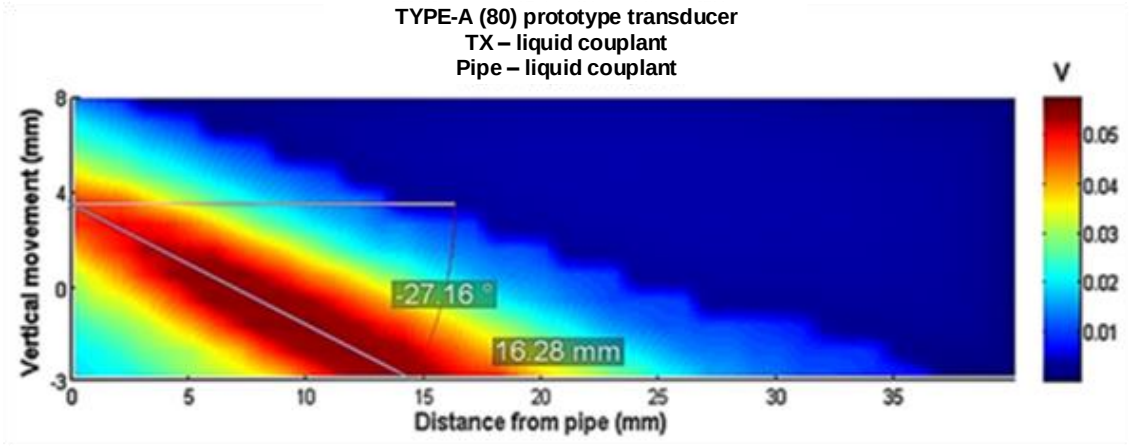

(b)

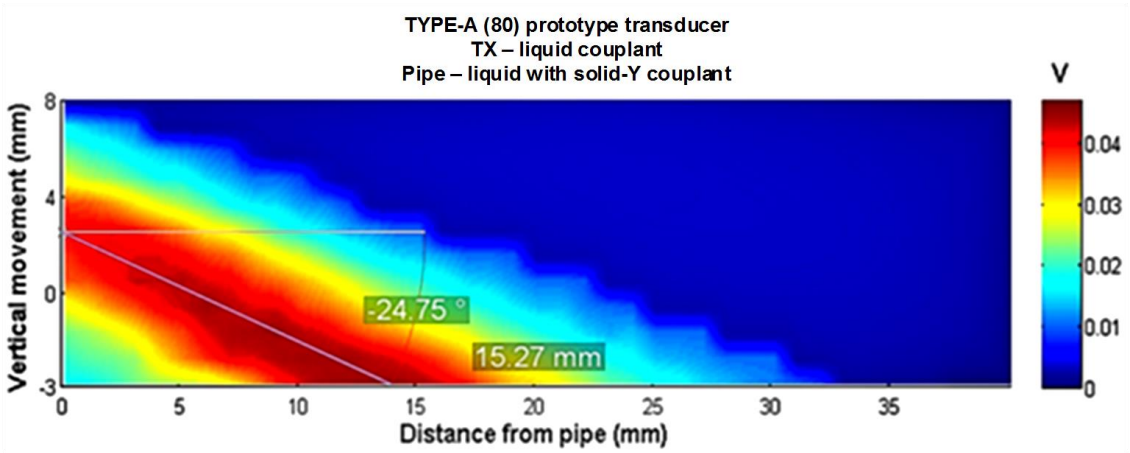

Figure 4.5: Acoustic maps for 22.4 mm pipe (80) sensor attached to prototype wedge with (a) only liquid couplant (b) combined liquid and solid-Y couplant on pipe.

A notable difference in the peak energy measured in the focal zone for the two tests was that with the solid-Y couplant at the wedge-to-pipe interface the maximum voltage was 57.7 mV whereas with the liquid only couplant less energy 47.2 mV was recorded.

Another observation was that the beams from both setups are not entirely symmetrical. The lower half of both beams (bottom left corner of acoustic maps) looks much wider than the top half in the top left corner. The beams in both setups have a focal zone which spans the entire pipe radius which is of great importance in order to determine the fluid properties from the velocity profile more accurately.

4.2.2.4. TYPE-B – prototype wedge configuration for 152.4 mm pipe

The acoustic maps from the 152.4 mm pipe transducer and prototype wedge configuration are shown in Figure 4.6. The first acoustic map in (a) was obtained with the 152.4 mm TYPE-B transducer attached to a wedge optimised for the 47.8 mm stainless steel pipe (liquid was used as the coupling material between the pipe and wedge). The result in (b) was from the measurement configuration using only the transducer and a 152.4 mm pipe wedge with no stainless steel pipe. These two tests were carried out since there was no readily available 152.4 mm stainless steel pipe spool piece similar to the ones used for the 22.4 mm and 47.8 mm transducers. However, the wedge used in Figure 4.6 (b) was optimised for a 152.4 mm pipe.

(a)

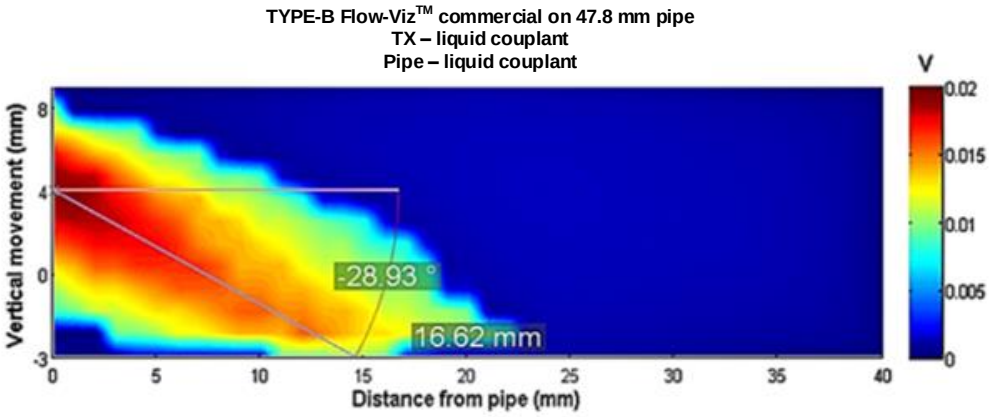

(b)

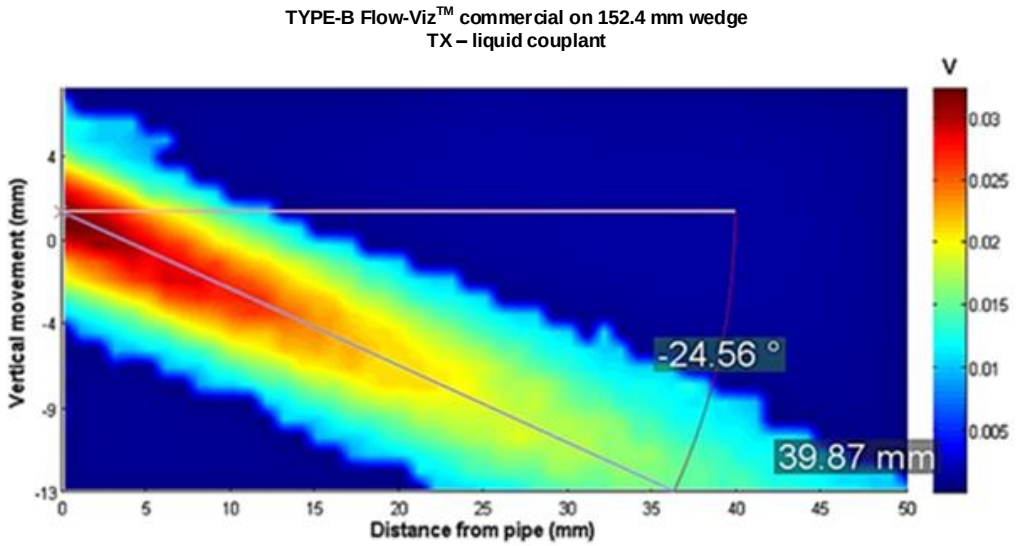

Figure 4.6: Acoustic maps for 152.4 mm pipe sensor attached to prototype wedge with (a) only liquid couplant on 47.8 mm pipe (b) no pipe attachment.

The focal zone for the setup in (a) with the pipe is at the pipe wall. For the setup with the wedge only the focal zone starting point is directly at the wedge wall. For both sensor setups the beams are more or less symmetrical. The sensor in Figure 4.6 (a) on the 47.8 mm wedge makes a much wider angle with the sensor reference line at 0 mm line, than the one attached to the 152.4 mm wedge.

The focal length in both setups appears to be shorter than expected for this 152.4 mm transducer. The angle the beam make with the horizontal is approximately 28.93°, covering a length of ~15 mm of the inner pipe diameter.

This result could be due to the setup in which the 152.4 mm pipe did not have any liquid couplant or pipe attachment. The reduced energy in both setups was due to the excitation pulse length limitation of the pulser/receiver electronics (see Section 4.2.1). Further tests need to be done with this sensor setup in order to validate the current focal zone and beam properties. Despite the significant reduction in beam energy (~30 mV peak), the overall beam shape agrees quite well with previous measurements from the 47.8 mm and 152.4 mm sensors.

4.2.2.5. TYPE-A – Flow-Viz^{TM} commercial sensor configuration for 47.8 mm pipe

The latest non-invasive Flow-Viz^{TM} commercial clamp-on sensor was tested with an integrated transducer-to-wedge couplant optimised for 47.8 mm pipes. This design requires only coupling material between the sensor unit and stainless steel pipe. Two couplants were used i.e. the liquid couplant and solid-Y couplant. Figure 4.7 depicts the measured acoustic maps obtained using the two different wedge-to-pipe coupling materials.

(a)

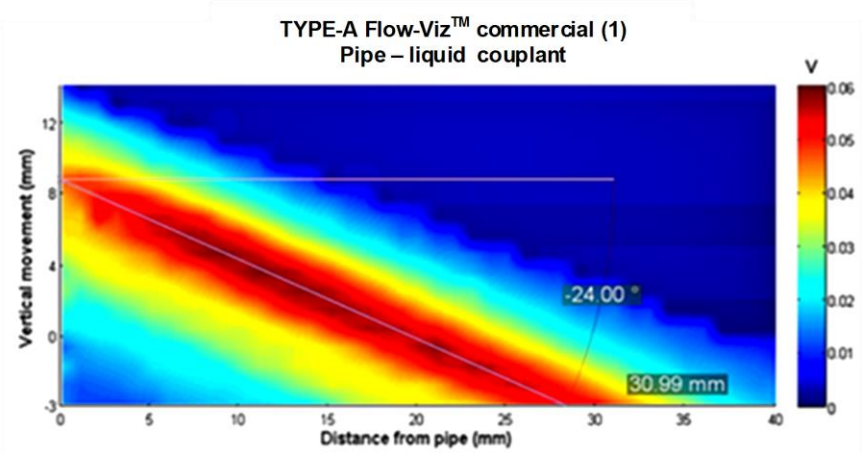

(b)

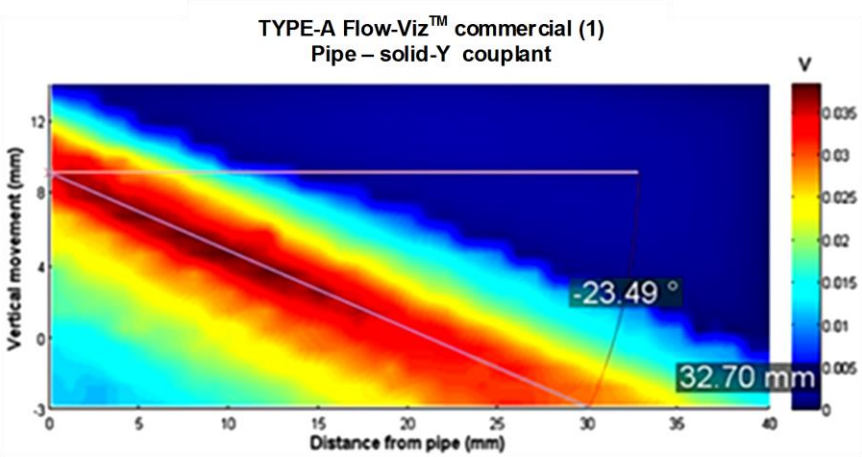

(c)

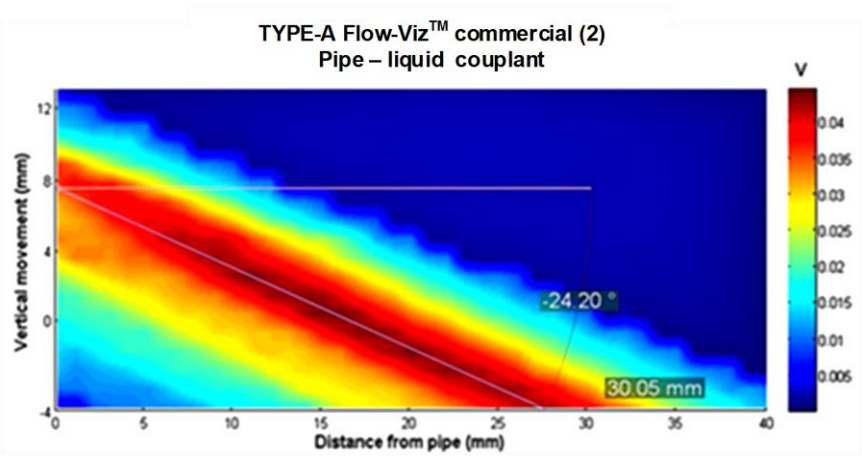

Figure 4.7: 47.8 mm Flow-Viz™ commercial sensor 1 with (a) liquid couplant and (b) solid-Y couplant at wedge-to-pipe (c) Flow-Viz™ commercial sensor 2 with liquid couplant at wedge-to-pipe interface

In order to test the quality and consistency of the Flow-Viz^{TM} manufacturing process two identical non-invasive sensors were tested and compared as shown Figure 4.7 (a) and (c). The beam shape are more similar than not, with focal zone length which extend to cover a horizontal length of ~27 mm which is more than the 47.8 mm with pipe inner centre at (23.9 mm). The difference in the measured peak energies between (a) and (c) can be attributed to slight differences in the test conditions, however by noting the similarities in the beam angles 24.00° and 24.20° as well as the focal zone lengths the overall measurement shows consistent designs.

These results are similar to the results obtained using the prototype wedge with regards to the position of the focal zone when solid-Y couplant is used in the wedge-to-pie position. With the liquid couplant alone, the focal zone starting point was located at approximately 5 mm from the pipe wall, with an angle of ~24° for both sensor 1 and sensor 2, shown as (a) and (c). The beams from this setup appeared to be slightly asymmetrical (wider towards the bottom left corner). The measurements showed that even with the integrated transducer-to-wedge couplant the effects of the wedge-to-pipe couplant are still similar as with the prototype sensor presented in Sections (4.2.2.1-4.2.2.3) and should thus be considered in the design of new sensor units.

By considering the beam energy across the length of the focal zone it can be observed that the liquid couplant is a more effective couplant than the solid couplant with the new Flow-Viz^{TM} sensor unit. The solid couplant seems to have more attenuating effects within this setup. As previously stated, the solid couplant is not suitable for high temperature conditions, thus the liquid couplant proves to be more reliable and versatile.

4.2.2.6. TYPE-A sensors – comparison of Flow-Viz^{TM} commercial and prototype configuration

After conducting the tests for 22.4 mm, 47.8 mm and 152.4 mm sensor configurations, a comparison of the 47.8 mm prototype and the Flow-Viz^{TM} was then carried out. The 47.8 mm sensor units were chosen for the comparison since 47.8 mm pipe-lines are more common in industrial setups compared to 22.4 mm ones. The other reason for this comparison was that, the 47.8 mm version of the commercial Flow-Viz^{TM} is a recent design and by comparing it with a 47.8 mm prototype more knowledge on the properties of the resultant beam through stainless steel is gained and future sensor designs can be improved. Figure 4.8 illustrates the comparison.

(a)

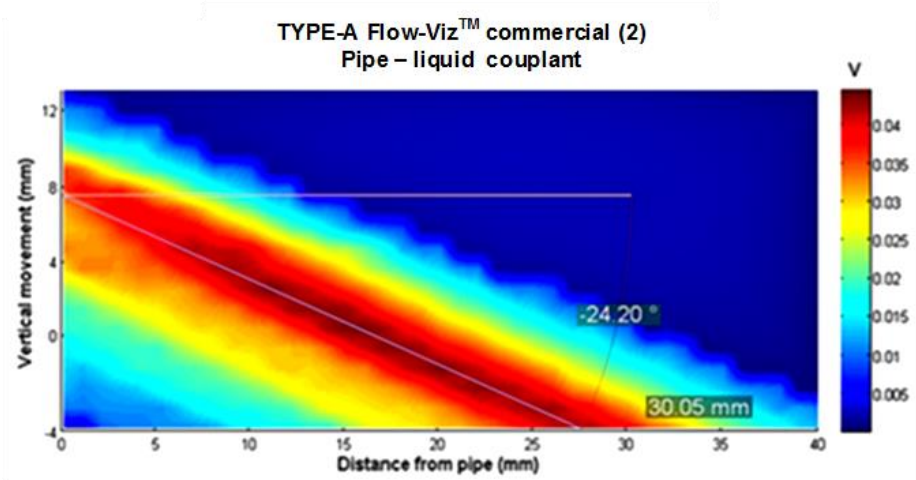

(b)

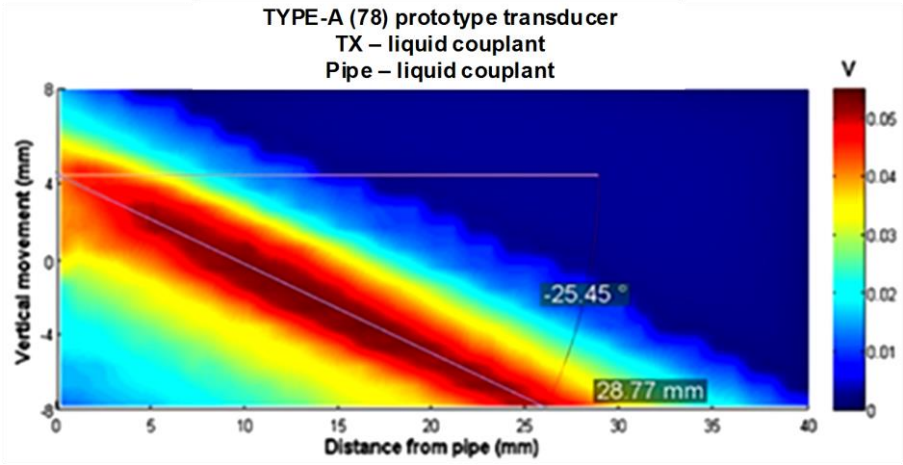

Figure 4.8: A comparison of the 47.8 mm (a) Flow-Viz™ commercial and (b) prototype sensor configuration with liquid wedge-to-pipe couplants.

It can be seen that the beam properties from the two different sensor units have slight differences in the shape of the focal zone as well as the beam angle. The focal zone shape for the commercial sensor is narrower but has the same width throughout the acoustic field, compared to that of the prototype wedge configuration which starts off wide and narrows (from ~20mm onwards) with distance. The narrower focal zone seen in the commercial sensor is more preferable as it increase lateral and spatial resolution.

The final comparison presented is important as it summarises the outcome of the acoustic characterisation of the non-invasive sensor technology through stainless steel. The acoustic test results give a better understanding of the how important couplants are in non-invasive sensor

technology. By changing between configurations with different solid couplants i.e. solid-X, solid-Y and solid-Z and combinations with liquid couplant it was seen that the shape, starting point and length of the focal zone can be significantly altered and thus have major impacts on the quality of the measured velocity profiles. From most of the tests it was seen that a solid couplant attenuates the beam significantly more than the liquid couplant and it conveniently draws the focal zone starting point to the pipe wall to increase the near wall accuracy of measured profiles. However, an exception was observed were higher energy was measured with the setup in which a thin filmed solid-X couplant was used as the transducer-to-wedge couplant. On the other hand the liquid couplant at the pipe interface is less attenuating and results in a focal zone which extends over the entire pipe radius. Table 4.2 and Table 4.3 summarise the results from the vertical pipe acoustic characterisation tests.

Table 4.2: An overview of the main properties of the acoustic couplants

TYPES OF ACOUSTIC COUPLANTS AND PROPERTIES			
Couplant type	**~Thickness of couplant**	**High temperature tolerance**	**Ease of installation**
Solid-X	*(< 1 mm)*	*low*	*low*
Solid-Y	*(2 mm max.)*	*low*	*low*
Solid-Z	*(2.5 mm)*	*low*	*low*
Liquid	*Thin film (< 1 mm)*	*High (slow drying)*	*high*

For solid couplants, regular checks on fastening required to eliminate air gaps and maintain accurate measurements. Installation surfaces to be cleaned thoroughly before application (Sanderson & Yeung, 2002).

Table 4.3: The effect of different sensor configurations on the resultant beam (vertical pipe tests)

NON-INVASIVE SENSOR BEAM PROPERTIES (STAINLESS STEEL PIPE)							
Sensor type	**Installation position (interface)**		**~Start of focal Zone from pipe wall [mm]**	**~Peak energy [mV]**	**Length of focal zone extends to pipe centre**	**~Doppler angle [°]**	**†Rating**
	TX-to-wedge	**Wedge-to-pipe**					
TYPE-A (79) 22.4 mm pipe	solid-X [2]	liquid [1]	3 [3]	127 [1]	YES [1]	65.0	8
	solid-X [2]	solid-Y + liquid [2]	0 [1]	93 [1]	YES [1]	66.0	7
TYPE-A (80) 22.4 mm pipe	liquid [1]	liquid [1]	3 [3]	57.7 [2]	YES [1]	65.0	8
	liquid [1]	solid-Y + liquid [2]	1 [2]	47.2 [3]	YES [1]	66.0	9
TYPE-A (78) 47.8 mm pipe	liquid [1]	liquid [1]	4 [4]	55.1 [2]	YES [1]	65.6	9
	liquid [1]	solid-Y + liquid [2]	0 [1]	53.3 [2]	YES [1]	68.1	7
	liquid [1]	solid-Z + liquid [4]	0 [1]	47.2 [4]	NO [4]	65.3	14
TYPE-A commercial 47.8 mm pipe (1)	liquid [1]	liquid [1]	5 [4]	60.3 [2]	YES [1]	66.0	9
TYPE-A commercial 47.8 mm pipe (1)	liquid [1]	solid-Y [3]	0 [1]	38.5 [4]	NO [4]	66.5	13
TYPE-A commercial 47.8 mm pipe (2)	liquid [1]	liquid [1]	5 [4]	44.6 [3]	YES [1]	65.8	10
TYPE-B commercial 152.4 mm pipe (1)	liquid [1]	liquid [1]	0 [1]	20.1 [4]	NO [4]	61.1	11
TYPE-B commercial 152.4 mm pipe (2)	liquid [1]	-	0 [1]	32.4 [4]	NO [4]	65.4	10

† Rating — the superscript rating values show how well the sensor setup performed for each of the properties which were evaluated. The rating of each property (column) is as follows: [1] Excellent, [2] Good, [3] Average and [4] Poor. The sensor setup with the **LOWEST** overall score shows the most suitable coupling configuration.

Table 4.3 summarises the effect of the different couplants on the resultant beam properties. Each sensor coupling configuration is rated based on different properties which are: the measured beam focal zone properties (start of focal zone, length of focal zone and peak energy [mV]), the couplant's temperature tolerance and ease of installation (described in Table 4.2).

The rating of each sensor configuration was carried out by assigning the ratings of: [1] Excellent, [2] Good, [3] Average and [4] Poor, for each property (column) which was evaluated. For example, a rating of one ([1]) was assigned to the setups with solid-X couplant in the *peak energy* column, since they resulted in the most focal zone energy compared to other sensor setups. The ratings for the couplants (*installation position*) at the different interfaces were based on the couplant's temperature tolerance and ease of installation (Table 4.2). The final rating score of each sensor setup was obtained by summing the singular scores obtained from the evaluation of each column attribute. Thus, the lowest overall score per row determined the most suitable sensor configuration.

The most preferable setup which had the highest intensity and a focal zone starting at the inner wall interface had the solid-X couplant on the transducer-to-wedge interface. However as previously mentioned this setup has a major drawback of using the solid couplant which is not suitable for use in high temperature and extreme industrial conditions. The most optimal setup considering the effect of operating conditions and ease of installation is that which utilises the liquid couplant at both interfaces or has direct integration between transducer and wedge. The acoustic energy from the liquid couplant at both interfaces also provided sufficient energy throughout the pipe radius.

These results will be used to further improve the existing non-invasive sensors. Future designs will consider integrating the acoustic properties of solid-X at the transducer-to-wedge interface, as the couplant resulted in the most energy across the focal area. The improved sensors will also have integrated coupling properties to adjust the focal point start position to be at the inner wall when using the liquid couplant at the wall interface. Based on these results the liquid couplant as a more reliable and versatile, the liquid couplant was used for the in-line rheology tests on the stainless steel flow loop which is presented in Section 4.3.

4.3. EVALUATION OF FLOW-VIZ^{TM} SYSTEM FOR IN-LINE RHEOLOGICAL CHARACTERISATION OF NON-NEWTONIAN FLUIDS

In-line rheological tests were performed using the stainless steel flow loop which comprised of three pipe test sections with inner pipe diameters of 22.4 mm, 35.1 mm and 47.8 mm. Two *(high and low)* concentrations of each of the fluids representing Power-law, Herschel-Bulkley and Bingham type fluids were used in order to fully evaluate the capabilities of the Flow-Viz^{TM} system for fluids with a wide range of viscosities. The Flow-Viz^{TM} sensor technology was installed onto the 47.8 mm stainless steel pipe. Results obtained using the Flow-Viz system were compared to those obtained using conventional tube viscometry. Tube viscometry results (pseudo rheograms) can be found in Appendices A.1 - A.3.

The test fluids and their concentrations are shown in Table 4.4. Two concentrations were chosen as they allow reliable testing of the measurement capabilities of tube viscometry and PUV+PD within the same fluid. By having a more dilute and more concentrated mixture of the same fluid, major inconsistencies in the measurement capabilities of the Flow-Viz^{TM} technology can be observed and analysed.

Table 4.4: Fluids used for in-line tests with different concentrations

Fluid	Concentrations used [%w/w]
Bentonite	7.48 and 5.4
Carboxymethyl cellulose (CMC)	7.70 and 5.16
Kaolin	38.40 and 30.79

4.3.1. Carboxymethyl cellulose (CMC) 7.7 %w/w

CMC is a model fluid that can be rheologically described using the Power-law model (see Chapter 2, Section 2.2.4). The test conditions which include the temperature, flowrates and pressure differences were all recorded with the instrumentation described in Chapter 3 (Section 3.2.2). The test procedure started off by tube viscometry measurements at different flowrates. The acquired data was then used to instantaneously plot the pseudo rheogram. The PUV+PD measurements were then taken concurrently in the 47.8 mm ID pipe test section in order to ensure constant test conditions for both measuring techniques. The test conditions for both in-line tests are shown in

Table 4.5.

Table 4.5: Test conditions for CMC 7.7% w/w

Temperature [°C]	Slurry density [kg/m^3]	Re_2 [-]	ΔP/L [kPa/m]	ΔP Length [m]	Magnetic Flow-meter [L/min]	Velocity Profile [L/min]	% difference in flow rate
21	1044	119	2.638	2.14	83.5	81.3	2.6

The Flow-Viz^{TM} unit can also be used to measure the flow rate of the test fluid. Table 4.3 shows a 2.6% difference when comparing to a magnetic flow meter. This percentage difference is within acceptable range based on previous research presented in Wiklund et al. (2007) and this shows that the Flow-Viz^{TM} unit can be reliably used as a flow metering instrument.

The Flow-Viz system offers a user interface to select and input the ultrasound parameters to optimise the velocity profile measurement depending on the test fluid. Table 4.6 shows the PUV parameters used for the test.

Table 4.6: Parameter settings used for PUV measurement in CMC 7.7 %w/w

c [m/s]	PRF [kHz]	Voltage gain [dB]	Velocity estimator	N_{rep}	Rheometric Method	Number of Cycles
1538	123.75	35	FFT	128	gradient	5

The points obtained from individual pipes were all co-linear showing that no wall slip was present during the tests. These results can be found in Appendix A.1.

The complete rheogram after applying the Rabinowitsch-Mooney transformation (described in Appendix C.1) is then presented and compared with the results obtained using the Flow-Viz^{TM} instrument (PUV+PD technique). Figure 4.10 shows the comparison for CMC 7.7% w/w.

The in-line rheological properties are determined using the velocity profile measured in the laminar flow regime. The rheogram is calculated by combining the pressure drop data and the shear rates obtained by applying the gradient method on the measured velocity profile.

The Doppler spectrum is shown in Figure 4.9. A Fast Fourier transform velocity estimator was used to compute the radial velocities and a smoothing filter was used to minimise noise fluctuations in the resulting velocity profile.

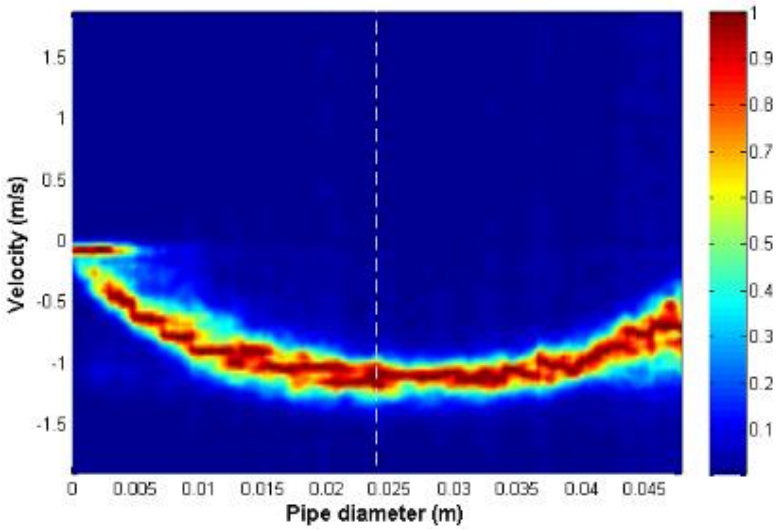

Figure 4.9: Power-spectrum for the velocity profile measurement, CMC 7.7%w/w

The power spectrum also shows that no significant energy losses of the ultrasound beam were presented by the CMC solution as seen from the normalised power distribution which is in the range (0.7-1) across the entire pipe diameter. A good profile was measured since CMC does not attenuate the ultrasound beam significantly. The power spectrum is expected to be symmetrical about the pipe axis however multiple reflections from the opposite wall occur and result in higher velocities instead of zero velocities at the wall. To eliminate this artefact the power spectrum is cropped at the opposite wall location and the first half of the profile at the near wall is used for calculations. The region of interest was the inner diameter of the 47.8 mm pipe.

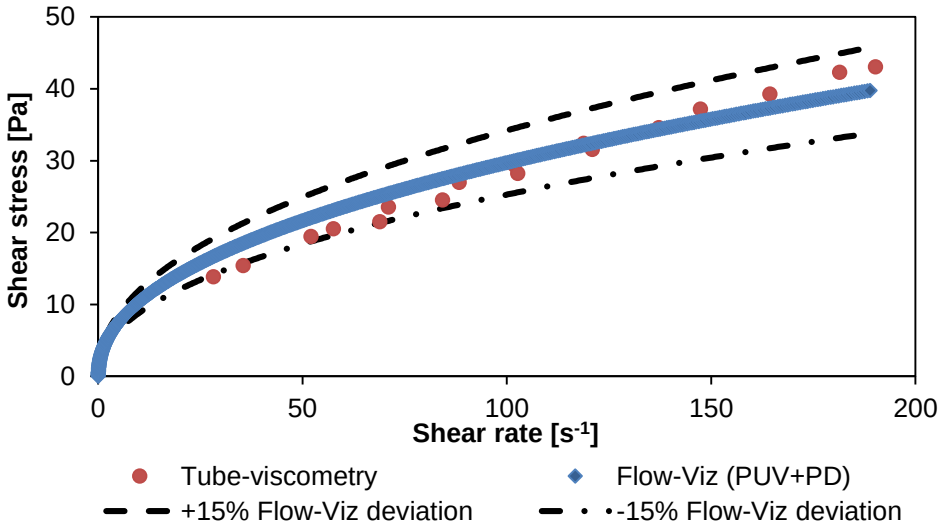

Figure 4.10: CMC 7.7 %w/w rheogram, comparison of tube-viscometer and Flow-Viz (PUV+PD)

The rheogram in Figure 4.10 shows an acceptable agreement of within ±15% for the whole shear rate range. This magnitude of percentage deviation was also noted for similar solutions, as presented in previous research work (Kotzé et al., 2008).

The rheograms agree better at higher shear rates (>100 s^{-1}) than at lower shear rates. The limitation of system components (lower range limit of pressure and flow transmitters) limits the in-line measurement of rheological properties at lower shear rates using the tube viscometry technique. However, the Flow-Viz™ instrument could measure and provide quantitative rheometric properties of the CMC solution at very low shear rate values (< 1 s^{-1}). Table 4.7 summarises values of the flow behaviour index *n*, and the corresponding consistency value *K* obtained from the two in-line techniques. These values were determined from the model based curve fitting procedures. The Power-law model was used as it gave a higher R^2 value to characterise the data over the shear rate range.

Table 4.7: Rheological parameters obtained from the two in-line techniques for CMC 7.7 %w/w

Parameters	Flow-Viz^{TM} (PUV+PD)	Tube viscometry
***K* [Pa.s^n]**	3.40	1.56
***n* [-]**	0.5	0.6

Differences in the calculated rheological parameters between the two in-line techniques are shown in Table 4.7. The differences are due to the mathematical curve fitting procedures which were used to obtain these values. The curve fitting procedures are aimed at reducing the overall error between the fitted model and the actual measurement values. Since the measurements from the Flow-Viz^{TM} instrument cover more points in the lower shear rate range where the tube-viscometer does not, there are bound to be notable differences. In addition, the rheological parameters calculated are dependent on the shear-rate range covered by the technique used. It is therefore important to compare the rheological characteristics over the same shear rate range covered by both techniques.

4.3.2. Carboxymethyl Cellulose (CMC) 5.16 %w/w

The second concentration of CMC used for the in-line tests was a more dilute mixture, with a relative density of 1.029 kg/m^3. The test conditions and the Flow-Viz^{TM} settings are given in Table 4.8 and Table 4.9.

Table 4.8: The test conditions for CMC 5.16 %w/w

Temperature [°C]	Slurry density [kg/m^3]	Re_2 [-]	ΔP/L [kPa/m]	ΔP Length [m]	Magnetic Flow-meter [L/min]	Velocity Profile [L/min]	% difference in flow rate
~19	1029	612	0.607	2.14	84.6	81.3	4

Table 4.9: Parameter settings used for PUV measurement in CMC 5.16 %w/w

c [m/s]	PRF [kHz]	Voltage gain [dB]	Velocity estimator	N_{rep}	Rheometric Method	Number of Cycles
1513	123.75	35	FFT	128	gradient	5

The temperature recorded during the test runs did not fluctuate by more than 2°C from the mean whilst the average pressure drop per meter across the 47.8 mm pipe test section was 2.64 kPa/m. The pseudo rheogram from the tube viscometry test is presented in Appendix A.1, illustrating that the no wall slip was observed during the test. Similarly to the more concentrated CMC solution, a good agreement (4%) in the measured flow-rate was noted.

The velocity profile measurement is shown in Figure 4.11. A similar parabolic velocity profile shape can be seen when compared to the profile obtained in CMC 7% w/w.

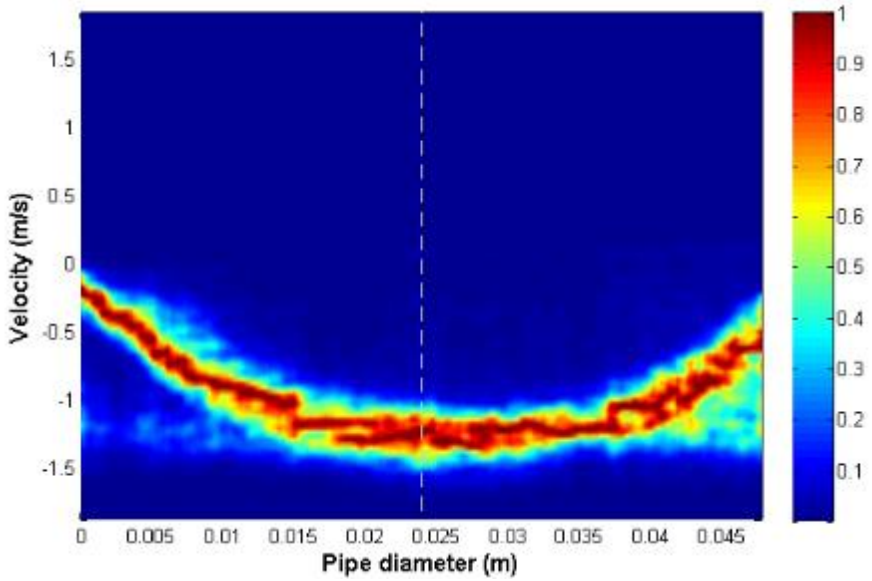

Figure 4.11: Power-spectrum for the velocity profile measurement, CMC 5.16%w/w

CMC did not attenuate the ultrasound energy significantly, as good signal-to-noise ratios were present. This can be seen in the spectrum image in Figure 4.11 where the acoustic energy was transmitted throughout the pipe diameter without much attenuation, except at distances towards the opposite pipe wall (0.04 m onwards). Figure 4.12 shows a comparison of the rheology obtained using the two in-line techniques.

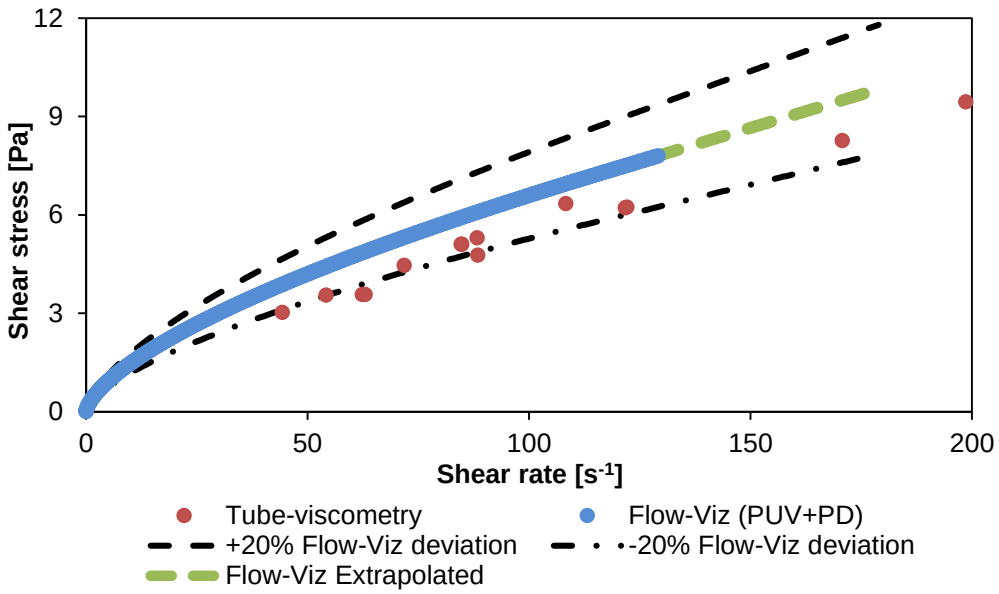

Figure 4.12: CMC 5.16 %w/w rheogram, comparison of tube-viscometer and Flow-Viz (PUV+PD)

Typical shear thinning behaviour of the CMC can be observed from the curvature of the plot.

The lowest shear rate measured using the tube-viscometer was ~40 s^{-1} which is much more than that measured using the Flow-Viz™ instrument (< 1 s^{-1}). The agreement between the data points over the shear rate range was about -20%. The ±20% deviation curves are shown in the rheogram as a measure of how good or acceptable the difference in is for the two techniques. With reference to previous research by Kotzé et al. (2008) which presents similar comparisons, a ±15% deviation was observed for CMC. This margin of deviation is expected since the two techniques determine the rheological properties based on different calculation i.e. the true shear rates for Flow-Viz™ are based on direct gradient method applied on the measured velocity profile. A single rheometric measurement with the Flow-Viz™ takes at most 2 minutes whilst that by the tube-viscometer requires about 30 minutes and during this time the flow conditions would not be the same. By observing the Flow-Viz™ data, it can be seen that there is a significant difference in the shear-rate range covered by the flow-curve which tends to be much less than that measured by the tube-viscometer. This is mainly due to the limitation of the pseudo shear rates which can be obtained in the 47.8 mm pipe test section and pump capability. The smaller pipes which offer higher shear-rates were only part of the tube viscometry measurements but were not used for the PUV+PD measurements. Although extrapolation of rheological data is not widely recommended

the shear rate range from (150 s^{-1} onwards) of the Flow-Viz^{TM} data using the originally obtained Power-law trend was done to clearly illustrate the graphical comparison of the two techniques.

Table 4.10 depicts the rheological parameters as measured by each technique. The rheological parameters were also determined from model based curve fitting using the same procedure used for CMC 7.7 %w/w.

Table 4.10: Rheological parameters obtained from the two in-line techniques for CMC 5.16 %w/w

Parameters	Flow-Viz^{TM} (PUV+PD)	Tube viscometry
***K* [Pa.s^n]**	0.25	0.15
***n* [-]**	0.7	0.8

4.3.3. Bentonite 7.48% w/w

Bentonite was used to evaluate the capability of the Flow-Viz^{TM} instrument in the rheological characterisation of fluids which can be described using the Bingham model. The methodology followed consisted of first carrying out the tube viscometry measurements in the 22.4 mm and 35.1 mm pipes and lastly in the 47.8 mm pipe where the ultrasound transducers for the PUV+PD measurements were installed. This approach was used as it allowed the PUV+PD measurements to be carried out interchangeably with the tube viscometry measurement within the same pipe section in order to ensure consistent tests conditions. The test conditions and the PUV+PD settings are shown in Table 4.11 and Table 4.12.

Table 4.11: The test conditions for Bentonite 7.48 %w/w

c [m/s]	PRF [kHz]	Voltage gain [dB]	Velocity estimator	N_{rep}	Rheometric Method	Number of Cycles
1584.7	123.75	35	FFT	128	gradient	5

Table 4.12: Parameter settings used for PUV measurement in Bentonite 7.48 %w/w

Temperature [°C]	Slurry density [kg/m^3]	Re_2 [-]	ΔP/L [kPa/m]	ΔP Length [m]	Magnetic Flow-meter [L/min]	Velocity Profile [L/min]	% difference in flow rate
~22	1048	103	2.782	2.14	67.5	65.2	3.4

The power-spectrum from the PUV+PD measurements are shown in Figure 4.13.

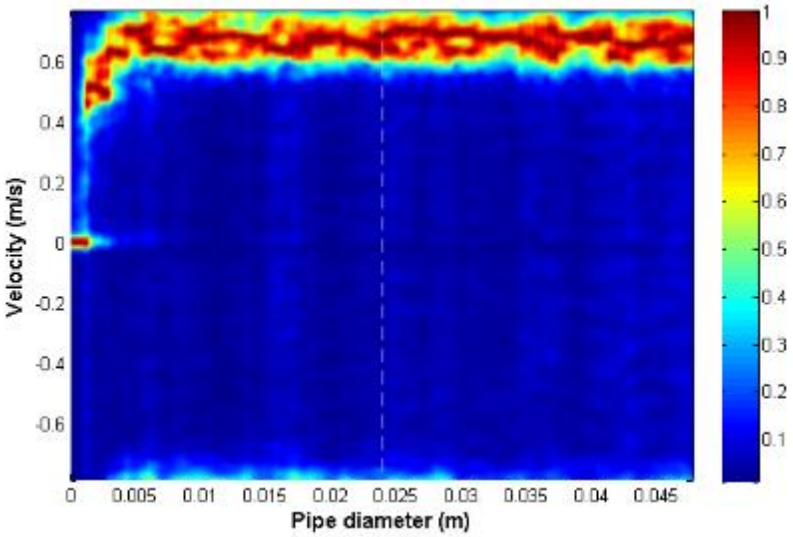

Figure 4.13: Power-spectrum for the velocity profile measurement, Bentonite 7.48 %w/w

The power spectrum shows that the acoustic energy was evenly distributed throughout the pipe and no artefacts were measured during the test. The power spectrum has a steep rise at the near wall and shows a large plug radius starting from 0.005 m to till the pipe centre at R = 0.0239 m. The observed plug radius shows the expected characteristic yield stress in a bentonite suspension. Based on the spectrum it can be seen that good signal-to-noise ratio was present (no artefacts in the spectrum). Figure 4.14 shows the rheograms obtained from the two in-line methods.

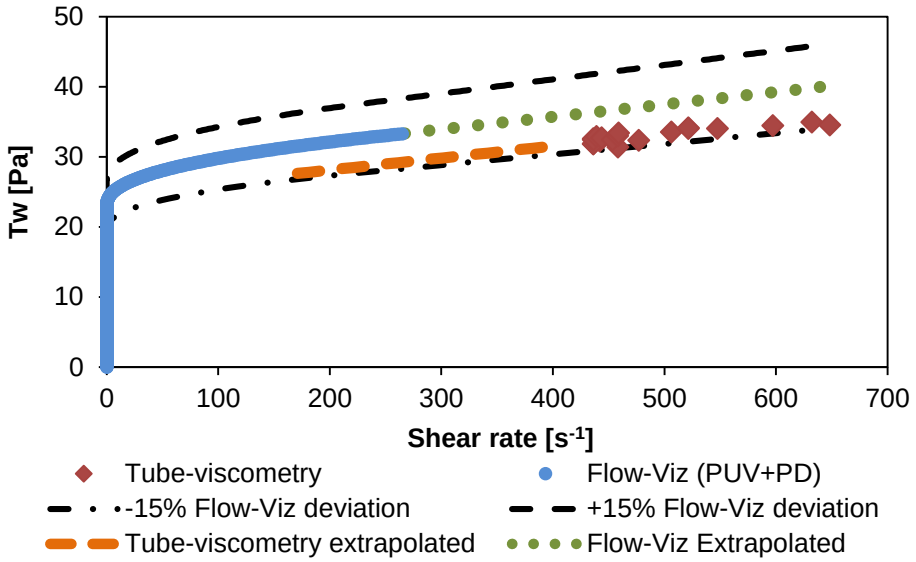

Figure 4.14: Bentonite 7.48% w/w rheogram, comparison of tube-viscometer and Flow-Viz (PUV+PD)

Within the shear-rate range (0-1000) s^{-1} there is good agreement between the results obtained from tube viscometry and PUV+PD (Flow-Viz^{TM}) since the tube viscometry data lies within -15% of the PUV+PD data. Tube viscometry data points range from ~430 s^{-1} to ~650, whereas those from Flow-Viz^{TM} extend up to 265 s^{-1}. The rheogram shows that, there is a significant difference in the shear rate range covered by the two techniques. However, it can be seen from the flow curve in Figure 4.14 that by extrapolating the tube viscometry data points that the two agree quite well. The PUV+PD measurement describes the rheological behaviour of the bentonite quite well at much lower shear rates compared to the tube-viscometer due to the velocity profile derived shear rates. In a similar manner to the CMC data, the lower shear rate range from the PUV+PD measurement was because the test was conducted within the larger pipe (47.8 mm). The larger 47.8 mm ID pipe limits the magnitude of the shear rate distribution for a given flow rate, compared to the smaller pipes which were included in the tube viscometry tests. This effect is also explained in Kotzé et al. (2015a) where shear rate range differences were also encountered, whilst using similar rheometric techniques i.e. tube viscometry and PUV+PD.

Furthermore, the lower range limitation of the magnetic flow-meter on the low end pseudo shear rates affected the overall tube viscometry pseudo shear rate range. By measuring flow data starting at a certain shear rate (due to lower range limitation), the flow and differential pressure data (Appendix A.2) for bentonite resulted in a pseudo flow curve with an almost flat curvature (linear line); with such data the Rabinowitsch-Mooney transformation slightly shifts the tube

viscometry based pseudo shear rates towards the upper end of the resultant rheogram (higher shear rates). Table 4.13 depicts the rheological parameters as determined from each technique.

Table 4.13: Rheological parameters obtained from the two in-line techniques for Bentonite 7.48 %w/w

Parameters	Flow-Viz^{TM} (PUV+PD)	Tube viscometry
K [Pa.s^n]	0.95	0.011
n [-]	0.4	1
T_y [Pa]	23.01	27.54

The Bingham model was used to characterise the tube viscometry data with a flow behaviour index of 1, since the technique was incapable of providing sufficient data at low shear rates (Kotzé et al., 2015a). With the PUV+PD technique, some curvature could be seen within the lower shear rate range and the Herschel-Bulkley model was used to better describe the rheological data, hence the difference in the value of the flow behaviour index (n = 0.4, for PUV+PD). Due to the differences in the lower shear rate range, a higher magnitude of the yield stress was obtained from the tube viscometry measurement as shown in Table 4.13.

4.3.4. Bentonite 5.4 %w/w

A more dilute bentonite suspension was also tested in order to evaluate the Flow-Viz^{TM} system at a lower viscosity range of the same suspension. The test conditions recorded are given in Figure 4.12 and Figure 4.13.

Table 4.14: The test conditions for Bentonite 5.4 %w/w

c [m/s]	PRF [kHz]	Voltage gain [dB]	Velocity estimator	N_{rep}	Rheometric Method	Number of Cycles
1497.5	123.75	35	FFT	128	gradient	5

Table 4.15: Main settings for the PUV measurement, Bentonite 5.4 %w/w

Temperature [°C]	Slurry density [kg/m^3]	Re_2 [-]	ΔP/L [kPa/m]	ΔP Length [m]	Magnetic Flow-meter [L/min]	Velocity Profile [L/min]	% difference in flow rate
~21.5	1037	616	0.540	2.14	69.3	61.8	10.8

Velocity profile measurements within the bentonite mixture were good since the bentonite suspension did not offer much attenuation to the beam. The spectrum image in Figure 4.15 shows a good measurement across the entire pipe diameter. The image shows a shorter plug radius as compared to the more concentrated Bentonite 7.48 %w/w; which corresponds to a decrease in the measured yield stress. The measured flow rates agreed quite well however a greater percentage difference was recorded for this test compared to the previous measurements (CMC and Bentonite 7.48 %w/w), possibly due to some random disturbance to the flow during the test.

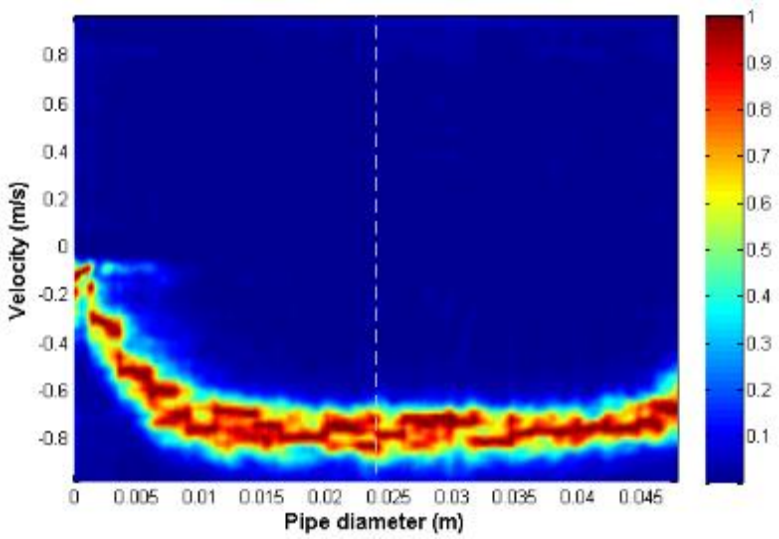

Figure 4.15: Power-spectrum for the velocity profile measurement, Bentonite 5.4 %w/w

The rheogram presented in Figure 4.16 shows the yield-stress properties of the Bentonite suspension over the measured shear rate range.

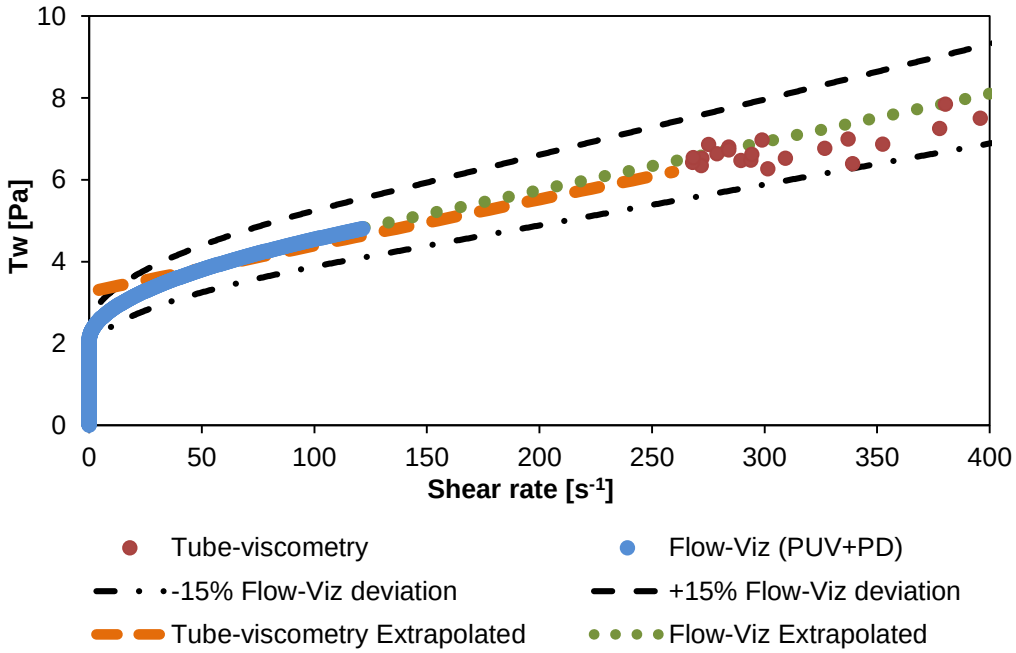

Figure 4.16: Bentonite 5.4 % w/w rheogram, comparison of tube-viscometer and Flow-Viz (PUV+PD)

The experimentally measured data from the two measurements agrees quite well as seen from the extrapolated tube viscometry flow curve. Similar to the more concentrated bentonite suspension, the difference in the shear rate ranges by the two techniques was mainly due to the lower shear rates measured in the 47.8 mm ID pipe, where the PUV+PD measurements were

taken. Tube viscometry evidently measured higher shear rates since it was carried out across three pipe test sections, where higher shear rates were experienced due to smaller pipe diameters. Even with the low concentration bentonite suspension, the lower range limits in the flow metering instruments notably contributed to the inadequate representation of the flow properties in the low shear rate region when using tube viscometry. Table 4.16 shows the rheological parameters as determined by each technique.

Table 4.16: Rheological parameters obtained from the two in-line techniques for Bentonite 5.4 %w/w

Parameters	Flow-Viz^{TM} (PUV+PD)	Tube viscometry
K [Pa.s^n]	0.23	0.01
n [-]	0.5	1
T_y [Pa]	2.08	3.36

The agreement of the two techniques also lies in ±15% interval for most of the profile, however it could be seen that major deviations were in the lower shear rate range, resulting in different yield stress values. The result shows that Flow-Viz^{TM} was able to provide detailed data at very low shear rates (< ~1 s^{-1}) where the tube viscometry technique was highly limited by flow metering. Even after true shear rates correction with the Rabinowitsch-Mooney transformation, the tube viscometry data could not be wholly compared to the Flow-Viz^{TM} data without applying extrapolation.

4.3.5. Kaolin 38.4 %w/w

Kaolin clay is typically used in the paper industry and is usually characterised as a yield-pseudoplastic. The test conditions are shown below in Table 4.17 and Table 4.18

Table 4.17: The test conditions for Kaolin 38.4 %w/w

c [m/s]	PRF [kHz]	Voltage gain [dB]	Velocity estimator	N_{rep}	Rheometric Method	Number of Cycles
1711.2	123.75	45	FFT	128	gradient	5

Table 4.18: Main settings for the PUV measurement, Kaolin 38.4 %w/w

Temperature [°C]	Slurry density [kg/m^3]	Re_2 [-]	ΔP/L [kPa/m]	ΔP Length [m]	Magnetic Flow-meter [L/min]	Velocity Profile [L/min]	% difference in flow rate
~20	1314	662	2.415	2.14	137.5	136.6	0.7

The flow conditions show that the flow was lamina with a Reynolds number, Re_2 of 662. The flow rate from the Flow-Viz^{TM} system (integration method) matched the electromagnetic flow meter to a higher degree (within 1%). Figure 4.17, shows the Doppler spectrum with significant attenuation especially from ~30 mm onwards. This is due to the highly attenuating physical properties of kaolin clay; this observation was also presented in Kotzé et al (2008, 2012). The attenuation was mostly at the opposite pipe wall and only data measured across half of the pipe diameter is required for calculating the fluid properties and volumetric flow rate. The velocity profile in Figure 4.17 shows that, plug flow was present and therefore a yield stress property could be measured.

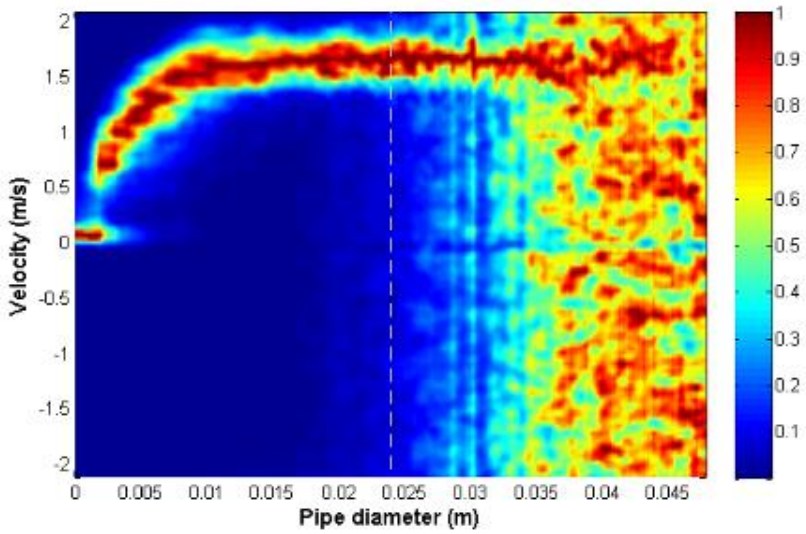

Figure 4.17: Power-spectrum for the velocity profile measurement, Kaolin 38.4 %w/w

The plug radius from the Kaolin fluid was not as pronounced as that observed in the bentonite profile presented in Section 4.3.3. The shorter plug radius corresponds with the lower yield stress value of 10.94 Pa. A larger shear rate range was covered compared to the bentonite PUV+PD measurements. This was because the PUV+PD measurement for kaolin suspensions were carried out at high enough flow rates.

The Flow-Viz^{TM} pulser/receiver voltage gain was adjusted to 45 dB as compared to 35 dB used for less attenuating CMC and bentonite suspensions. Even with the highly attenuating kaolin clay suspension it was still possible to measure across the pipe radius non-invasively through high grade stainless steel. Figure 4.18 shows the comparison between the results obtained using conventional tube viscometry and the in-line Flow-Viz^{TM} system.

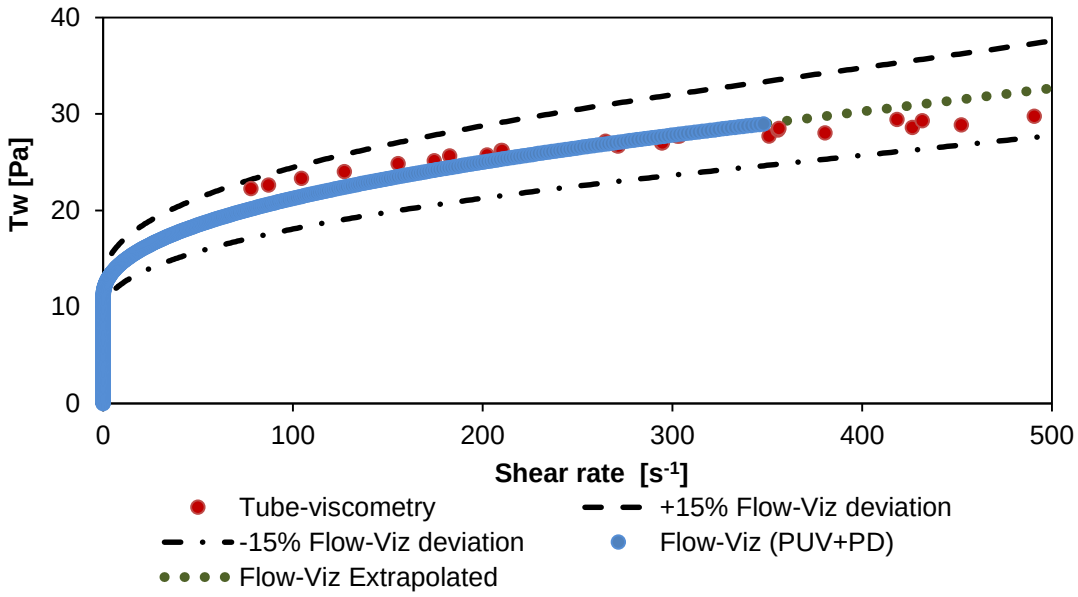

Figure 4.18: Kaolin 38.4 %w/w rheogram, comparison of tube-viscometer and Flow-Viz (PUV+PD)

The rheogram for the concentrated Kaolin suspension shows good agreement (well within ±15%) over the shear rate range where the data from the two techniques overlaps. The Herschel-Bulkley model was used to characterise the flow data, however it can be argued that the Bingham model describe the tube viscometry data appropriately, since there was no data in the lower shear rate range. As with previous measurements, the Flow-Viz^{TM} unit consistently provided meaningful data points even at very low shear rate values (< 1 s^{-1}). Table 4.19 depicts the rheological parameters obtained by curve-fitting using the Herschel-Bulkley model.

Table 4.19: Rheological parameters obtained from the two in-line techniques for Kaolin 38.4 %w/w

Parameters	Flow-Viz™ (PUV+PD)	Tube viscometry
***K* [Pa.s^n]**	1.31	3.78
***n* [-]**	0.5	0.3
T_y [Pa]	10.94	10

The rheological parameters (τ_y, K, n) tube viscometry were obtained from model based curve fitting. The yield stress values from the two techniques agreed quite well (~9% difference), although the tube viscometry value was not determined directly from shear stress measurement at very low shear rates.

4.3.6. Kaolin 30.79 %w/w

The test conditions and parameters from the more dilute solids concentration of Kaolin clay (30.79 %w/w) are shown in Figure 4.17 and Figure 4.18.

Table 4. 20: The test conditions for Kaolin 30.79 %w/w (ΔP, Q) are the pressure drop and flowrate.

c [m/s]	PRF [kHz]	Voltage gain [dB]	Velocity estimator	N_{rep}	Rheometric Method	Number of Cycles
1620.6	123.75	45	FFT	128	gradient	5

Table 4. 21: Main settings for the PUV measurement, Kaolin 30.79 %w/w

Temperature [°C]	Slurry density [kg/m^3]	Re_2 [-]	ΔP/L [kPa/m]	ΔP Length [m]	Magnetic Flow-meter [L/min]	Velocity Profile [L/min]	% difference in flow rate
~19	1237	1907	0.865	2.14	141	140.4	0.4

The pseudo rheogram in Appendix A.3 shows that no-slip condition was observed for the pipe tests, since data was colinear. The power spectrum from the PUV+PD measurement also shows significant attenuation as seen from the first concentration of kaolin (Figure 4.17). The pulser voltage gain was also set to 45 dB, with a linear gain slope of 1. Despite the attenuation, a

satisfactory velocity profile could still be measured non-invasively through high grade stainless steel. The spectrum image is shown in Figure 4.19.

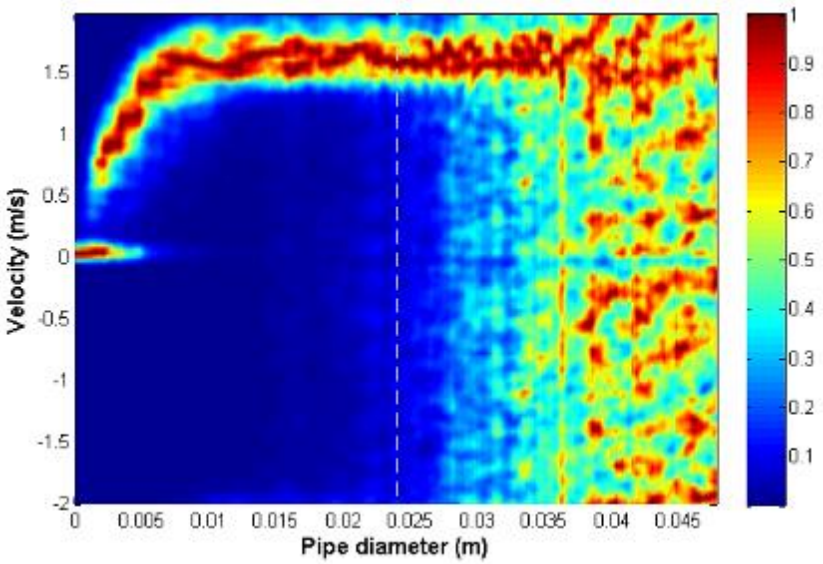

Figure 4.19: Power-spectrum for the velocity profile measurement, Kaolin 30.79 %w/w

The flow curve is depicted in Figure 4.20. The Rabinowitsch-Mooney correction factor for the pseudo-shear rate data had lower value and did not result in much higher true shear rates compared to the tube viscometry data obtained in bentonite suspensions.

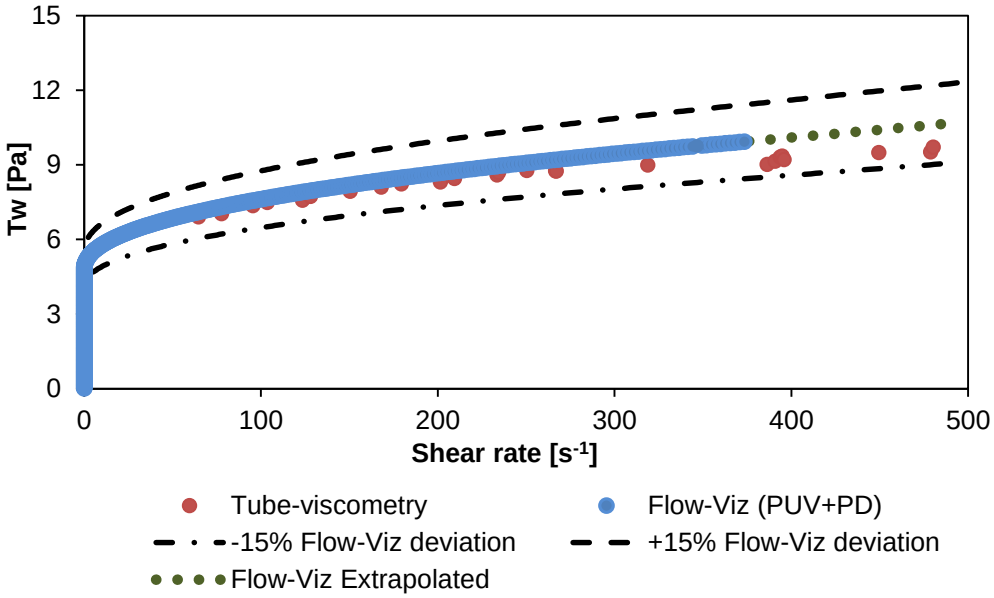

Figure 4.20: Kaolin 30.79 %w/w rheogram, comparison of tube-viscometer and Flow-Viz (PUV+PD)

The measured flow behaviour using the two different methods shows good agreement (within 15%) for most of the shear rate range. The tube viscometry data was fitted with a Herschel-Bulkley constitutive model in order to determine the rheological parameters. Table 4.22 depicts the rheological parameters as measured by each technique.

Table 4.22: Rheological parameters obtained from the two in-line techniques for Kaolin 38.4 %w/w

Parameters	Flow-Viz^{TM} (PUV+PD)	Tube viscometry
K [Pa.s^n]	0.36	0.34
n [-]	0.5	0.4
T_y [Pa]	4.76	5

The yield stress values for the two tests are much closer values due to the tube viscometry data which was also available at relatively lower shear rates (~50 s^{-1}) compared to the bentonite tests. For this tests the whole range of flow properties were in good agreement. The Flow-Viz^{TM} system proved to be consistent in both concentrations with the highly attenuating kaolin clay as it provided meaningful rheological data at very low shear rates.

4.4. CONCLUSIONS

The acoustic characterisation results showed that using different coupling materials influenced the ultrasound beam angle (or Doppler angle), which is very important for accurate velocity profile measurements. By using only the liquid couplant at the sensor's wedge-to-pipe interface, the focal zone is further away from the inner pipe wall (~5 mm). The angle was found to be ~24°, making the Doppler angle smaller ~66°.The same effects with regards to the location of the focal point and length of the focal zone were observed with both the new Flow-Viz^{TM} commercial sensor unit and the prototype sensors.

A significant increase in acoustic energy was observed when the thin solid-X couplant was used at the transducer-to-wedge interface of the 22.4 mm pipe. With this couplant, the peak to peak voltages were double compared to the setup where liquid couplant was used as the transducer-to-pipe couplant. However, it must be noted that the transducer used during the solid-X couplant test had a different design compared to the transducer used with liquid coupling material.

For industrial applications the solid couplant between the transducer to wedge is not ideal since installation is more difficult and it has a limited temperature range. In this case the integrated design of the black sensor configuration is ideal i.e. with direct integration between ultrasound transducer and wedge. Although most setups with a solid couplant shifts a focal zone closer to the inner pipe wall it is less suitable for industrial applications. The liquid couplant can withstand a greater range of temperatures and is easier to install and is therefore ideal for industrial installations. The next step will be to redesign the black sensor configuration so that the focal point is at the pipe-liquid interface when using the liquid coupling material. The focal zone should also be as long as possible or at least cover the pipe radius and have maximum energy output for accurate measurements in attenuating industrial fluids such as kaolin clay and cementitious pastes.

The liquid couplant was chosen for the in-line rheological characterisation tests as the wedge-to-pipe interface in order evaluate the Flow-Viz^{TM} system with an industrial installation method. The Flow-Viz^{TM} system was evaluated against conventional tube viscometry and results showed good agreement (within ±15%) of each other, for most of the fluids tested. Kaolin suspensions were the most attenuating and the gain value had to be set to 45 dB compared with 35 dB used for bentonite suspensions and CMC solutions. The major difference noted especially for bentonite suspensions

was that of the shear rate range covered by the Flow-Viz^{TM} instrument was less than that covered by the tube-viscometer. This difference was mainly due the different was due to the smaller pipe diameters which were used for the tube viscometry measurements (22.4 mm and 35.1 mm), compared to the PUV+PD which was carried out in the largest pipe diameter section (47.8) which results in lower radial shear rates at a given pump flow rate. The Rabinowitsch-Mooney correction also contributed to the shifted shear rates in the tube viscometry rheograms, especially for bentonite measurements. The flow metering also had lower range limitations which also contributed to insufficient tube viscometry data points in the lower shear rate range (< 100 s^{-1}). The Flow-Viz^{TM} instrument was able to measure at much lower shear rates (< 1 s^{-1}) compared to the tube viscometer, however is was limited at high shear rates within the specific pipe diameter. The rheological parameters were as a result different compared to the parameters fitted using the tube data. It is therefore important to compare the results over the same shear rate range. The important advantage of the Flow-Viz^{TM} system is that a complete rheogram or viscosities over a shear rate range can be determined in a few minutes whereas the tube viscometry tests can take from 30 minutes to over an hour. Based on the results it was shown that the Flow-Viz^{TM} system can accurately characterise non-Newtonian fluids as validated with the conventional tube viscometry measurements. Additionally, the Flow-Viz^{TM} system is able to fully characterise fluids even at extremely low shear rates (< 1 s^{-1}) where conventional tube viscometry is limited.

CHAPTER FIVE: SUMMARY, CONCLUSIONS, CONTRIBUTIONS AND RECOMMENDATIONS

5.1. SUMMARY

This research contributed to the ongoing development of the PUV+PD in-line rheometric technique specifically the Flow-Viz^{TM} system, and a brief summary of the main literature in the field is reviewed here to highlight the main gap which this work addressed. Publications from as early as 1993 in Brunn et al. (1993), reveal that in-line fluid rheology based on the PUV+PD technique has been used and developed in a number of research laboratories. Most of the past work has showed the significance of PUV+PD as a reliable tool for in-line rheology (Wiklund et al., 2001; Ouriev & Windhab (1999)).

Similar research was also conducted and presented in (Wiklund et al., 2002) and (Wiklund et al., 2006). These studies were aimed at showing the applicability of the technique in a wide range of industrial suspensions such as pulp suspensions, cheese sauce, yoghurt and rape-seed oil. A few years later Birkhofer et al. (2008) then highlighted the linear dependence of the decrease in velocity of sound to the formation of crystalline fat in the cocoa butter process. This work proved that it was possible to characterise the shear crystallisation of cocoa butter in line, using the PUV+PD method. This study which was carried out within the same time frame with (Wiklund et al., 2007) also resulted in the development of an improved application software which integrates the velocity profile and flow loop sensor data (temperature, flow and pressure) into one software application. The developed software made use of the ActiveX library provided by Met-Flow SA to communicate with the UVP-DUO monitor. One of the aims was to directly obtain the Demodulated Echo Amplitude (DMEA) data from the UVP-DUO to enhance signal processing using alternative algorithms.

Most of the earlier PUV+PD setups utilised flow-adaptor type ultrasound sensors. The transition from flow adaptor based ultrasound sensor technology with cavities to delay line sensors for velocity profile measurements was introduced during the study by Kotzé, et al. (2012 & 2013). During this study, novel sensors were developed which used the delay line material, such that the transducer front surface was installed flush with the pipe inner wall. The delay line sensors were an improvement; however, a non-invasive solution was still needed for industrial applications that have strict hygienic and safety requirements. From the past work, a non-invasive rheometric

system called Flow-Viz™ was then developed, but its capabilities and limitations had not yet been fully evaluated over a wide range of industrial fluids (Kotzé, 2014; Wiklund et al., 2014). The system included more capable pulser/receiver electronics which allowed for a greater spatial resolution across the pipe diameter. The pulser/receiver electronics described in (Kotze et al., 2015b; Wiklund et al., 2014) had faster microprocessors based on FPGA technology and were thus able to provide real-time FFT processing for improved in-line performance and monitoring of velocity profiles. This development formed part of the collaborative research between SP and CPUT.

The current research work presented in this thesis covered two aspects, which were: the acoustic characterisation of the non-invasive sensor technology through industrial stainless steel (316L) pipes and the evaluation of the newly developed Flow-Viz^{TM} in-line rheometric system against conventional tube viscometry.

The acoustic characterisation tests were aimed at determining the acoustic beam properties emitted from the transducers from each of the non-invasive sensor units, firstly without any coupling media, and secondly in a setup in which they are mounted to stainless steel pipes. Tests were carried out for the 22.4 mm, 47.8 mm and 152.4 mm prototype and commercial sensor units. By using an advanced needle hydrophone and XYZ-scanning system, beam properties such as the beam intensity (peak-voltage), focal zone shape and location as well as the Doppler angle were determined.

The Flow-Viz^{TM} TYPE-A sensors for 47.8 mm pipes which were acoustically characterised, were then used as part of the Flow-Viz^{TM} system for in-line rheological characterisation tests. Two concentrations of each of the model suspensions (CMC, bentonite and kaolin clay) were used within an experimental flow loop at CPUT (FPRC) laboratories in Cape Town. Good agreement (±15%) was achieved between the two in-line techniques, despite some differences in the shear rate ranges covered due to pipe size limitations.

5.2. RECOMMENDATIONS FOR FUTURE RESEARCH

Several technical difficulties were noted during the course of the experimental tests. These are described for each of the tests conducted i.e. acoustic characterisation of ultrasound sensors and the in-line rheology tests.

- **Acoustic characterisation**

The major technical shortcoming with the acoustic characterisation tests was the pulser/receiver pulse length setting. The effect of this was noted for the TYPE-B transducers which produced shorter beams with less energy than expected, although the beam shape was symmetrical and consistent with the other transducers (TYPE-A). This limitation was due to the shorter pulse length which was used to excite the transducer.

For more accurate representations of the acoustic field, a higher resolution (> 8 bit) digitiser could have been used to measure the acoustic intensity ($V_{pk\text{-}pk}$ voltages). With a higher resolution digitiser, smaller voltage fluctuations between adjacent spatial points can be measured and actually be able to show important acoustic field properties.

- **In-line rheology tests**

Shear rate range differences between conventional tube viscometry and PUV+PD made it complex to ascertain the differences in the rheograms obtained from the two techniques. The tube viscometry data was shifted in the higher shear rate region due to differences in the pipe test sections used for PUV+PD and tube viscometry. PUV+PD was carried out in the pipe section with the largest pipe diameter whereas tube viscometry which was carried out in smaller pipes resulted in higher shear rates. Additionally, the magnetic flowmeters could not measure low flow-rates below ~0.1 l/s due to lower range limitations, thus making it difficult to provide very low shear rate data with the tube-viscometer. At these low shear-rates the Flow-Viz^{TM} system was able to provide meaningful rheological information. To overcome this limitation, extrapolation of the tube viscometry data to lower shear-rates was done, however this is not always accurate for most fluids where details of the flow behaviour of the fluid are not known apriori and thus comparison of the rheological data (flow-curves) should then be carried out within similar shear rate ranges.

Other drawbacks were those associated with the attenuating effects of the model suspensions especially kaolin clay. For all other test fluids the velocity of sound measurement was carried out in-line whilst using a 35 dB voltage gain for the velocity profile measurements, however for kaolin a voltage gain of 45 dB was used for the velocity measurements. An off-line velocity of sound test described in Section 3.2.7 was conducted for kaolin clay. The limitation was that velocity of sound could not be measured for kaolin in-line due to high attenuation of the ultrasound energy.

With the remote seal sensor technology in the pressure transmitters used for the tube viscometry some problems were that an offset pressure could be measured if the seals were mounted facing an upward vertical direction perpendicular to the flow direction. Thus the pressure taps (remote seals) were positioned sideways as shown in Figure 3.31, or in a downward position to eliminate measuring the significant pressure build-up due to air. Based on the magnitude of the differential pressure measured during the tests, a more suitable lower range pressure transmitter could have been used. Ranging the high pressure transmitters which were used for the tests to lower spans resulted in greater errors in the measured values (as shown by the manufactures turndown ratio specification).

For future research aimed at advancing the PUV+PD methodology for in-rheology and the Flow-Viz^{TM} system the following outstanding matters are outlined:

- In-depth knowledge about the transducer's acoustic field after propagating through stainless steel (316L) properties could be obtained by designing a fully automated scanning system wherein three dimensional acoustic maps are obtained. By measuring with a higher resolution digitiser, 3D acoustic maps with more accurate data will be made available to gain further insight into the actual geometry of the pulsed ultrasound beams.

- The in-line, real-time rheometric capabilities of the Flow-Viz^{TM} system can be further tested and improved by extending the range of testing fluids to actual industrial fluids such as wastewater sludge and various food products.

- The accurate measurement of the velocity of sound value still needs to be addressed. For example, from the tests with the highly attenuating kaolin suspensions it was evident that improved pulser/receiver electronics and transducers still need to be developed. Another option would be to develop a pulser/receiver which is integrated with the main system but

is utilised as a dedicated sound velocity measurement unit, separate from the primary pulser/receiver for velocity profile measurement. Additionally the detection of the opposite wall interface could also be improved by using more efficient algorithms, and hence increase the accuracy of in-line sound velocity measurements.

- Tests with sensors optimised for larger pipe diameters can be conducted with suitable coupling wedges or mounting cases.

- Another area which needs further improvement is the use of more advanced pressure sensors where the membrane is installed around the inner pipe wall to eliminate problems with pressure offsets, clogging of fluids, etc. Sensor setups of this kind will greatly improve the acquired pressure data for shear stress calculations.

5.3. CONCLUSIONS

The main outcomes of this work were detailed acoustic characterisation maps of the Flow-Viz^{TM} system non-invasive sensors and an evaluation of the Flow-Viz^{TM} rheometric system against conventional tube viscometry within an experimental flow loop.

The in-line tests were conducted with three model fluids, and good agreement (±15%) over the same shear-rate ranges was achieved for the two techniques. The tube viscometry technique was quite limited in the low-shear rate range whereas the Flow-Viz^{TM} was able to provide meaningful data, even up to low as (< 1 s^{-1}). This observation showed that with extremely low shear-rate data the Flow-Viz^{TM} system is able to fully characterise fluids and determined more reliable values of the yield stress without any extrapolation. Velocity measurements in kaolin were measured using a higher voltage gain from the pulser in order to overcome the attenuating effects of kaolin.

For the acoustic characterisation transducers optimised for 22.4 mm, 47.8 mm and 152.4 mm pipes were characterised in single transducer characterisation as well as in vertical pipe tests. The ideal beam after propagating through the pipe walls should be as narrow as possible whilst providing a high energy focal zone which extends throughout the pipe diameter. The beam angle and location of the beam focal zone were seen to deviate when using different solid and liquid couplants.

The overall analysis of the acoustic characterisation data revealed that the solid couplants (solid-X, solid-Y and solid-Z) result in a larger Doppler angle and a focal zone which is directly at the pipe wall although the overall beam energy is reduced when compared to the liquid couplant. The liquid couplant offers less attenuation when used as a wedge-to-pipe couplant, resulting in a beam which covers the pipe radius although the focal zone does not start at the pipe wall (~5 mm away). The most energy was generated by having a thin solid-X couplant at the transducer-to-wedge interface with liquid couplant at the wedge-to-pipe boundary. The beam from this setup had a focal zone directly at the pipe wall and had a focal zone with almost double the energy compared to the other configurations. Despite these differences, the liquid couplant was noted to be more versatile as an industrial couplant as it is more convenient to install for industrial usage. Furthermore, the liquid couplant can be used in high temperature conditions compared to the solid couplants which have poor thermal properties. The liquid couplant does not evaporate when left for months, on an installation pipe and thus is more reliable and cost effective. However using external couplants is not desirable as this can introduce artifacts when improper coupling is done, hence the drive towards an integrated sensor unit with the acoustic couplants in one sensor unit.

The acoustic characterisation data will be used to develop the next generation non-invasive sensors by considering the advantages of an integrated transducer-to-wedge setup, with optimised thermal properties to cater for the industrial requirements in higher temperature environments. The new sensor unit will also have an optimised beam with a focal zone which starts at the pipe wall and extends farther over the pipe radius. With such an integrated sensor more accurate in-line rheological characterisation is then possible in a wide range of industrial fluids and applications, such as food products, oil drilling, paper-pulp and cosmetics.

5.4. CONTRIBUTIONS

By completing the research objectives the following contributions were made:

- The non-invasive sensor technology, which is part of the Flow-Viz^{TM} system, had not been acoustically characterised in order to determine important beam properties. The sensor technology was for the first time characterised where the ultrasound beam propagates through high grade stainless steel (316L) pipes.

- Several acoustic couplants (solid and liquid) for mounting of ultrasound sensors were evaluated during the acoustic characterisation tests, and their influence on the resultant beam critical properties (i.e. focal zone shape and Doppler angle) were noted. This information will now be used to design improved, next generation non-invasive sensors.

- The newly developed Flow-Viz^{TM} system which had not yet been fully tested in a wide range of industrial fluids was evaluated against conventional tube viscometry in three different fluids exhibiting a wide range of different rheological properties. Results showed good agreement (within ±15%), thus showing the reliability of Flow-Viz^{TM} as an in-line rheometric unit.

REFERENCES

Barber, W.D., Eberhard, J.W. & Karr, S.G. 1985. A new time domain technique for velocity measurements using Doppler ultrasound. *Biomedical Engineering, IEEE Transactions on*, (3): 213–229.

Barnes, H.A. & Hutton, J.F. 1989. *An introduction to rheology*. Elsevier.

Barnes, H.A. 2000. *A handbook of elementary rheology*. University of Wales, Institute of Non-Newtonian Fluid Mechanics Aberystwyth, England.

Bechtold, J., 2006. *Jill Bechtold's home page: Department of Astronomy, University of Arizona.* [Online] Available at:http://boojum.as.arizona.edu/~jill/NS102_2006/Lectures/Lecture12/turbulent.html[Accessed 12 October 2014].

Birkhofer, B. H. et al., 2008. Monitoring of fat crystallization process using UVP–PD technique. *Flow Measurement and Instrumentation,* Volume 19, pp. 163-169.

Birkhofer, B. H., 2007. *Ultrasonic In-line Characterisation of Suspensions.* Zurich: ETH (Zurich).

Birkhofer, B., Jeelani, S.A.K., Ouriev, B. & Windhab, E.J. 2004. In-line characterization and rheometry of concentrated suspensions using ultrasound. *Proceedings-4th ISUD, Sapporo, Japan*: 65–68.

Birkhofer, B.H., Jeelani, S.A.K., Windhab, E.J., Ouriev, B., Lisner, K.-J., Braun, P. & Zeng, Y. 2008. Monitoring of fat crystallization process using UVP–PD technique. *Flow Measurement and Instrumentation*, 19(3-4): 163–169.

Blauert, J. & Xiang, N. 2008. *Acoustics for Engineers*. Berlin, Heidelberg: Springer Berlin Heidelberg.

Brunn, P. O., Vorwerk & S. R., 1993. Optical and Acoustic Rheometers: Three Examples. *Appl. Rheol,* 3(20).

Cengel, Y.A. 2010. *Fluid mechanics*. Tata McGraw-Hill Education.

Chhabra, R. P. & Richardson, J. F., 1999. *Non-Newtonian Flow in the Process Industries.* 1st ed. Oxford: Butterworth-Heinemann.

Cullen, P.J., Duffy, A.P., O'Donnell, C.P. & O'Callaghan, D.J. 2000. Process viscometry for the food industry. Trends in Food Science & Technology, 11(12): 451–457.

David, J. & Cheeke, N., 2002. *Fundamentals and Applications of Ultrasonic Waves.* Boca Raton, Florida: CRC Press

Haldenwang, R. et al., 2012. Sludge pipe flow pressure drop prediction using composite Power-law friction factor–Reynolds number correlations based on different non-Newtonian Reynolds numbers. *Water SA,* 38(4).

Haldewang, R., 2003. *Flow of Non-Newtonian Fluids in Open Channels.* Cape Town, South Africa: Cape Peninsula Univeristy of Technology.

Jensen, J. A., 1996. *Estimation Of Blood Velocities Using Ultrasound: A Signal Processing Approach.* New York: Cambridge University Press.

Jorgensen, J. E., Campau, D. N. & Baker, D. W., 1973. Physical characteristics and mathematical modelling of pulsed ultrasonic flowmeter. *Medical and Biological Engineering,* 11(4), pp. 404-421.

Kotzé, R., 2011. *Detailed Non-Newtonian Flow Behaviour Measurements Using A Pulsed Ultrasound Velocimetry Method: Evaluation, Optimisation & Application.* Cape Town, South-Africa: CPUT, Cape Town.

Kotzé, R., Haldenwang, R. & Slatter, P., 2008. *Rheologial Characterisation of highly concentrated mineral suspensions using an ultrasonic velocity profiler.* Prague, Czech Technical University in Prague, Faculty of Civil Engineering.

Kotzé, R., Haldenwang, R. & Wiklund, J., 2012. *OPTIMISATION OF UVP MEASUREMENTS USING NEW TRANSDUCER TECHNOLOGY AND ADVANCED SIGNAL PROCESSING TECHNIQUES.* Dresden, Germany, Department Magnetohydrodynamics, Institute of Fluid Dynamics, Helmholtz-Zentrum Dresden-Rossendorf, pp. 3-6.

Kotzé, R., Haldenwang, R., Fester, V. & Rössle, W. 2015a. In-line rheological characterisation of wastewater sludges using non-invasive ultrasound sensor technology. Water SA, 41(5): 683.

Kotzé, R., Haldenwang, R., Fester, V. & Rössle, W., 2014a. A feasibility study of in-line rheological characterisation of a wastewater sludge using ultrasound technology. *Water SA,* 40(4).

Kotzé, R., Ricci, S. & Wiklund, J., 2014b. *Performance tests of a new non-invasive sensor unit and ultrasound electronics.* Strasbourg, France, Ubertone.

Kotze, R., Ricci, S., Birkhofer, B. & Wiklund, J. 2015b. Performance tests of a non-invasive sensor unit and ultrasound electronics. Flow Measurement and Instrumentation: 1–8.

Kotzé, R., Wiklund, J. & Haldenwang, R. 2013. Optimisation of Pulsed Ultrasonic Velocimetry system and transducer technology for industrial applications. *Ultrasonics*, 53(2): 459–469.

Krautkramer, J. & Krautkramer, H. 1990. Ultrasonic Testing of Materials. 4th ed. Heidelberg: Springer-Verlag Berlin Heidelberg.

Kuttruff, H., 1991. *Ultrasonics: Fundamentals and Applictions..* London and New York: Elsevier Applied Science.

MET-FLOW SA, 2002. *UVP Monitor Model UVP-DUO With Software Version 3. User's Guide.* Lausanne, Switzerland: Met-Flow SA.

Metzger, T. G., 2002. *The Rheology Handbook: For users of rotational & oscillation rheometers.* Hannover: Curt R. Vincentz Verlag.

Metzner, A.B. & Reed, J.C. 1963. Flow of Non-Newtonian Fluids - Correlation of the Laminar, Transition, and Turbulent-flow Regions. *American Institute of Chemical Engineers*, 1(4): 434–440.

Morris, A. & Langari, R. 2012. *Measurement and instrumentation: Theory and application*. Waltham, MA, USA: Academic Press, Elsevier.

Nave, R., 1998. *Fluid Velocity Profile.* [Online] Available at:http://hyperphysics.phy-astr.gsu.edu/hbase/pfric.html
[Accessed 13 October 2014].

Ouriev, B. & Windhab, E. 2003. Transient flow of highly concentrated suspensions investigated using the ultrasound velocity profiler–pressure difference method. *Measurement Science and Technology*, 14(11): 1963.

Ouriev, B. & Windhab, E. J., 1999. *STUDY OF FLOW PROCESSES OF CONCENTRATED SUSPENSIONS USING IN-LINE NON INVASIVE RHEOLOGICAL TECHNIQUE.* Villigen, Switzerland, s.n.

Ouriev, B. 2002. Investigation of the Wall Slip Effect in Highly Concentrated Disperse Systems by Means of Non-Invasive UVP-PD Method in the Pressure Driven Shear Flow1. *Colloid Journal*, 64(6): 740–745.

Ouriev, B., 2000. *Ultrasound Doppler Based In-line Rheometry of Highly Concentrated Suspensions.* Zurich, Switzerland: ETH dissertaion No. 13523.

Povey, M.J. 1997. *Ultrasonic techniques for fluids characterization*. Academic Press.

Powell, R.L. 2008. Experimental techniques for multiphase flows. *Physics of Fluids*, 20(4): 040605.

Roberts, I. 2001. In-line and on-line rheology measurement. In Instrumentation and Sensors for the Food Industry. Nestle´ Research Centre, Lausanne: Woodhead Publishing: 403–422.

Rudman, M., Blackburn, H.M., Graham, L.J.W. & Pullum, L. 2004. Turbulent pipe flow of shear-thinning fluids. *Journal of Non-Newtonian Fluid Mechanics*, 118(1): 33–48.

Satomura, S., 1957. Ultrasonic Doppler Method for the Inspection of Cardiac Functions. *The Journal of the Acoustical Society of America,* 29(11), p. 1181.

Shutilov, V. A., 1980. *Fundamental Physics of Ultrasound - English Translation by Michael E. Alferieff.* Amsterdam, Netherlands: Gordon and Breach Science Publishers.

Signal-Processing, SA, 1999. *ignal-processing.com.* [Online] Available at:
http://www.signal-processing.com/us_field.html [Accessed 17 October 2014].

Slatter, P. T. & Lazarus, J. H., 1993. *Critical flow in slurry pipelines. 12th International Conference on Slurry Handling and Pipeline Transport, HYDROTRANSPORT 12.* Brugge, Belgium, British Hydromechanics Research Group.

Steffe, J. F., 1996. *Rheological Methods in Food Process Engineering.* 2nd ed. USA: Freeman Press.

Steger, R., 1994. *OptischUnd Akustische Metoden in Der Rheometrie.* Erlangen: University of Erlangen.

Takeda, Y. 1986. Velocity profile measurement by ultrasound Doppler shift method. *International journal of heat and fluid flow*, 7(4): 313–318.

Takeda, Y. 1999. Ultrasonic Doppler method for velocity profile measurement in fluid dynamics and fluid engineering. *Experiments in fluids*, 26(3): 177–178.

Umchid, S. 2014. Measurement of the field characteristics from High Intensity Focused Ultrasound transducer. In Biomedical Engineering International Conference (BMEiCON), 2014 7th. IEEE: 1–5.

Wang, L., McCarthy, K.L. & McCarthy, M.J. 2004. Effect of temperature gradient on ultrasonic Doppler velocimetry measurement during pipe flow. *Food research international*, 37(6): 633–642.

Wiklund, J. & Stading, M. 2008. Application of in-line ultrasound Doppler-based UVP–PD rheometry method to concentrated model and industrial suspensions. *Flow Measurement and Instrumentation*, 19(3-4): 171–179.

Wiklund, J. et al., 2014. *Flow-VizTM – A fully integrated and commercial in-line fluid characterization system for industrial applications.* Strasbourg, France, Ubertone.

Wiklund, J., Johansson, M., Shaik, J., Fischer, P., Stading, M. & Hermansson, A.-M. 2001. In-Line rheological measurements of complex model fluids using an ultrasound UVP-PD based method. *ANNUAL TRANSACTIONS-NORDIC RHEOLOGY SOCIETY*, 8: 128–130.

Wiklund, J., Johansson, M., Shaik, J., Fischer, P., Windhab, E., Stading, M., Hermansson, A.-M. & others. 2002. In-line ultrasound based rheometry of industrial and model suspensions flowing through pipes. In *Trans. Third International Symposium on Ultrasonic Doppler Methods for Fluid Engineering, EFPL, Lausanne, Switzerland*. 69–76.

Wiklund, J., Ricci, S., Haldenwang, Meacci, V., Stading, M. & Kotzé, R. 2014. Flow-Viz^{TM} – A fully integrated and commercial in-line fluid characterization system for industrial applications. In *9th ISUD Conference*. International Symposium on Ultrasonic Doppler Methods for Fluid Mechanics and Fluid Engineering. (Ubertone) Strasbourg, France: Ubertone.

Wiklund, J., Shahram, I. & Stading, M. 2007. Methodology for in-line rheology by ultrasound Doppler velocity profiling and pressure difference techniques. *Chemical Engineering Science*, 62(16): 4277–4293.

Wiklund, J.A., Stading, M., Pettersson, A.J. & Rasmuson, A. 2006. A comparative study of UVP and LDA techniques for pulp suspensions in pipe flow. *AIChE Journal*, 52(2): 484–495.

Windhab, E.J. & Ouriev, B. 2002. Rheological study of concentrated suspensions in pressure-driven shear flow using a novel in-line ultrasound Doppler method. *Experiments in Fluids*, 32(2): 204–211.

Wood, A. B., 1941. *A Textbook of Sound.* London: Bell and Sons.

Yamamoto, M., Carrillo, J., Insunza, A., Mari, G. & Ville, Y. 2006. Error introduced into velocity measurements by inappropriate Doppler angle assignment. Ultrasound in Obstetrics & Gynecology, 28(6): 853–854.

Zhou, Y., Simmons, R., Zhong, P. & Zhai, L. 2006. Measurement of high intensity focused ultrasound fields by a fiber optic probe hydrophone. , 120(2): 676–685.

APPENDIX A.1: Pseudo-rheograms for CMC (7.7 & 5.16) w/w%

CMC 7.7%w/w

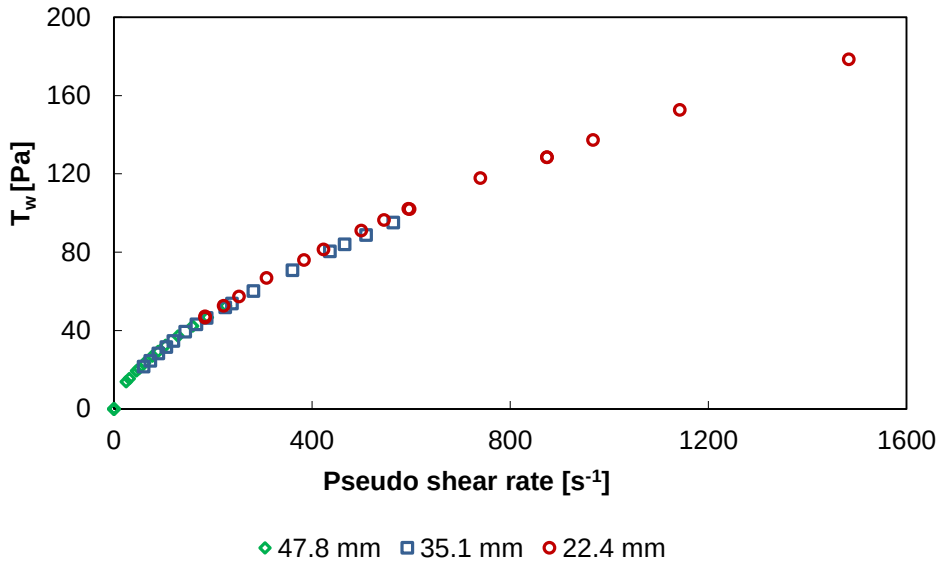

CMC 5.16%w/w

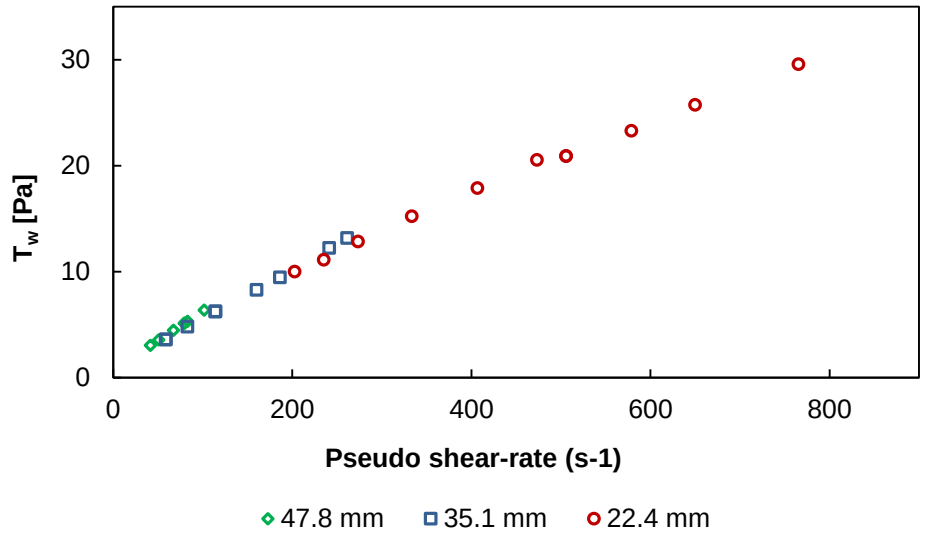

APPENDIX A.2: Pseudo-rheograms for Bentonite (7.48 & 5.4) %w/w

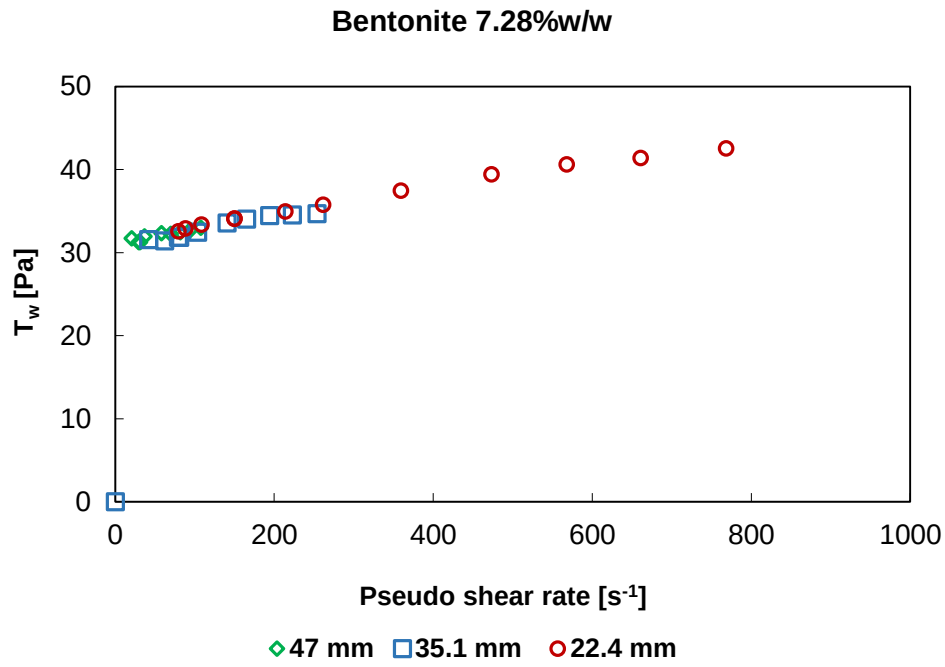

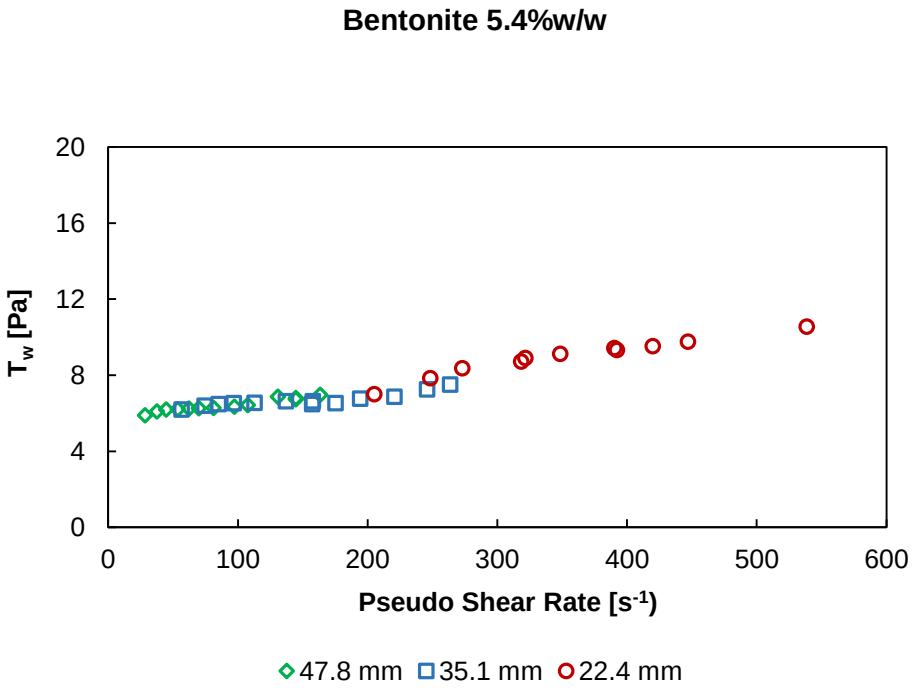

APPENDIX A.3: Pseudo-rheograms for Kaolin (38.4 & 30.79) %w/w

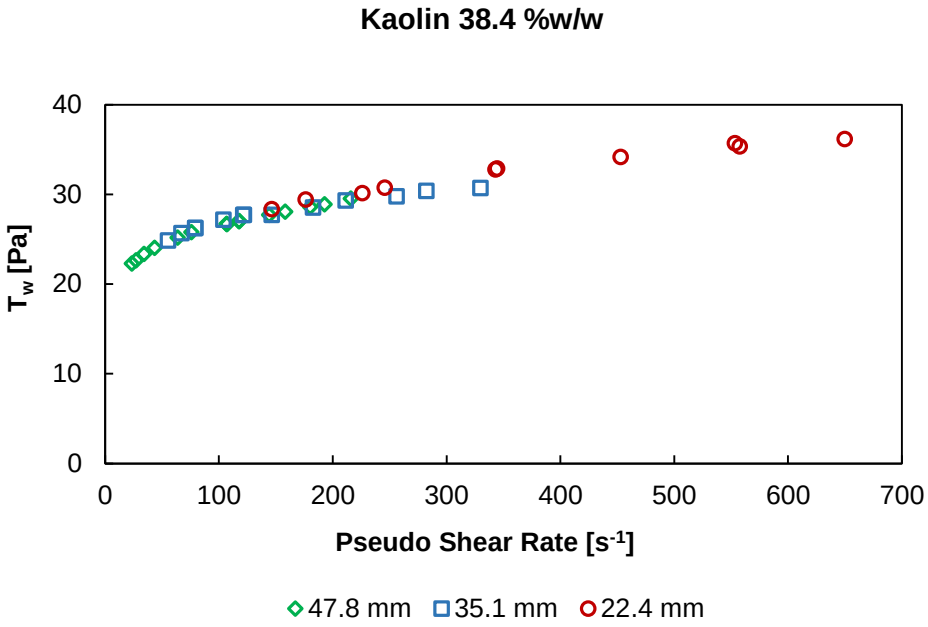

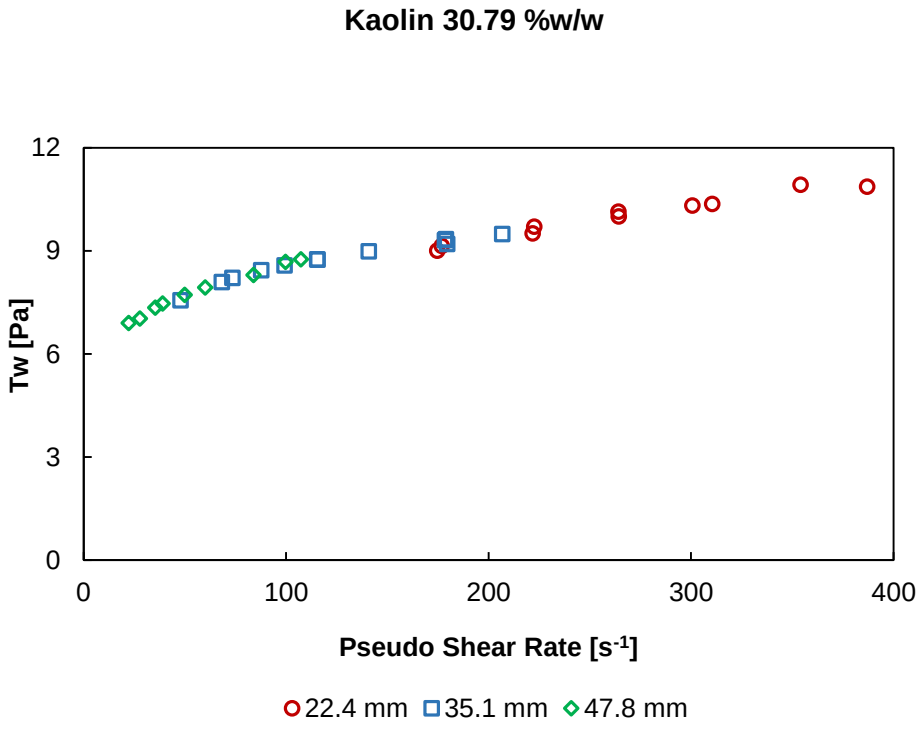

APPENDIX B.1: Velocity profile relationships for Power-law fluids

This section further describes the pipe flow relationships for fluids which can be characterised by the Power-law model. Assuming no-slip conditions for Power-law fluids, Equations B.1.1 and B.1.2 can be equated and integrated to give the radial velocity, shear rate and viscosity profiles:

$$\tau = K(\dot{\gamma})^n \ ; \ \mu = K(\dot{\gamma})^{n-1} \tag{B.1.1}$$

$$\frac{F}{A} = \tau_{yx} = \mu\left(-\frac{dV_x}{dy}\right) = \mu\dot{\gamma}_{yx} \tag{B.1.2}$$

The velocity distribution/profile is then given as:

$$v = \left(\frac{nR}{(1+n)}\right)\left(\frac{R\Delta P}{2LK}\right)^{\frac{1}{n}}\left(1-\left(\frac{r}{R}\right)^{1+\frac{1}{n}}\right) \tag{B.1.3}$$

The radial shear rate and viscosity profiles are described by B1.4 and B1.5 respectively:

$$\dot{\gamma} = \left(\frac{r\Delta P}{2LK}\right)^{\frac{1}{n}} \tag{B.1.4}$$

$$\mu = \frac{\tau}{\dot{\gamma}} = K\left(\frac{r\Delta P}{2LK}\right)^{1-\frac{1}{n}} \tag{B.1.5}$$

Figure B1.1 shows an illustration of the cylindrical lamina across the pipe radius i.e. the velocity profile of the fluid.

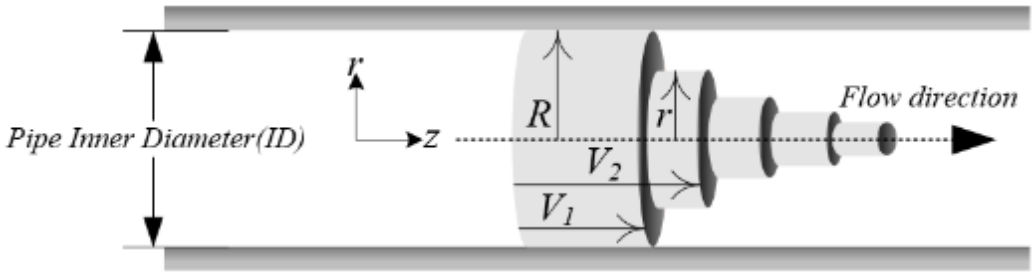

Figure B1.1: Fluid velocity profile in pipe flow (adapted from Nave, 1998)

The wall shear rate and the corresponding viscosity are described by the relationship in Equation B.1.6.

$$\dot{\gamma}_w = \left(\frac{R\Delta P}{2LK}\right)^{\frac{1}{n}} \tag{B.1.6}$$

$$\mu_w = \frac{\tau_w}{\dot{\gamma}_w} = K\left(\frac{R\Delta P}{2LK}\right)^{1-\frac{1}{n}} \tag{B.1.7}$$

Therefore the flow rate can be expressed as:

$$Q = 2\pi\int_0^R v dr = \left(\frac{\pi n R^3}{(3n+1)}\right)\left(\frac{R\Delta P}{2LK}\right)^{\frac{1}{n}} \tag{B.1.8}$$

APPENDIX B.2: Velocity profile relationships for yield-stress fluids

For yield stress fluids, that is fluids which only flow after a threshold stress value has been exceeded; a solid plug core flowing in the middle of the pipe is observed since in that region the shear stress is less than the yield stress. This is shown schematically in Figure B2.1

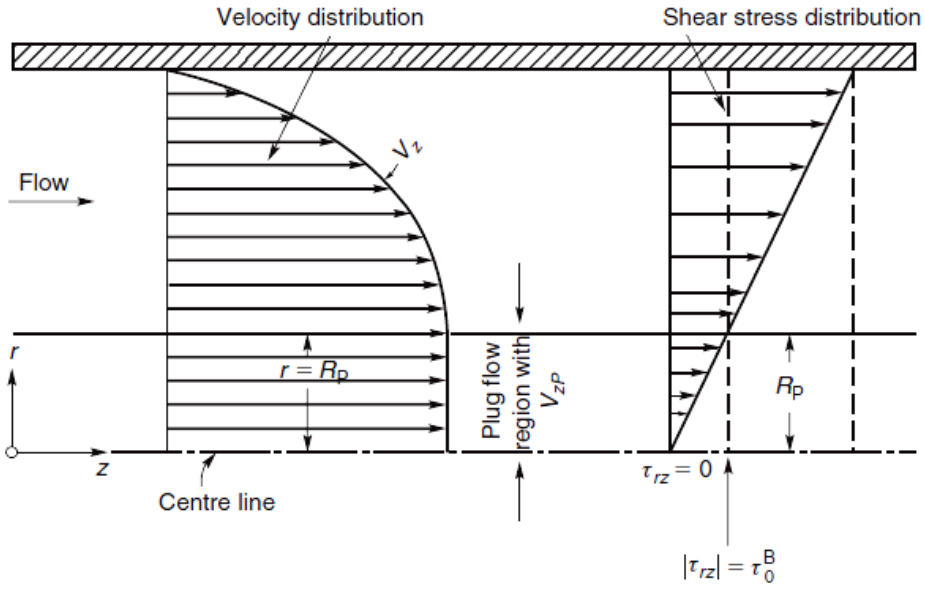

Figure B2.1: Velocity distribution for a yield-stress fluid in a pipe (Chhabra & Richardson, 1999)

In the annular area $R_{plug} < r < R$, the velocity will gradually decrease from the constant plug velocity to zero at the pipe wall. Also within this region the shear stress is greater than the yield stress of the fluid. By combining the Equations in B.2.1 and integrating with respect to r results in the velocity distribution shown in B.2.2.

$$\tau_{rz} = \left(\frac{-\Delta P}{L}\right)\frac{r}{2} \; ; \; \tau_{rz} = \tau_0^H + K\left(\frac{-\Delta P}{L}\right)^n \tag{B.2.1}$$

$$v = \left(\frac{nR}{(1+n)}\right)\left(\frac{R\Delta P}{2LK}\right)^{\frac{1}{n}}\left(\left(1-\frac{R_{plug}}{R}\right)^{(n+1)/n} - \left(\frac{r}{R}-\frac{R_{plug}}{R}\right)^{1+\frac{1}{n}}\right) \tag{B.2.2}$$

The shear rate and viscosity distributions are then described by B2.3 and B2.4 respectively:

$$\dot{\gamma} = \left(\frac{\Delta P}{2LK}\right)^{\frac{1}{n}}\left(\left(r - R_{plug}\right)^{\frac{1}{n}}\right) \tag{B.2.3}$$

$$\mu = \frac{\tau}{\dot{\gamma}} = K\left(\frac{R\Delta P}{2LK}\right)^{1-\frac{1}{n}}\left(\frac{r}{\left(r - R_{plug}\right)^{\frac{1}{n}}}\right), \tag{B.2.4}$$

where, $R_{plug} = \frac{2L\tau_y}{\Delta P}$ is the plug radius. At the pipe wall, the shear rate and viscosity are:

$$\dot{\gamma}_w = \left(\frac{\Delta P}{2LK}\right)^{\frac{1}{n}}\left(\left(R - R_{plug}\right)^{\frac{1}{n}}\right) \tag{B.2.5}$$

$$\mu_w = \frac{\tau_w}{\dot{\gamma}_w} = K\left(\frac{\Delta P}{2LK}\right)^{1-\frac{1}{n}}\left(\frac{R}{\left(R - R_{plug}\right)^{\frac{1}{n}}}\right) \tag{B.2.6}$$

The volumetric flow rate is given by:

$$Q = \pi v_{plug} {R_{plug}}^2 + \frac{\pi n R^2 \left(R - R_{plug}\right)^{1+\frac{1}{n}}}{(n+1)}\left(\frac{\Delta P}{2LK}\right)^{\frac{1}{n}} \cdots$$
$$\left[1 - \frac{2n}{(3n+1)}\left(1 - \frac{R_{plug}}{R}\right)^2 - \frac{2nR_{plug}}{(2n+1)R}\left(1 - \frac{R_{plug}}{R}\right) - \left(\frac{R_{plug}}{R}\right)^2\right] \tag{B.2.7}$$

Figure B.2.2 shows the velocity distribution of yield stress fluids described by the Bingham model. A number of curves are drawn with different values of *c*, where $c = \tau_w / \tau_y = R_{plug} / R$. The constant is a ratio which expresses the relationship between a fluid's yield stress and its corresponding plug radius (Steffe, 1996). The higher the *c* value, the higher the fluid's yield stress.

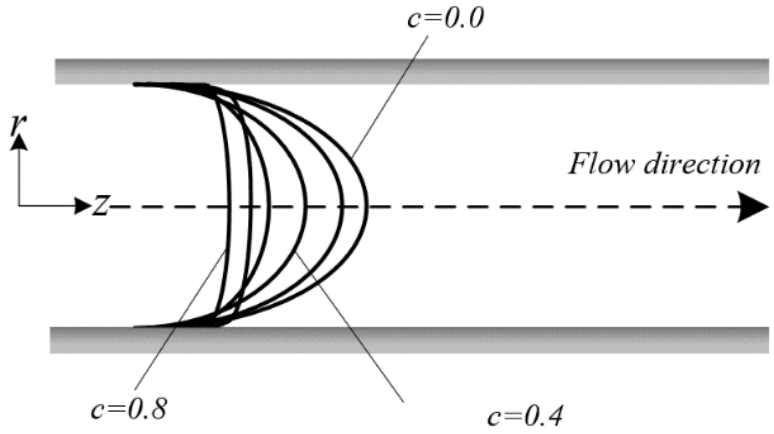

Figure B.2.2: Velocity profiles for Bingham fluids in laminar pipe flow (Steffe, 1996)

APPENDIX C.1: Rabinowitsch-Mooney correction for tube viscometry flow data

After measuring raw tube viscometry data i.e. flow rates and corresponding pressure drops across different pipe test sections, the true shear rates are obtained by applying the Rabinowitsch-Mooney. From pipe flow theory, the shear-stress varies from a maximum at the pipe wall to zero at the centre. Equation C.1.1 describes the shear stress distribution.

$$\tau = \frac{r}{2}\left(\frac{-\Delta P}{L}\right) \tag{C.1.1}$$

By differentiating the parabolic Newtonian velocity profile, the wall shear rate ($r = R$) is then found by the following formula:

$$\dot{\gamma}_{wN} = \frac{4Q}{\pi R^3} = \frac{8V}{D} \tag{C.1.2}$$

A shown in (Holland & Bragg, 1995), the resulting equation after mathematical manipulation gives the non-Newtonian true shear rate as:

$$f(\tau_w) = \frac{8V}{D}\left\{\left(\frac{3}{4}\right) + \frac{d\left(\log 8V/D\right)}{4d\left(\log \tau_w\right)}\right\} \tag{C.1.3}$$

The true wall shear rate can be written in the form:

$$\dot{\gamma}_w = \dot{\gamma}_{wN}\left(\frac{3n'+1}{4n'}\right) \tag{C.1.4}$$

where n' is given by the expression:

$$n' = \frac{d\left(\log \tau_w\right)}{d\left(\log \dot{\gamma}_{wN}\right)} \tag{C1.5}$$

The value of n' is the slope of the of the log–log plot of pseudo shear stress against the pseudo shear rate $\dot{\gamma}_{wN}$ (Holland & Bragg, 1995).

- **Rabinowitsch-Mooney transformation**

The Rabinowitsch-Mooney transformation is clearly a useful tool. Basically the transformation enables the conversion of the pseudo rheogram to the true rheogram for non-Newtonian fluids in lamina flow (Steffe, 1996). By using graphical plotting and curve fitting methods, the procedure is summarised as follows:

- From the raw tube viscometry data (flow rates and pressure drops), construct a $D\Delta P/4L$ vs $8V/D$ for all pipe data on the same graph. If all pipe data from different pipes is collinear, then no wall slip was experienced. Data in the turbulent region is noted as it deviates from the main locus of collinear points.

- Secondly, fit a mathematical function to the laminar flow data and obtain the first derivative of the equation. This value of *n'* is determined by evaluating the differentiated function at the different shear rates.
- Calculate $\dot{\gamma}_w$ using Equation C.1.4.
- Plot τ_w against $\dot{\gamma}_w$ on a logarithmic scale.
- Fit the appropriate equation (Herschel-Bulkley, Power-law or Bingham plastic model) to suit the data.

From these equations, the rheological parameters τ_w, *K* and *n* can be computed. The true rheogram for the non-Newtonian fluid is then obtained.

The main sources of error when using tube viscometry arise from wall slip and entrance or exit losses (Chhabra & Richardson, 1999). Barnes & Hutton (1989) highlight that precautionary measures have to be taken in defining and measuring the pressure gradient $\Delta P/\Delta l$. If the pressure in the external reservoir supplying the capillary and the receiving vessel are measured, then, unless the ratio of tube length to radius is approximately (100 times larger) an allowance must be made for entrance and exit effects. These arise from the following sources for all types of liquid:

(i) Viscous and inertial losses in the converging stream up to the entrance.
(ii) Redistribution of the entrance velocities to achieve the steady state velocity profile within the tube.
(iii) Similar points as mentioned in (i) and (ii) also at the exit.

As for the mitigation of wall slip effects, Chhabra & Richardson (1999) suggest that three pipe diameters be used. This is beneficial in the sense that if the data sets coincide it means that there is no wall slip. However in the case that the pipe data does not coincide, a slip correction factor must be applied (Steffe, 1996).